# FLOW AND MIXING TIME STUDIES IN BIOREACTORS

**A DISSERTATION**

**Submitted in partial fulfilment of the**
**requirements for the award of the degree**
**of**
**MASTER OF TECHNOLOGY**
**IN**
**BIOPROCESS ENGINEERING**

**By**

**SHIVANI SINGH RAJPUT**


**DEPARTMENT OF BIOTECHNOLOGY**
**INDIAN INSTITUTE OF TECHNOLOGY ROORKEE**
**ROORKEE -247667**
**MAY , 2018**

## DECLARATION

I hereby assure that the work presented in this dissertation report entitled **" Flow and Mixing Time studies in Bioreactors"** is submitted towards completion of dissertation work in M.Tech (Bioprocess Engineering) at the Indian Institute of Technology Roorkee, is an authetic record of my original work carried out under the guidance of Dr. Vimal Kumar, Assistant Professor. I have not submitted the matter embodied in this dissertation report for the award of any other degree.

Place: Roorkee Shivani Singh Rajput

Date:

## CERTIFICATE

This is to certify that Ms. Shivani Singh Rajput has completed the dissertation report entitled **" Flow and Mixing Time studies in Bioreactors"** under my supervision. This is to certify that the above statement made by the candidate is correct to the best of my knowledge

Dr. Vimal Kumar
Associate Professor,
Department of Chemical Engineering
Indian Institute of Technology, Roorkee

Dr. Sanjoy Ghosh
Associate Professor
Department of Biotechnology
Indian Institute of Technology, Roorkee

# ACKNOWLEDGEMENTS

First and foremost, I want to thank my mentors **Dr. Sanjoy Ghosh and Dr. Vimal Kumar** for their continuous support of my project and its related research, for their patience, motivation, and immense knowledge. Their assistance, guidance and insight helped me in all the time of research and writing of this report. I sincerely appreciate the help and support provided by the entire research team of Mass Transfer research lab, Instrument analysis Lab and Biochemical Engineering Lab. I am highly indebted to **Mr. Sohail Rasool Lone** and **Mr. Vikash Vashisth** for their guidance and constant supervision as well as for providing necessary information regarding the project & also for their support in completing the project. I would like to express my special gratitude and thanks to **Mr. Shailendra Singh** and **Mr. Kartik Gehlot** for giving me such attention and time.

Signature

# ABSTRACT

Rheological behaviour of three commercially relevant biological cultures: *E.coli* BL21, *Botryococcus braunii* and *Pichia stiptis* is investigated in the present work. These cultures were rheologically characterized and correlation between viscosity and biomass concentration was studied. For all the three cultures studied, all samples taken were proven to be Newtonian fluids and effective viscosity was quite close to that of the nutrient medium. Dynamic viscous properties such as storage modulus, loss modulus and complex viscosity were measured to determine if the culture exhibit viscous or elastic dominant behavior. It was found that all the cell cultures investigated exhibit viscoelastic behavior. Response Surface Methodology (RSM) study was conducted to determine the optimum operational parameters of a bioreactor for Newtonian cultures. It was done for two different combinations of impellers: Rushton-Rushton impeller and Rushton impeller- Marine propeller.

Further, the mixing behaviour of different cultures in a laboratory scale 7L bioreactor was investigated numerically assuming single phase flow behaviour, i.e. in the absence of air. For the numerical modelling of flow and mixing behaviour in the bioreactor k-ε model for turbulence and moving reference frame (MRF) approach for rotating flow was employed. Mixing time study was conducted for all the cultures at varying agitation rates (i.e. 100, 200, 350 and 600 rpm). The species transport model was used to determine mixing characteristics in the bioreactor. The mixing behaviour was reported at different locations in the reactor, where the dead points are observed with flow behaviour predictions. The results obtained can be useful for designing of bioreactor for the processing for these cultures for commercial purposes.

# CONTENTS

# LIST OF TABLES

# LIST OF FIGURES

# NOMENCLATURE

| Symbol | Description |
|---|---|
| ANOVA | Analysis of variance |
| RSM | Response surface Methodology |
| VVM | Volume of gas per culture volume per minute |
| DO | Dissolved Oxygen |
| $k_L A$ | Mass transfer coefficient |
| STR | Stirred Tank reactor |
| 2D | 2 Dimensional |
| 3D | 3 Dimensional |
| Df | degree of freedom |
| VIF | Variance Inflation factor |
| LPM | Liters per minute |
| RPM | Revolutions per minute |
| Conc | Concentration |
| Pt | Point |
| LB Broth | Luria Bertani Broth |
| Bb | *Botryococcus braunii* |
| CFD | Computational Fluid Dynamics |
| MRF | Multiple Reference Frame |
| SM | Sliding Mesh |
| G' | Storage Modulus |
| G'' | Loss Modulus |
| L | Liter |
| FEM | Finite Element Method |
| FVM | Finite Volume Method |
| TS | Total Solid Concentration |
| CMC | Carboxymethyl cellulose |
| $\eta'$ | viscous component of complex viscosity |
| $\eta''$ | elastic component of complex viscosity |
| $\omega$ | Frequency |

| | |
|---|---|
| G* | complex modulus |
| (x,y,z) | Coordinates |
| (u,v,w) | Velocity Components |
| T | Time |
| ρ | Density |
| P | Pressure |
| $E_t$ | Total Energy |
| ζ | Stress |
| Q | Heat flux |
| Re | Reynolds number |
| Pr | Prandtl Number |
| κ | kinetic energy |
| E | Dissipation |
| $\mu_t$ | eddy viscosity |
| $P_b$ | Effect of buoyancy |
| β | coefficient of thermal expansion |
| δ | phase angle |
| Np | Power Number |

# CHAPTER 1

# INTRODUCTION

Biological cultures are complex materials whose complexity is still not completely understood by the researchers. The studies concerning rheological properties of culture are especially lacking. Rheology is the branch of physics that deals with the deformation and flow of materials under external applied forces. Rheometer is generally used for measuring rheological properties. The Rheological properties are different for different kind of materials mostly depending on the physical and chemical state of a material. Thus Rheological properties of polymers solution will differ from concentrated protein formulations, pastes and creams. Rheological properties of cells and tissues generally resemble those of soft matter, such as polymeric systems, gels, suspensions, emulsions etc. These materials exhibit both solid and fluid like behaviour and are considered to be viscoelastic. However, viscoplastic behaviour is also observed in some cases. Plasticity here implies very large deformations of a material once the stress crosses a certain yield limit. Cellular materials are unique because of their property of producing active response to stresses. The cells have the ability to convert mechanical external stresses into biochemical signals (and vice versa) known as mechanotransduction.

The cultures studied in this thesis are viscoelastic in nature i.e. they exhibit properties of both viscous and elastic materials. Some of the cultures especially at high biomass concentration can exhibit Non- Newtonian Behaviour. Non Newtonian Fluids are the fluid whose viscosity depends on shear rate. Normally the biological cultures are either Newtonian or shear thinning (Viscosity decreases as shear rate increases).

The aim of rheological studies is to improve the performance of biological fermentation process by optimizing important growth parameters like temperature, pH, light intensity, and energy for mixing.

Three Types of biological cultures are studied for this project:

1. *E.coli* BL21 (Bacteria)
2. *Botryococcus braunii* (Algae)
3. *Pichia Stiptis*(Fungus)

*E.coli* is the most utilized bacteria for the production of biomolecules. BL21 strain of *E.coli* is highly useful for the production of recombinant proteins. *E.coli* BL21 is compatible with rich medium such as Luria Bertani or Terrific broth. *E.coli* has also been widely used for producing low molecular weight compounds and homologous metabolites. Thus a better understanding of *E.coli* physiology can help improve production process. Moreover, the relationship between bacterial population dynamics and environmental stimuli can be found by investing bacterial growth under different shear conditions. Characterization of bacterial populations can also be done by identifying their viscosity patterns as they are unique for each strain.

*Botryococcus braunii* (Bb) is a green, pyramid-shaped planktonic microalga that has emerged as a great alternative energy source in the field of biotechnology. It can be naturally found in temperate or tropical oligotrophic lakes and estuaries, and the presence of elevated levels of dissolved inorganic phosphorus will provide favourable environment for its growth. The species is of special attention as it can produce high amounts of hydrocarbons, especially oils in the form of Triterpenes. The fast depletion of mineral oil reserves and environmental deterioration due to the emission of greenhouse gases like carbon dioxide and methane is increasing the risk of global warming. Thus the need of the hour is to find a sustainable source of energy. Algae-to-fuel technology can potentially be one such sustainable method. Some major benefits algae has over other technologies is that it is a non- food resource, do not need external resources and has very high biomass yield. However, commercialization of the algae biofuel production is still not possible because of its high energy requirements and the cost involved with it.

A potential research area that can help combat these limitations and improve the concentration and optimize the reaction parameters is rheological studies. The other areas which can be improved with rheology is its downstream processing methods like harvesting and dewatering. Rheological characterization of algae can help in understanding of potential issues that may arise during the fermentation process. Overall, rheological properties of algal slurries may have direct impact on the energy demand and efficiency of algae biofuel production.

*Pichia stipitis* is yeast that is widely known for being used in the fermentation of xylose to ethanol and other products from hemicellulose which is one of the most inexhaustible biomass on earth. *Pichia stipitis* can grow in both aerobic and oxygen limited conditions and is very economical due to its ability to directly convert xylose to ethanol. A high biomass

concentration is required for economical bioethanol production. The culture has the potential of becoming shear-thinning if desirable biomass concentration is obtained. The increase in viscosity can however adversely mass transfer and mixing in the bioreactor and thus can reduce the efficiency and productivity of the whole process. Shear stresses are primarily generated due to agitation and aeration and necessary to maintain adequate oxygen mass transfer and short mixing time. The yeast cell cultures can be more sensitive to the hydrodynamic characteristics of a bioreactor than the bacterial and algae cell culture. Thus it is highly desirable to operate the bioreactor at optimum conditions and the bioreactor should be designed carefully to meet the requirements. The elastic response of the cell membrane is its ability to restore reversibly the integrity of cells and resist the damage and the deformation and it can be studied via dynamic Rheology. The steady yield stress can moreover assist in deciding the operating parameters in case of highly viscous culture.

It can be concluded from above cases that it will be highly beneficial to predict the performance of the reactor before setting up the actual experiment. Computation Fluid Dynamics (CFD) is a very useful tool to virtually determine the performance of a reactor and effect of various parameters on the flow and mass transfer behaviour of a culture. It uses physics, applied Mathematics and computational software to give results like velocity profile, mixing time, torque and power efficiency of a bioreactor. The Fluent software employed for computational fluid dynamics simulations relies on basic mass, linear momentum and energy balance equations balance equations of fluid mechanics to give the required results. It discretizes the fluid domains as defined by the user and approximate the results on the basis of the size of the grid employed. However, the actual modelling of such a complex three dimensional flow in a bioreactor with a pair of rotating impeller can be quite challenging. Multiple Reference Frames (MRF) or Sliding meshes (SM) are commonly used techniques to model the rotation of the impeller in the bioreactor. The main aim in our study is to visualize the mixing characteristics of species in a 7L bioreactor by employing a tracer and derive computational results with the CFD software FLUENT.

# CHAPTER 2

# LITERATURE REVIEW

In this section, the basic concepts used during this study are explained with relevant equations. Similar studies conducted by various researchers are also briefly discussed to explain the motive of this thesis.

Rheology is the study of characteristics of fluids when external force is applied to them. It generally applies to substances that have a complex microstructure, such as sludges, suspensions and polymers as well as many additives, bodily fluids (*e.g.*, blood) and other biological materials. Newtonian fluids can by apparent viscosity which varies with temperature, but constant for different strain rate. The viscosity of non-Newtonian fluids changes with the strain rate.

Dynamic Rheology is generally used to characterize viscoelastic materials. Dynamic modulus (sometimes complex modulus) is the ratio of stress to strain under vibratory conditions. For purely elastic materials the stress and strain occur in phase. In purely viscous materials, there is a phase difference of 90 degree ( $\prod$ /2 radian) between stress and strain. Viscoelastic materials display behaviour somewhere in between that of purely viscous and purely elastic materials and shows some phase lag.

The linear viscoelastic functions can be represented by either a complex modulus, G*, or a complex viscosity, η*, where

$\eta^* = \eta' - i\eta''$

η’ is viscous component of complex viscosity and η’’ is elastic component of complex viscosity

Similarly, complex modulus, G* is

$G^* = G' + iG''$

G’ is Storage Modulus and G’’- Loss Modulus

Components of complex modulus and complex viscosity are interrelated by

$G' = \omega \eta''$

$G'' = \omega \eta'$

where $\omega$ is frequency

The **storage modulus** represents elasticity of the material or the energy storage during the deformation. On the other hand, **the loss modulus** describes the viscous characteristics of a material, or the energy dissipation that are associated with the flow.

For a perfectly elastic material,

$G' = G^*$ and $G'' = 0$,

whereas for a Newtonian fluid,

$\eta'' = \mu$ and $\eta'' = 0$

If $G'' \neq 0$, it implies viscous irreversible deformation.

**Wileman et al, (2012)** studied Rheological properties of microalgae slurries as a function of biomass concentration for *Nannochloris sp., Chlorella vulgaris*, and *Phaeodactylum tricornutum*. For smaller biomass concentrations, all of them are Newtonian fluids. However, at higher biomass concentrations, *Nannochloris sp*. and *C. vulgaris*, displayed shear thinning non-Newtonian behaviour with varying degrees consistency index and power index. *P. tricornutum*, was still a Newtonian fluid up to 80 kg/m3. The pumping effectiveness is different for various types of algae especially in Non Newtonian regime.

**Patricio et al, (2014)** investigated the activity of growing living bacteria using real-time and in situ rheology in stationary and oscillatory shear. Staphylococcus aureus strain COL and its isogenic cell wall autolysis mutant was used for the same. In the early stages of growth, the viscosity of both strains increases with the population of cells. However, the viscosity of the two strains differs significantly during the exponential phase of growth. The viscous and elastic moduli of strain COL was also obtained with oscillatory shear, exhibit power-law behaviours and varies on the basis of the stage of bacterial growth.

**Gabelle et al. (2012)** studied the rheological properties and mass transfer during the growth of submerged cultures of fungi *Trichoderma reesei*. They noticed that as biomass concentration is increased, the culture broth exhibits shear-thinning behaviour, affecting both mixing and oxygen transfer. Fungi and enzyme yields were also shown to strongly depend on the ability to supply oxygen to the broth and, and thus main focus was on gas–liquid mass

transfer predictions. A rheology of the broth was explained using power law. Power consumption was calculated for 3L and 20 L Bioreactors and mass transfer correlations were derived. Experimental results and recently developed correlations were compared and it was concluded hydrodynamic properties and mass transfer in a bioreactor can be estimated by using model fluids.

**Shi et al, (1992)** studied the rheological Properties of Mammalian Cell Culture Suspensions: Hybridoma and HeLa Cell Lines. They observed that both cell suspensions exhibited shear thinning behaviour. From the measured viscoelastic properties, the yield stress was also calculated. The methods of determining the shear sensitivity and the viscous and the elastic components of mammalian cell suspensions was explained in detail

In the present study, Response surface Methodology (RSM) was employed to find optimum parameters for operation of bioreactor for *E.coli* BL21. RSM is used to model experimental responses. The application of RSM is to approximate the optimum reaction parameter and save economic resources in conducting experiments at sub-optimal conditions.

**Bakonyi et al, (2012)** compared various *E. coli* Strains for optimum biohydrogen Production by using Response Surface Methodology. The two factors that were to be optimized were substrate concentration and pH. Response recorded was yield of bioH2 production and aim was to maximize it. The results revealed that the genetically engineered E. coli (DJT 135) strain under optimized conditions could give 1.5 times higher yield compared to the wild-type E. coli (XL1-BLUE).

**Dubey et al (2011)** used RSM to optimize Nitrilase Production by recombinant *E.coli*. The main aim was to optimize the different component of the medium for best response( growth and enzyme activity). The factors here were concentration of fructose, tryptone, yeast extract and lactose. Central composite design was successfully used to get the ideal concentration of these medium components.

Computational fluid dynamics is used in present study to visualize flow in a bioreactor. CFD generally uses methods like Finite Element Method (FEM), Finite Volume Method (FVM), and Finite Difference Method (FDM) to arrive at the results. The governing equation of CFD are the Non-linear Navier Stokes equation which describe

1. The conservation of mass
2. Conservation of momentum
3. Conservation of energy

For these methods, complexity is of the order of $O(N^3)$ where N represent the degrees of freedom.

The Navier Stokes equation are given below:

Continuity: $\frac{\partial \rho}{\partial t} + \frac{\partial (\rho u)}{\partial x} + \frac{\partial (\rho v)}{\partial y} + \frac{\partial (\rho w)}{\partial z} = 0$

X-Momentum: $\frac{\partial (\rho u)}{\partial t} + \frac{\partial (\rho u^2)}{\partial x} + \frac{\partial (\rho uv)}{\partial y} + \frac{\partial (\rho uw)}{\partial z} = -\frac{\partial p}{\partial x} + \frac{1}{Re}\left[\frac{\partial \zeta_{xx}}{\partial x} + \frac{\partial \zeta_{xy}}{\partial y} + \frac{\partial \zeta_{xz}}{\partial z}\right.$

Y-Momentum: $\frac{\partial (\rho v)}{\partial t} + \frac{\partial (\rho uv)}{\partial x} + \frac{\partial (\rho v^2)}{\partial y} + \frac{\partial (\rho vw)}{\partial z} = -\frac{\partial p}{\partial y} + \frac{1}{Re}\left[\frac{\partial \zeta_{xy}}{\partial x} + \frac{\partial \zeta_{yy}}{\partial y} + \frac{\partial \zeta_{yz}}{\partial z}\right.$

Z-Momentum: $\frac{\partial (\rho w)}{\partial t} + \frac{\partial (\rho uw)}{\partial x} + \frac{\partial (\rho vw)}{\partial y} + \frac{\partial (\rho w^2)}{\partial z} = -\frac{\partial p}{\partial z} + \frac{1}{Re}\left[\frac{\partial \zeta_{xz}}{\partial x} + \frac{\partial \zeta_{yz}}{\partial y} + \frac{\partial \zeta_{zz}}{\partial z}\right.$

Energy: $\frac{\partial (E_t)}{\partial t} + \frac{\partial (uE_t)}{\partial x} + \frac{\partial (vE_t)}{\partial y} + \frac{\partial (wE_t)}{\partial z} = -\frac{\partial (up)}{\partial x} - \frac{\partial (vp)}{\partial y} - \frac{\partial (wp)}{\partial z} - \frac{1}{Re*Pr}\left[\frac{\partial q_x}{\partial x} + \frac{\partial q_y}{\partial y} + \frac{\partial q_z}{\partial z}\right] + \frac{1}{Re}\left[\frac{\partial (u\zeta_{x\,x} + v\zeta_{xy} + w\zeta_{xz})}{\partial x} + \frac{\partial (u\zeta_{x\,y} + v\zeta_{yy} + w\zeta_{yz})}{\partial y} + \frac{\partial (u\zeta_{x\,z} + v\zeta_{yz} + w\zeta_{zz})}{\partial z}\right]$

**Montante et al,(2005)** worked on identifying a proper CFD strategy to determine mixing time in stirred tanks reactor for both Newtonian and non-Newtonian fluids. Mixing time was predicted using the time needed for a tracer to become homogeneous. The whole tracer dispersion process was simulated and studied. It was found that various parameters like the discretization scheme, the exact location of probes and tracer injection do not affect the end results significantly.

**Taghavi et al, (2011)** performed experimental and CFD studies to get power consumption in a dual Rushton turbine stirred tank reactor. Flow field and power consumption of a single phase and gas–liquid phase for Rushton turbines was investigated. Results obtained from CFD simulation were compared with experimental and literature data and were found to be in agreement.

**Ameur et al, (2012**) worked on Computation fluid dynamics of shear thinning fluids. CFD characterization was done for the flow generated by curved-blade impellers in a cylindrical unbaffled vessel. The fluids simulated have a shear thinning behaviour. The effect of the impeller speed, the fluid rheology and the number of impeller blades on the flow patterns and the power consumption was investigated. The power consumption was higher for extreme shear thinning fluids. Mixing Power was also highly influenced by Reynolds number and number of impeller blades. Low power law index, high Reynolds number and low blade number yield the best result.

**Wu et al, (2007)** studied CFD Simulation of Non-Newtonian Fluid Flow in Anaerobic Digesters. Mathematical model predicting the flow fields was also developed. The liquid manure employed in the digester was assumed to be a non-Newtonian fluid, and continuity, momentum, and k-ε standard turbulence equations, and non-Newtonian power law model was used for this study. The flow patterns obtained for Newtonian and non-Newtonian fluids were then qualitatively compared. Simulation was performed for different pump power inputs and total solid concentration (TS) in the liquid manure. The optimal power inputs were then determined by comparing the results.

# CHAPTER 3

# MOTIVATION AND OBJECTIVES

**1:** The objective of initial work is to understand the rheology of viscous shear thinning material which might behave like culture. Carboxymethyl cellulose (CMC) in its sodium salt form and Xanthan gum are thus used in this study to understand the rheological behaviour of shear thinning fluids.

**2:** Rheological characterization of the culture is to be done. G', G'' and complex viscosity vs Frequency curve and Stress vs strain curve were determined and are assumed to provide sufficient information about the rheology of the culture.

**3:** To find application of rheology in process parameter optimization. It is assumed that there is some correlation between the stress exerted by a viscous fluid and the acceptable tip rotation speed of the impeller for a culture

**4:** To simulate the mixing flow model in a lab scale bioreactor. Mixing flow is to be modeled using ANSYS Workbench 16.0. Species transport model is to be used for this purpose.

# CHAPTER 4

# MATERIALS AND METHODS

## 4.1 Rheological characterization of reference materials

Carboxymethyl cellulose (CMC) in its sodium salt form and Xanthun Gum were formed at various concentrations with water as a medium and mixed using Magnetic fluid mixer. Modular Compact Rheometer is used for all Rheological Experiments conducted in this study. It is equipped with a ball-bearing motor and provides measurements in rotational and also for special applications in oscillatory mode. In this study, gap sizes of 0.1 mm and measuring system PP50 which is suitable for Newtonian and low viscosity fluids.

## 4.2 E.coli BL21

The E.coli BL21 strain was used for the set of experiments. It was obtained from Physical Chemistry Lab, University of Kentucky. Stock culture of the isolate preserved in 20% glycerol at -80 ºC and subcultured monthly on YPD agar plates. The freshly grown culture from the agar plates was then transferred to a 250 mL flask containing a 25 g/l seed culture medium (pH 7.0), comprising of yeast extract 5 (g/l), Casein enzymic hydrolysate (10 g/l) and sodium chloride(10 g/l) for inoculum development. The inoculum was incubated at 37ºC at 180 rpm in a shaker for 12 h. The fermentation is to be carried out in a 7 L STR containing 5 L of production medium. The production medium (pH 7.5) consisted of 5% inoculum, 5% (w/v) yeast extract,10 %(w/v) Casein enzymic hydrolysate and 10% (w/v) NaCl.

To find the optimum reactor parameters for maximum mass transfer coefficient ($k_La$) to carry out the fermentation, RSM ( Response Surface Methodology) study was conducted.

A 7 L stirred tank reactor (STR) containing

1. Two six-bladed Rushton turbine impellers
2. One Rushton Impeller and One marine impeller

was filled with 5 L distilled water to measure the mass transfer coefficient ($k_L a$) value in Newtonian system since the culture to used will also be Newtonian as proved in this study. The $k_La$ value was measured using the static gassing-out method. At the start of the experiment, nitrogen is passed through the reactor till there is no dissolved oxygen and then air was passed through the reactor till it reaches saturation. To find the $k_La$ value, oxygen concentration w.r.t time was measured during the aeration using Dissolved oxygen probe.

The three parameters used in the study are

1. Agitation rate - A
2. Air Flow Rate- B
3. Impeller Spacing - C

Optimum values of these parameters were found by conducting series of experiments as designed by the Design Expert software version 7.0.0. Each experiment was performed under different conditions of agitation rate, air flow rate and Impeller Spacing as described in experimental design (Table 4.1).

**Table 4.1:** Value of Independent Variables Used for Optimization in RSM Study

| Factor | Name | Units | Type | Low Actual | High Actual | Low Coded | High Coded | Mean | Std. Dev. |
|---|---|---|---|---|---|---|---|---|---|
| A | Agitation rate | RPM | Numeric | 100 | 600 | -1 | 1 | 350 | 182.574 |
| B | Air flow rate | vvm. | Numeric | 0.2 | 2.4 | -1 | 1 | 1.3 | 0.803 |
| C | Impeller spacing | Cm | Numeric | 4 | 8 | -1 | 1 | 6 | 1.461 |

A multiple regression analysis of the obtained data was then done in terms of mass transfer coefficients to obtain a correlation between A, B, C and $k_L A$.

A second-order polynomial equation was the best fit to mathematically explain this correlation:

$$Y = x_0 + x_1A + x_2B + x_3C + x_{11}A^2 + x_{22}B^2 + x_{33}C^2 + x_{12}AB + x_{13}AC + x_{23}BC$$

where Response – Y, Intercept coefficient – x0, linear coefficients - x1, x2, x3 , Squared coefficients - x11, x22, and x33; Interaction coefficients - x12, x13, and x23

The fit of the regressed empirical model was also statistically confirmed through $R^2$ and F-values from the ANOVA of the developed model.

2D Response plots showing how the interaction different factors is effecting the response is then plotted and explained to find the major contributing factor to response.

The E.coli BL21 culture was then fermented in a bioreactor at 37ºC under the optimum conditions. It was studied for its biomass change with time by measuring the optical density at regular intervals for the sample collected. The Rheological study was also done for these samples and Apparent Viscosity, Loss Modulus, Storage modulus and complex viscosity curves were obtained for comparison.

### *4.3 Botryococcus braunii*

The Algae *Botryococcus braunii* was also characterized used in this experiment. It was processed in a 3 L flat panel photobioreactor. The inoculum is prepared in BG 11media whose composition is given in Table 4.1. Working volume of the bioreactor was 2.87 l and 10% inoculum was mixed with medium to initialize the reactor. Bioreactor was maintained at pH 7.8 and air supplied into the reactor had 20% $CO_2$ and light intensity was 133 µmol/$m^2$s. The working temperature was 27 ºC.

For determining the rheological properties, algae samples at different biomass concentration were prepared. A known volume of the culture was collected from the bioreactor at fixed time interval and centrifuged for 5 min at 600 rpm. The supernatant was then decanted and the obtained dry cells were again suspended in the medium. The algae concentration was measured in grams of dry weight per litre of sample.

**Table 4.2:** BG11 Medium Composition(Source: Biocyclopedia.com)

**TABLE 6.2**
**BG11 Medium Composition**

| Reagents | Per Liter |
|---|---|
| $NaNO_3^a$ | 1.5 g |
| $K_2HPO_4 * 3H_2O$ | 0.004 g |
| $MgSO_4 * 7H_2O$ | 0.075 g |
| $CaCl_2 * 2H_2O$ | 0.027 g |
| Citric acid ($C_6H_8O_7$) | 0.006 g |
| Ammonium ferric citrate ($C_6H_8O_7 * n$Fe $* n NH_3$) | 0.006 g |
| $EDTANa_2Mg$ | 0.001 g |
| $Na_2CO_3$ | 0.02 g |
| Microelement stock solution | 1 ml |
| ***Microelement Stock Solution*** | |
| $H_3BO_3$ | 2.860 g |
| $MnCl_2 * 4H_2O$ | 1.810 g |
| $ZnSO_4 * 7H_2O$ | 0.222 g |
| $Na_2MoO_4 * 2H_2O$ | 0.390 g |
| $CuSO_4 * 5H_2O$ | 0.079 g |
| $Co(NO_3)_2 * 6H_2O$ | 0.0494 g |

pH = 7.4
[a]To be omitted for $N_2$-fixing cyanobacteria

### *4.4 Pichia stiptis*

*Pichia stipitis* used in this study was grown at 30°C and maintained at 4°C on agar slants. The adapted culture was maintained in a medium containing 10 g/l yeast extract,1g/l Potassium biphosphate (KH2PO4), 1g/l Ammonium Sulphate ($(NH_4)_2SO_4$), 1 g/l Magnesium Chloride ($MgCl_2.7H_2O$) and 20 g/l Glucose. 20. The pH was maintained near 5.0.

Fermentation experiment was carried out in a 5L reactor with a 2l working volume. Rushton impeller was used for mixing. The culture at a concentration of 10% (v/v) was used as inoculum. Media used contain 10 g/l yeast extract, 1g/l Potassium Biphosphate (KH2PO4), 1g/l Ammonium Sulphate ((NH4)2SO4), 1 g/l Magnesium Chloride (MgCl2.7H2O) and 60

g/l Glucose. The culture was grown at 30°C and at 150 rev min. The Samples were withdrawn at 4h interval, and analysed for biomass growth and rheology.

### 4.5 . Numerical Modelling of Flow and Mixing Characteristics

The flow in a7L fully baffled bioreactor equipped with a pair of Rushton impellers was simulated using commercial computation fluid dynamics software Fluent 16.2. The Geometry was first constructed in Gambit 2.4.6. Bioreactor designed was similar to the one used for E.coli BL21 experiments. Inner diameter of cylindrical bioreactor was 18 cm and outer diameter was 21.4 cm and height of the reactor was 28 cm. Four Baffles placed on the four sides of the bioreactor had length = 20.2 cm, breadth = 1.8 cm and width = 1.2 mm. Cooling Coil constructed in the reactor to maintain the temperature had a diameter of 1cm and height of 27 cm. Sparger used has a height of 24 cm and diameter of 0.71 cm. The impeller shaft was also cylindrical and had a diameter of 1.2 cm and height of 28 cm. Two Rushton impellers with six blades was constructed with the impeller spacing of 5 cm. Overall diameter of the impeller constructed was 5.942 cm. The impeller blades were cubical and had a length of 2.71 cm, breadth of 1.6 cm and width of 0.98 mm. The impeller disk supporting these blades has the height of 0.9 cm and diameter of 3.12 cm. The meshing was done by dividing the volume into two parts:

1. Moving fluid region

2. Static fluid domain

The grids in the impeller region rotate with the impeller at a rotation speed same as that of moving fluid. The grid in the tank remains stationary. The two grids slide past each other at a cylindrical interface. The meshing was done using ‘bottoms up’ approach. The edges were meshed first followed by faces and finally the volume was meshed. Quad grids were generated wherever possible otherwise Tri- Pave meshing was employed for face meshing. The Tet/Hybrid meshing with type TGrid was employed for volume meshing. The grid constructed for the simulations consisted of 6,26,416 cells which is a good number to get accurate results. Constant boundary conditions were set for all the boundaries and a rotating reference frame (RRF) approach was followed where the impeller is immobilized and the flow is occurring with respect to the rotating frame. The fluids employed are given in Table

4.3. They are simulated for four impeller speeds: 100 rpm, 150 rpm, 350 rpm and 600 rpm and results were thus compared.

**Table 4.3:** Fluids used for CFD simulation

| Culture Name | Viscosity (Pa.s) | Type of Fluid | Consistency Index | Power Law Index | Agitation (RPM) |
|---|---|---|---|---|---|
| E.coli Bl21 | 0.000914 | Newtonian | 0.000914 | 1 | 100 |
| *Pichia stiptis* | 0.000956 | Newtonian | 0.000956 | 1 | 150 |
| E.coli Bl21 | 0.000823 | Newtonian | 0.000823 | 1 | 350 |
| Water | 0.00103 | Newtonian | 0.00103 | 1 | 600 |
| *P. tricornutum* | 0.0025 | Newtonian | 0.0025 | 1 | 100 |
| *P. tricornutum* | 0.0025 | Newtonian | 0.0025 | 1 | 150 |
| *P. tricornutum* | 0.0025 | Newtonian | 0.0025 | 1 | 350 |
| *P. tricornutum* | 0.0025 | Newtonian | 0.0025 | 1 | 600 |
| *Beauveria bassiana* | 0.015 | Shear thinning | 0.02281 | 0.4221 | 100 |
| *Beauveria bassiana* | 0.015 | Shear thinning | 0.02281 | 0.4221 | 150 |
| *Beauveria bassiana* | 0.015 | Shear thinning | 0.02281 | 0.4221 | 350 |
| *Beauveria bassiana* | 0.015 | Shear thinning | 0.02281 | 0.4221 | 600 |

The simulations were done in single phase. Reynold number was in the order of $10^5$ hence turbulent flow can be considered in all the cases. Pressure based solver was used and ansolute velocity formulation was employed to develop velocity profile. The standard *k–ε* model with 2 equations was used for solving turbulent single phase flow.

**Transport equations for standard k-epsilon model**

For turbulent kinetic energy κ

$$\frac{\partial}{\partial t}(\rho\kappa) + \frac{\partial}{\partial x_i}(\rho\kappa u_i) = \frac{\partial}{\partial x_j}\left[\frac{\left(\mu + \frac{\mu_t}{\sigma_\kappa}\right)\partial\kappa}{\partial x_j}\right] + P_\kappa + P_b - \rho\varepsilon - Y_M + S_\kappa$$

For dissipation $\epsilon$

$$\frac{\partial}{\partial t}(\rho\varepsilon) + \frac{\partial}{\partial x_i}(\rho\varepsilon u_i) = \frac{\partial}{\partial x_j}\left[\frac{\left(\mu + \frac{\mu_t}{\sigma_\varepsilon}\right)\partial\varepsilon}{\partial x_j}\right] + C_{1\varepsilon}\frac{\varepsilon}{\kappa}(P_\kappa + C_{3\varepsilon}P_b) - C_{2\varepsilon}\rho\frac{\varepsilon^2}{\kappa} + S_\varepsilon$$

where $E_{ij}$ is component of rate of deformation and $\mu_t$ is eddy viscosity.

$$\mu_t = \frac{\rho C_\mu \kappa^2}{\varepsilon}$$

$$P_\kappa = -\frac{\rho \overrightarrow{u_i' u_j'} \partial u_j}{\partial x_i}$$

$$P_\kappa = \mu_t S^2$$

In the above equation k and $P_k$ are production terms, where S is the modulus of the mean rate-of-strain tensor, defined as :

$$S = \sqrt{2S_{ij}S_{ij}}$$

where $P_b$ is effect of buoyancy and is given by

$$P_b = \frac{\beta g_i \mu_t}{Pr_t}\frac{\partial T}{\partial x_i}$$

Model constant were

$C_{1\varepsilon}$ = 1.44, $C_{2\varepsilon}$ = 1.92, $C_\mu$ = 1.44, $\sigma_\kappa$ = 1.0, $\sigma_\varepsilon$ = 1.3

In case of Non Newtonian fluid, Non- Newtonian Power law model was first enable before starting the simulations.

Solution method used for Pressure – Velocity Coupling was SIMPLE where spatial Discretization gradients were least squares cell based and second order scheme was used for solving Pressure and second Order Upwind scheme for Momentum, turbulent kinetic energy and turbulent dissipation rate. In order to get the accurate results the fully developed single-phase flow field was first calculated by running the iterations for steady state. The simulations were run till we get constant continuity value. The simulations were then run for

unsteady state with the time step size of 0.0001 s and Number of time steps were kept at 3000 for all the set of simulations.

Mixing characteristics were determined using species transport model. In the species transport model, a tracer is used and modelled as having same properties as the fluid used. Defined tracer has the volume of less than 1% of total volume of the tank. Total seven points were plotted inside the tank. The area weighted average of the mass fraction of the species was then plotted with respect to flow time for all these points. The flow time here represent the mean residence time of the tracer. The transient formulation was solved using first order implicit formulation. Dimensions of the different point used to monitor tracer concentration are mentioned in Table 4.4

**Table 4.4:** Dimensions of different point at which tracer is monitored

| Point | X Coordinate (cm) | Y Coordinate (cm) | Z Coordinate (cm) |
|---|---|---|---|
| Point 1 | 0 | 0 | 0 |
| Point 2 | 8.585 | 0 | 0 |
| Point 3 | -8.585 | 0 | 0 |
| Point 4 | 6.345 | 9.375 | 0 |
| Point 5 | -6.345 | 9.375 | 0 |
| Point 6 | 8.585 | 27 | 0 |
| Point 7 | -8.585 | 27 | 0 |

These points are represented with respect to the geometry in Fig 4.1.

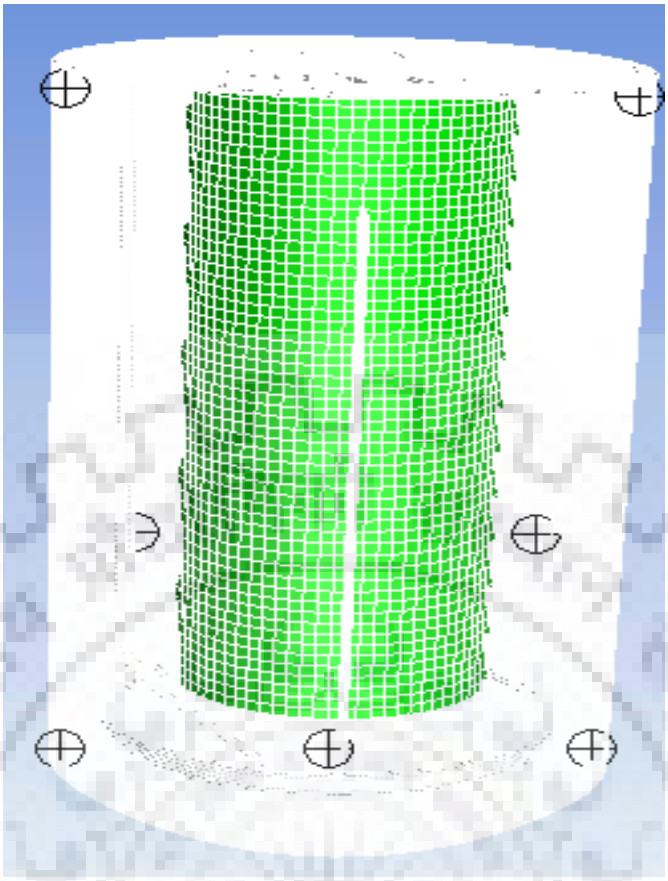

**Fig 4.1:** Tracer Monitor Points represented in the computational domain

# CHAPTER 5

# RESULTS AND DISCUSSIONS

## 5.1 Rheological behaviour of reference fluids

Rheological measurement of water is carried out at different temperatures since water is used in all the samples as a medium. Carboxy methyl cellulose (CMC) and Xanthan gum have been known to mimic the behaviour of highly viscous culture. The Rheological studies for them were conducted for reference purposes.

It can be clearly observed that water is a Newtonian fluid and viscosity decreases with increase in temperature.

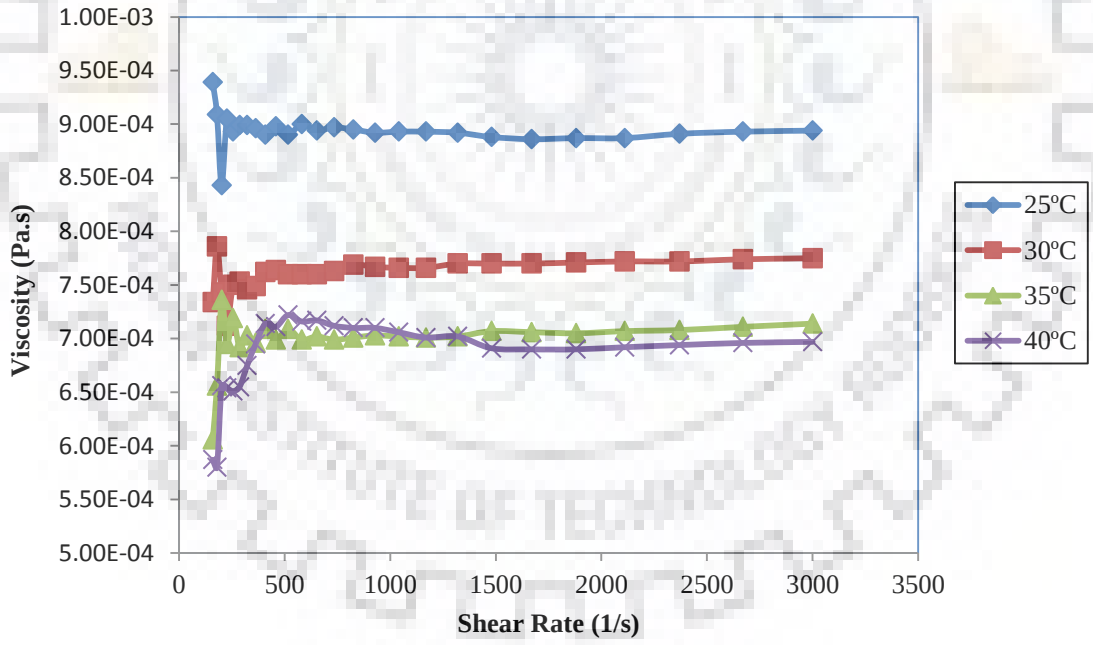


**Fig 5.1:** Viscosity curve for water at different temperature

Dynamic rheology of water is also measured for reference which is storage modulus dominated.

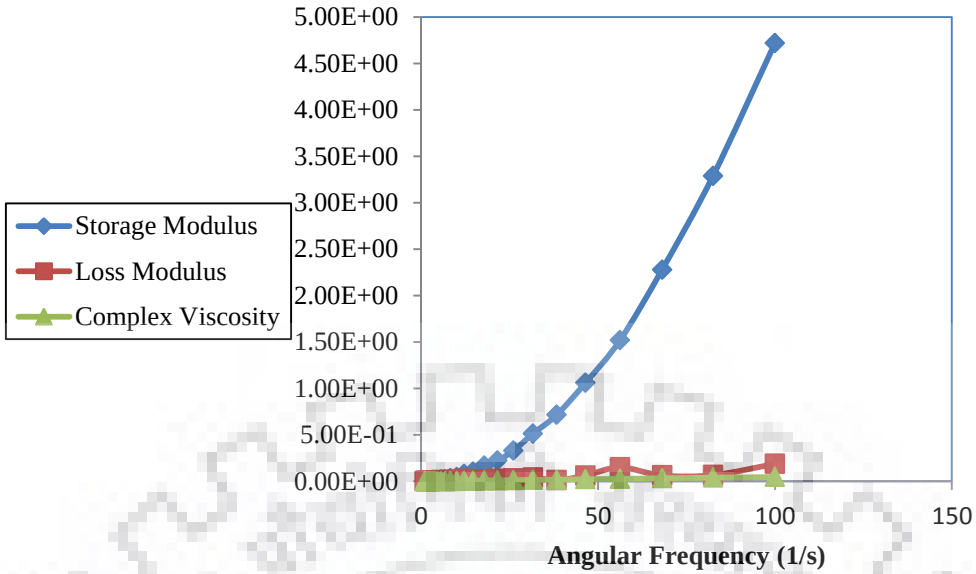


**Fig 5.2**: Dynamic Rheology Curve for water

Rheology of CMC was also measured at 4 different temperatures. In this case, the fluid is not Newtonian. The power law and consistency index is subsequently measured for the different concentration of CMC solution in water. Figures 5.3-5.5 show the dynamic rheology for CMC solution with 1, 2 and 4 % concentrations. Storage Modulus of 1% solution is comparatively higher than 2% and 4 % CMC solution indicating higher ability to store deformation energy in an elastic manner. This may be due to higher degree of cross linking at 1%. The loss modulus is a measure of energy dissipation indicating the hardness or stiffness of a material. The trend similar to storage modulus was observed here where 1% solution is found to have the highest loss modulus. Complex Viscosity depends on complex modulus which is dependent on both storage and loss modulus. Thus similar trend is observed for complex modulus

**Table 5.1:** Consistency index and power index for different concentration of CMC solution in water at different temperature

| Concentration | Temperature | Consistency Index | Power Index |
|---|---|---|---|
| | 25 | 3.422 | 0.128 |
| 0.2 | 30 | 3.2395 | 0.119 |
| | 35 | 2.6535 | 0.136 |
| | 40 | 1.8897 | 0.157 |
| | 25 | 8.1578 | 0.037 |
| 0.4 | 30 | 6.0124 | 0.074 |
| | 35 | 7.0599 | 0.083 |
| | 40 | 4.7254 | 0.105 |
| | 25 | 8.1803 | 0.082 |
| 0.6 | 30 | 8.9387 | 0.052 |
| | 35 | 6.8893 | 0.102 |
| | 40 | 6.7792 | 0.056 |
| | 25 | 10.513 | 0.072 |
| 0.8 | 30 | 7.2024 | 0.102 |
| | 35 | 7.2236 | 0.102 |
| | 40 | 5.1784 | 0.126 |
| | 25 | 4.6287 | 0.18 |
| 1 | 30 | 5.2365 | 0.161 |
| | 35 | 3.8357 | 0.191 |
| | 40 | 3.0823 | 0.201 |
| | 25 | 1.9818 | 0.395 |
| 2 | 30 | 1.487 | 0.421 |
| | 35 | 1.1974 | 0.441 |
| | 40 | 0.9251 | 0.47 |
| | 25 | 8.908 | 0.388 |
| 4 | 30 | 6.9117 | 0.414 |
| | 35 | 5.4516 | 0.437 |
| | 40 | 3.209 | 0.518 |

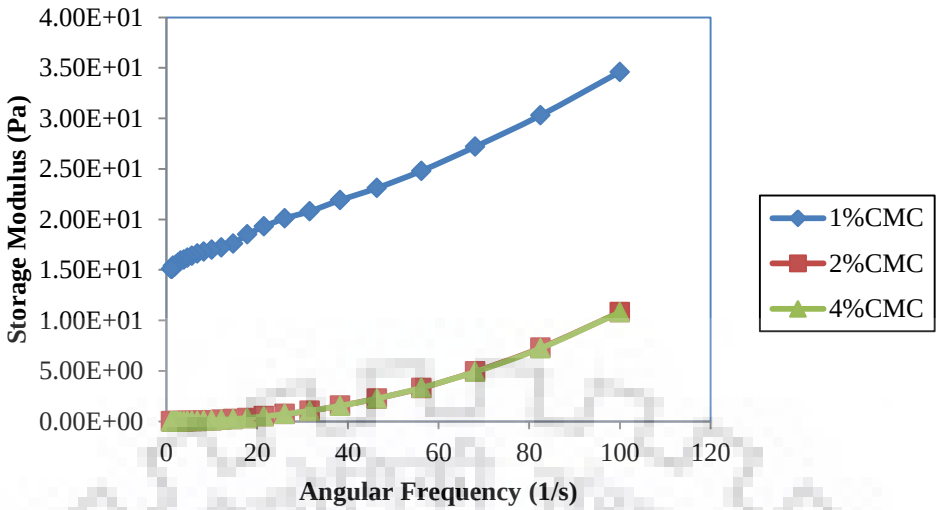


**Fig 5.3 :** Variation of Storage modulus of CMC vs angular frequency and concentration

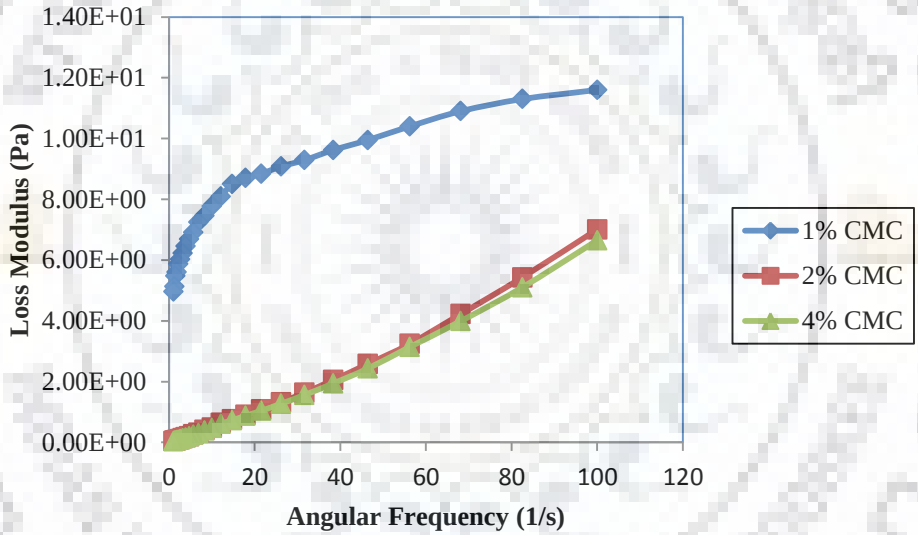


**Fig 5.4:** Variation of Loss modulus of CMC vs angular frequency and concentration

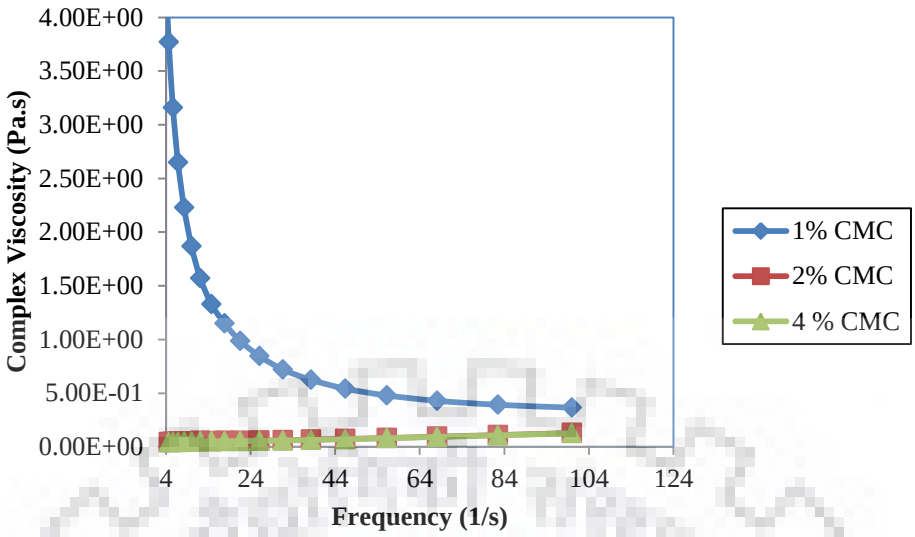


**Fig 5.5:** Variation of Complex Viscosity of CMC vs angular frequency and concentration

Phase angle was also calculated using the formula

$$tan(\delta) = G"/G'$$

where δ is the phase angle, G' is bulk modulus and G" is storage modulus. If tan(δ) is greater than unity, it indicates more "liquid like properties" while this value less than unity will indicate more " solid like properties" . The tangent of Phase angle calculated was less than 1 for 1% CMC solution. It is less than 1 for lower frequency values while is slightly greater than 1 for higher frequency values in case of 2% CMC solution. In case of 4% CMC solution, this value is greater than 1 even for low values of frequency indicating prominent 'solid like' properties. Similarly Rheology for Xanthun gum was measured for two different temperatures. The consistency index and power index found are reported below:

**Table 5.2:** Consistency index and power index for different concentration of Xanthan gum solution in water at different temperature

| Conc (wt%) | Temp (°C) | Consistency Index | Power Index |
|---|---|---|---|
| 0.25 | 30 | 1.0695 | 0.3512 |
| 0.25 | 37 | 0.8145 | 0.3608 |
| 0.5 | 30 | 4.089 | 0.2674 |
| 0.5 | 37 | 3.2206 | 0.2746 |
| 1 | 30 | 13.06 | 0.2322 |
| 1 | 37 | 11.619 | 0.2241 |

As, can be concluded from Table 5.1 and Table 5.2, consistency index (k) decreases with temperature for the same concentration while power index (n) increases with temperature. Moreover, Power index is found to be inversely proportional to concentration and consistency index is directly proportional to concentration. This is in agreement to the already published literature. Storage modulus, loss modulus and complex viscosity for Xanthan gum as function of frequency are illustrated in Fig 5.6, Fig 5.7 and Fig 5.8 respectively.

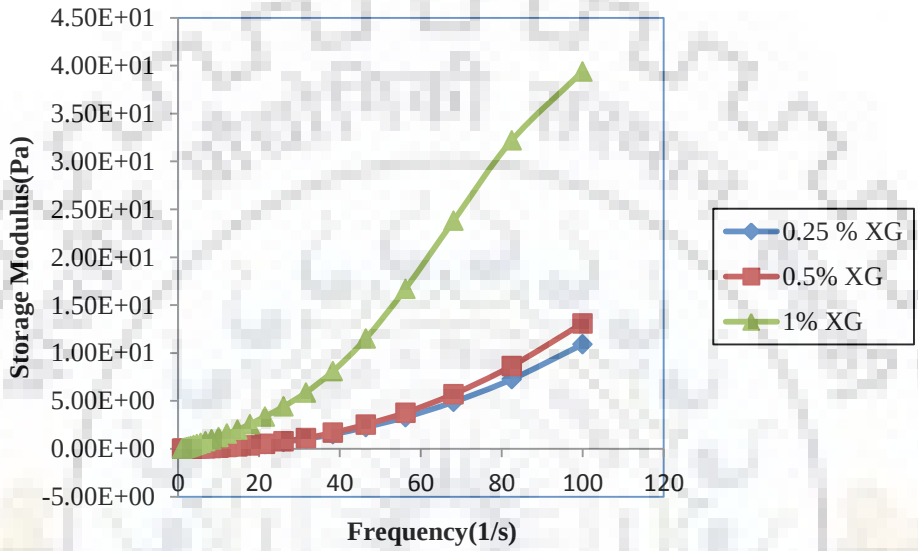


**Fig 5.6 :** Variation of Storage modulus of Xanthan gum vs angular frequency and concentration

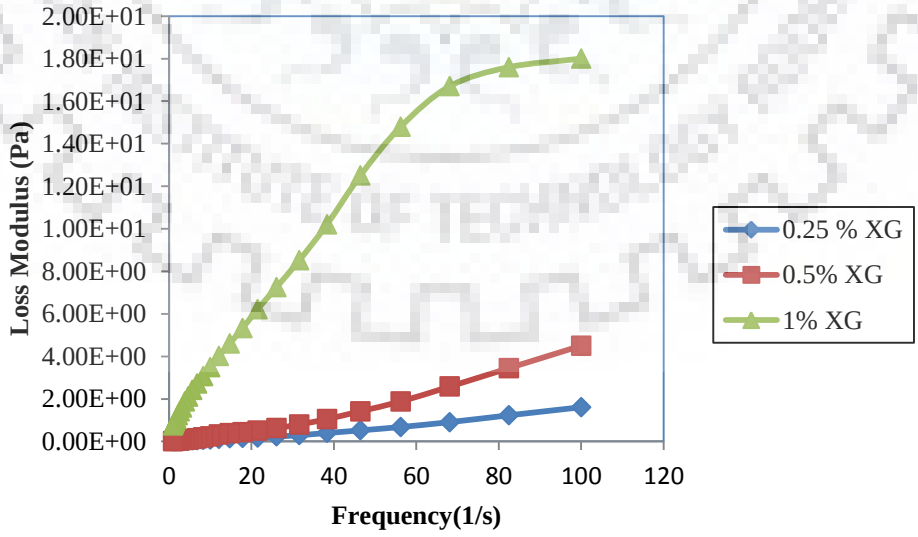


**Fig 5.7:** Variation of loss modulus of Xanthan gum vs angular frequency and concentration

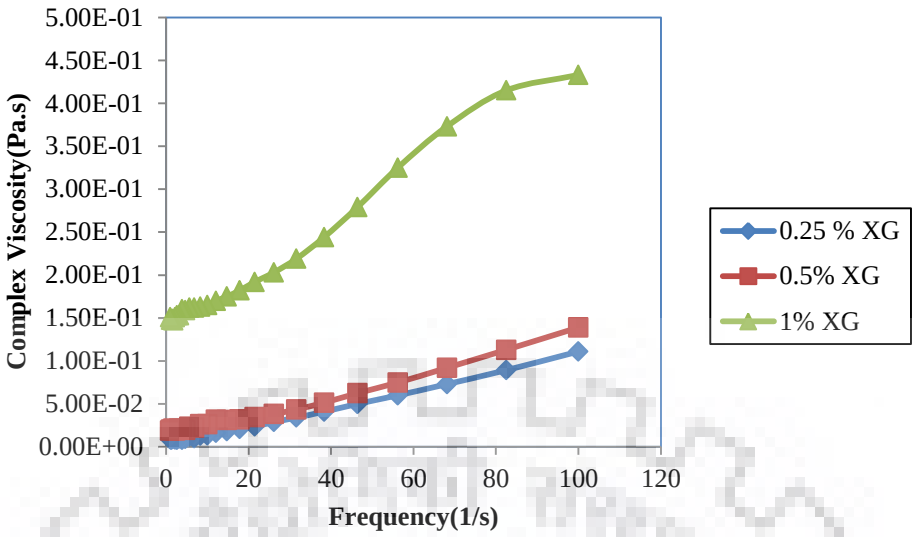


**Fig 5.8:** Variation of complex Viscosity of Xanthan gum vs angular frequency and concentration

In this case it can be clearly seen that storage modulus, loss modulus and complex viscosity are all directly proportional to frequency and concentration. The phase angle is calculated for these three different concentrations of Xanthan gum. The tangent for phase angle measured was less than 1 for 0.25 per solution implying 'liquid like' behaviour while it is greater than 1 for 0.5 and 1 percent solution implying 'solid like' behaviour

## 5.2 E.coli BL21

### 5.2.1 RSM Study

Response surface methodology (RSM) is one of the most famous statistical methods to study the dependence of response on various quantitative parameters. It is widely used to optimize the response which is influenced by different independent variables to a varying degree. The primary goal of this RSM Study is the design of experiments and to derive a reliable mathematical model of the process. Box-Behnken design (BBD) was employed using a full factorial matrix and the three physical parameters that are considered to have the most effect on volumetric mass transfer coefficient ($k_La$) are agitation rate (A), air flow rate (B) and spacing between the two impellers (C).

RSM study was conducted for two different combinations of impellers:

(a) Rushton- Rushton
(b) Rushton – Marine Propeller

#### 5.2.1.1 Rushton – Rushton

The software was designed with 2 centre points and 15 experimental runs. The variables that significantly affected the mass transfer coefficient were determined using a confidence level above 95% . The optimum conditions for maximum mass transfer coefficient were calculated and evaluated using Design Expert software version 7.0.0. Experimental data and result of mass transfer coefficient for the pair of Rushton impeller is given in Table 5.3. The degree of freedom evaluation shows that degree of freedom for model is 9 while for residuals , it is 5. Df for lack of fit is 3 and for pure error, it is 2. For all the cases, variance inflation factor is close to 1 which signifies accurate estimation of coefficients. Table 5.4 shows the values of VIF and Ri values for the model obtained

**Table 5.3:** Experimental data and results of BBD for mass transfer coefficient in case of Rushton-Rushton Impeller combination

| Run | Factor 1 A: Agitation Rate RPM | Factor 2 B: Air Flow Rate vvm | Factor 3 C: Impeller Spacing cm | Mass Transfer Coefficient $k_La$ (1/min) | |
|---|---|---|---|---|---|
| | | | | Experimental | Predicted |
| 1 | 350 | 1.3 | 6 | 1.0978 | 1.0467 |
| 2 | 350 | 2.4 | 4 | 0.658 | 0.8162 |
| 3 | 600 | 2.4 | 6 | 2.2281 | 2.1241 |
| 4 | 350 | 0.2 | 8 | 0.616 | 0.4577 |
| 5 | 350 | 1.3 | 6 | 1.056 | 1.0467 |
| 6 | 600 | 0.2 | 6 | 1.7689 | 1.8006 |
| 7 | 350 | 0.2 | 4 | 0.4126 | 0.4351 |
| 8 | 600 | 1.3 | 8 | 1.8976 | 2.0241 |
| 9 | 350 | 2.4 | 8 | 1.1615 | 1.1390 |
| 10 | 100 | 0.2 | 6 | 0.1462 | 0.2502 |
| 11 | 100 | 1.3 | 4 | 0.6352 | 0.5087 |
| 12 | 600 | 1.3 | 4 | 1.9543 | 1.9000 |
| 13 | 100 | 1.3 | 8 | 0.6758 | 0.7300 |
| 14 | 100 | 2.4 | 6 | 1.0209 | 0.9891 |
| 15 | 350 | 0.2 | 6 | 0.9863 | 0.6139 |

**Table 5.4:** VIF and RI value for mass transfer coefficient model for Rushton- Rushton Impeller system

| Term | StdErr** | VIF | Ri-Squared |
|---|---|---|---|
| A | 0.35 | 1 | 0 |
| B | 0.35 | 1 | 0 |
| C | 0.35 | 1 | 0 |
| AB | 0.5 | 1 | 0 |
| AC | 0.5 | 1 | 0 |
| BC | 0.5 | 1 | 0 |
| $A^2$ | 0.52 | 1.01 | 0.011 |
| $B^2$ | 0.52 | 1.01 | 0.011 |
| $C^2$ | 0.52 | 1.01 | 0.011 |

A quadratic model using regression analysis was developed for this data.

**Final Equation in Terms of Coded Factors:**

$$k_La = +1.05+(0.67* A)+(0.27 * B)+(0.086* C)-( 0.10* A * B)-(0.024 *A*C)+(0.075*B*C) +(0.41*A^2 ) – (0.17 *B^2 )- (0.17* C^2)$$

The statistical significance of this model was verified using the Fisher's test for the analysis of variance (ANOVA), which confirmed that the second-order polynomial function is a good fit for the experimental data. (Table 5.5 )

**Table 5.5:** ANOVA for all the model terms for Rushton Rushton Impeller Combination

| **Source** | **Sum of Squares** | **df** | **Mean Square** | **F Value** | **p Value Prob > F** |
|---|---|---|---|---|---|
| Model | 5.2 | 9 | 0.58 | 24.27 | 0.0013 |
| A-Agitation rate | *3.61* | *1* | *3.61* | *151.52* | *< 0.0001* |
| B-Air flow rate | *0.56* | *1* | *0.56* | *23.72* | *0.0046* |
| C-Impeller spacing | *0.06* | *1* | *0.06* | *2.51* | *0.1742* |
| AB | *0.043* | *1* | *0.043* | *1.81* | *0.2359* |
| AC | *2.37E-03* | *1* | *2.37E-03* | *0.099* | *0.7652* |
| BC | *0.023* | *1* | *0.023* | *0.95* | *0.3754* |
| $A^2$ | *0.63* | *1* | *0.63* | *26.28* | *0.0037* |
| $B^2$ | *0.1* | *1* | *0.1* | *4.34* | *0.0918* |
| $C^2$ | *0.1* | *1* | *0.1* | *4.35* | *0.0913* |
| Residual | 0.12 | 5 | 0.024 | | |
| Lack of Fit | *0.11* | *3* | *0.038* | *11.83* | *0.0789* |
| Pure Error | *6.35E-03* | *2* | *3.17E-03* | | |
| Cor Total | 5.32 | 14 | | | |

The Model F-value of 24.27 implies the model is significant. Values of "Prob > F" less than 0.0500 indicate model terms are significant. In this case A, B, $A^2$ are significant model terms. The "Lack of Fit F-value" of 11.83 implies there is a 7.89% chance that a "Lack of Fit F-value" this large could occur due to noise. "Adeq Precision" measures the signal to noise ratio. A ratio greater than 4 is desirable. Our ratio of 14.878 indicates an adequate signal. This model can thus be applied for design of experiments. Additional information about the accuracy of model is given in Table 5.6. Fig 5.9 shows a good agreement between predicted and experimental values

**Tabe 5.6:** ANOVA Parameters of the second order model derived for Rushton-Rushton Impeller Combination

| | |
|---|---|
| Std. Dev. | 0.15 |
| Mean | 1.09 |
| C.V. % | 14.18 |
| PRESS | 1.82 |
| R-Squared | 0.9776 |
| Adj R-Squared | 0.9373 |

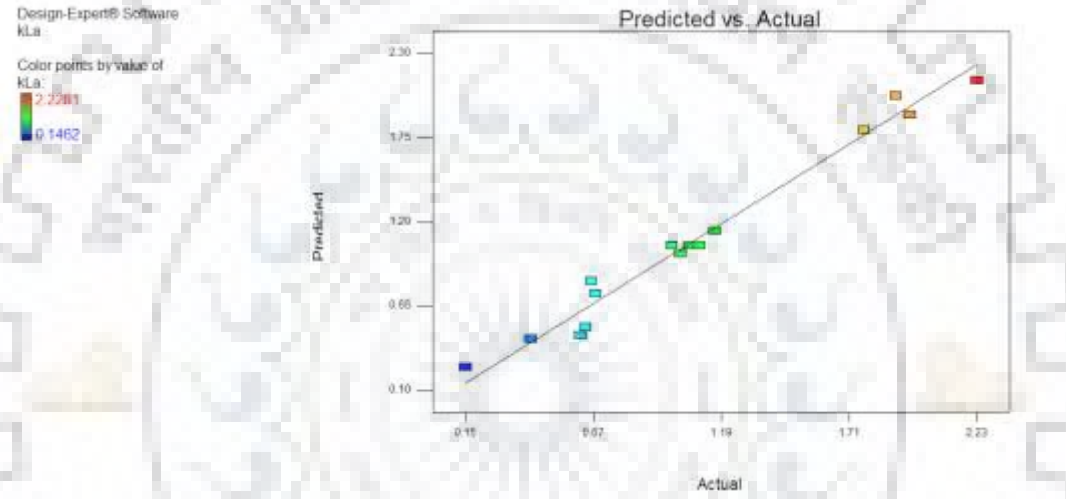


**Fig 5.9**: Relation between actual and predicted values for $k_La$ estimation of Rushton – Rushton impeller combination.

To study the interactive effect of the A, B and C on mass transfer coefficient, three response curves were generated and are represented in Fig 5.10. Fig 5.10(a) represent interactive effect of agitation rate and air flow rate for a fixed impeller spacing of 6 cm. It shows that $k_La$ value increases with increase in flow rate and agitation rate. Fig 5.10(b) indicate the interaction between agitation rate and impeller spacing for a fixed value of air flow rate. $k_La$ value as expected is small for small values of agitation rate. However for $k_La$ value increases as impeller spacing increases from 4 to 6 cm and then decreases again for 8 cm.Similarly, Fig 5.10(c) shows the interaction between impeller spacing and air flow rate. The distance between two impellers can have a huge impact on mass transfer. The material exchange in between the circulation loops is highly dependent on impeller spacing. A inaccurate impeller spacing may result in inefficient mixing of liquid in the upper or lower regions of the vessel.

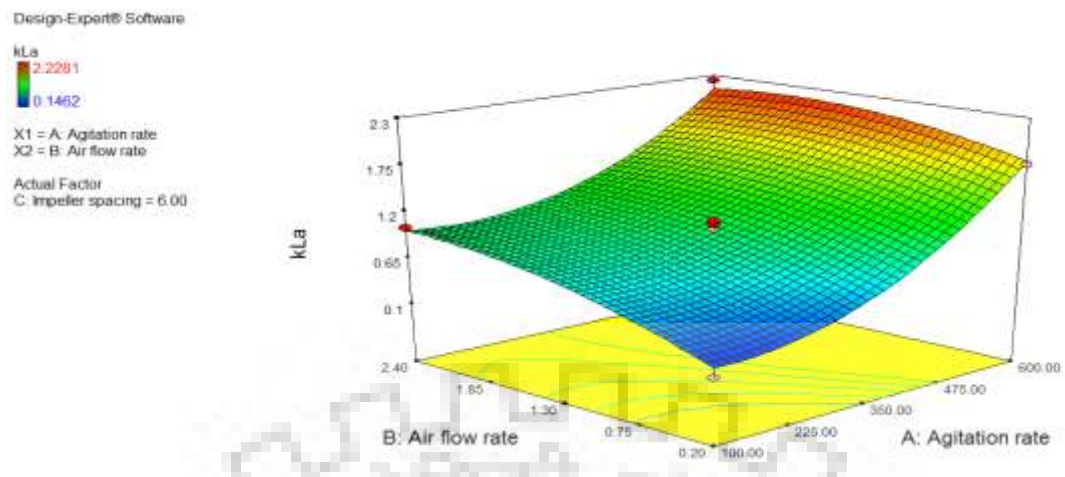


**(a)**

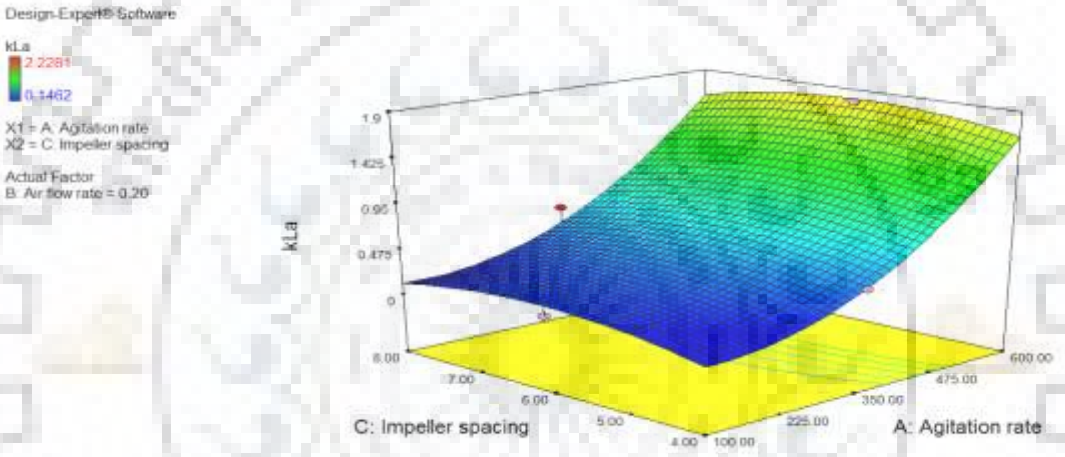


**(b)**

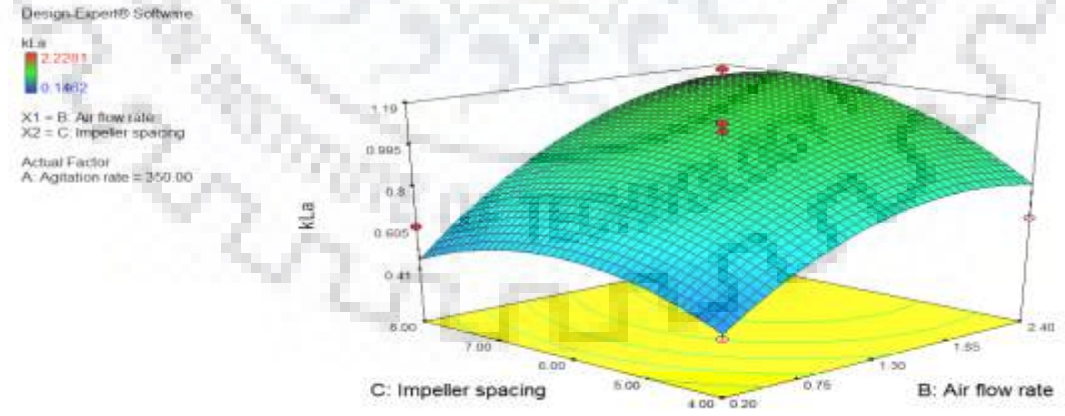


**(c)**

**Fig 5.10:** Dependece of $k_La$ for Rushton- Ruston Impeller combition on possible combination of (a) agitation rate and air flow rate, (b) agitation rate and impeller spacing, (c) air flow rate and impeller spacing

Optimum values of the three parameters were found using this data. Four different set of experiments will be carried out according to the process parameters laid out in Table 5.7 to understand the suitability of the developed model.

**Table 5.7:** Experimental range of variables studied during designing of experiments for Rushton-Rushton Impeller Combination

| Run No. | Agitation (RPM) | Aeration (vvm) | Impeller spacing (cm) | $k_La$,1/min. |
|---|---|---|---|---|
| Optimized | 600 | 1.91 | 6.61 | 2.18 |
| 6 | 600 | 0.2 | 6 | 1.77 |
| 1 | 350 | 0.2 | 6 | 0.6139 |
| 10 | 100 | 0.2 | 6 | 0.15 |

### 5.2.1.2 Rushton Impeller–Marine Propeller

The optimum conditions for maximum mass transfer coefficient were calculated in similar way for the combination of Rushton and marine impeller using Design Expert software version 7.0.0. Experimental data and result of mass transfer coefficient for the pair of Rushton impeller is given in Table 5.8. The degree of freedom evaluation is same as the case for Rushton- Rushton impeller combination. Table 5.9 represents the variance inflation factor (VIF) and Ri values for the model formed. The values shows the significance of the model formed

**Table 5.8:** Experimental data and results of BBD for mass transfer coefficient in case of Rushton Impeller -Marine Propeller combination

| Run | Factor 1 A: Agitation Rate RPM | Factor 2 B: Air Flow Rate vvm | Factor 3 C: Impeller Spacing cm | Mass Transfer Coefficient $k_La$ 1/min | |
|---|---|---|---|---|---|
| | | | | Experimental | Predicted |
| 1 | 100 | 1.3 | 8 | 0.6372 | 0.6195 |
| 2 | 100 | 1.3 | 4 | 0.7658 | 0.6037 |
| 3 | 350 | 2.4 | 4 | 1.4812 | 1.4693 |
| 4 | 350 | 1.3 | 6 | 1.1271 | 1.1375 |
| 5 | 600 | 0.2 | 6 | 1.8581 | 1.6841 |
| 6 | 350 | 1.3 | 6 | 1.0907 | 1.1375 |
| 7 | 100 | 0.2 | 6 | 0.1752 | 0.1811 |
| 8 | 350 | 2.4 | 8 | 1.2911 | 1.1349 |
| 9 | 600 | 1.3 | 8 | 1.3391 | 1.5012 |
| 10 | 350 | 1.3 | 6 | 1.1947 | 1.1375 |
| 11 | 100 | 2.4 | 6 | 0.9766 | 1.1506 |
| 12 | 350 | 0.2 | 8 | 0.5751 | 0.5871 |
| 13 | 350 | 0.2 | 6 | 0.6146 | 0.7796 |
| 14 | 600 | 1.3 | 4 | 2.0174 | 2.0352 |
| 15 | 600 | 2.4 | 6 | 1.9667 | 1.9609 |

**Table 5.9:** VIF and RI value for mass transfer coefficient model for Rushton Impeller - Marine Propeller system

| Term | Std Err** | VIF | Ri-Squared |
|---|---|---|---|
| A | 0.35 | 1 | 0 |
| B | 0.35 | 1 | 0 |
| C | 0.35 | 1 | 0 |
| AB | 0.5 | 1 | 0 |
| AC | 0.5 | 1 | 0 |
| BC | 0.5 | 1 | 0 |
| $A^2$ | 0.52 | 1.01 | 0.011 |
| $B^2$ | 0.52 | 1.01 | 0.011 |
| $C^2$ | 0.52 | 1.01 | 0.011 |

Ideal VIF is 1.0. Ideal Ri-squared is 0.0. A quadratic model using regression analysis was developed for this data.

**Final Equation in Terms of Coded Factors:**

$k_La$= +1.14+(0.58* A) +(0.31* B)-(0.13* C)-(0.17* A * B)-(0.14* A * C) -(0.038* B * C)

+(0.15* $A^2$ )-(0.046* $B^2$) – (0.10* $C^2$)

The statistical significance of this model was verified using the Fisher's test for the analysis of variance (ANOVA), which confirmed that the second-order polynomial function is a good fit for the experimental data. (Table 5.10)

**Table 5.10:** ANOVA for all the model terms for Rushton Impeller-Marine Propeller Combination

| **Source** | **Sum of Squares** | **Df** | **Mean Square** | **F Value** | **p-value Prob > F** |
|---|---|---|---|---|---|
| Model | 3.93 | 9 | 0.44 | 12.96 | 0.0058 |
| A-Agitation rate | *2.68* | *1* | *2.68* | *79.4* | *0.0003* |
| B-Air flow rate | *0.78* | *1* | *0.78* | *23.05* | *0.0049* |
| C-Impeller spacing | *0.13* | *1* | *0.13* | *3.99* | *0.1024* |
| AB | *0.12* | *1* | *0.12* | *3.56* | *0.1178* |
| AC | *0.076* | *1* | *0.076* | *2.24* | *0.1946* |
| BC | *5.67E-03* | *1* | *5.67E-03* | *0.17* | *0.6986* |
| $A^2$ | *0.086* | *1* | *0.086* | *2.57* | *0.1701* |
| $B^2$ | *7.94E-03* | *1* | *7.94E-03* | *0.24* | *0.648* |
| C*2* | *0.037* | *1* | *0.037* | *1.11* | *0.3404* |
| Residual | 0.17 | 5 | 0.034 | | |
| Lack of Fit | *0.16* | *3* | *0.054* | *19.5* | *0.0492* |
| Pure Error | *5.57E-03* | *2* | *2.79E-03* | | |
| Cor Total | 4.1 | 14 | | | |

The Model F-value of 12.96 implies the model is significant. Additional information about the accuracy of model is given in Table 5.11

**Tabe 5.11:** ANOVA Parameters of the second order model derived for Rushton Impeller-Marine Propeller Combination

| | |
|---|---|
| Std. Dev. | 0.18 |
| Mean | 1.14 |
| C.V. % | 16.09 |
| PRESS | 2.62 |
| R-Squared | 0.9589 |
| Adj R-Squared | 0.8849 |
| Adeq Precision | 12.37 |

"Adeq Precision" measures the signal to noise ratio. A ratio greater than 4 is desirable. The ratio of 12.370 for this experiment implies an adequate signal. This model can be thus be used to design experiments. Fig 5.11 denote a good agreement between predicted and experimental values

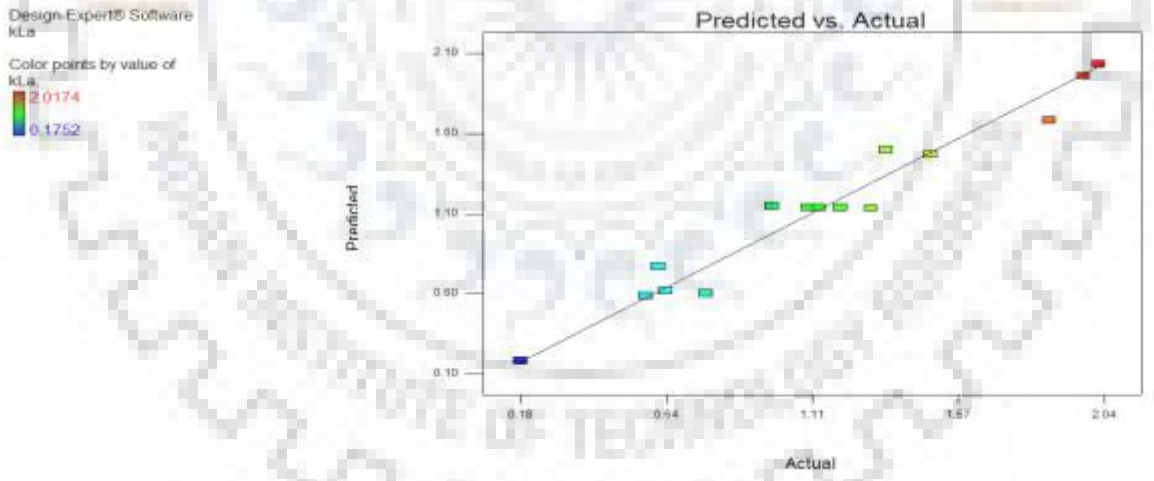


**Fig 5.11:** Relation between actual and predicted values for $k_La$ estimation of Rushton Impeller -Marine Propeller combination

As, can be seen from the second order polynomial correlation obtained for mass transfer coefficient, in case of Rushton- Marine Impeller combination Agitation Rate doesn't play a significant role. This fact is further illustrated by the reponse curves depicting the interaction between the three parameters as shown in Fig 5.12.

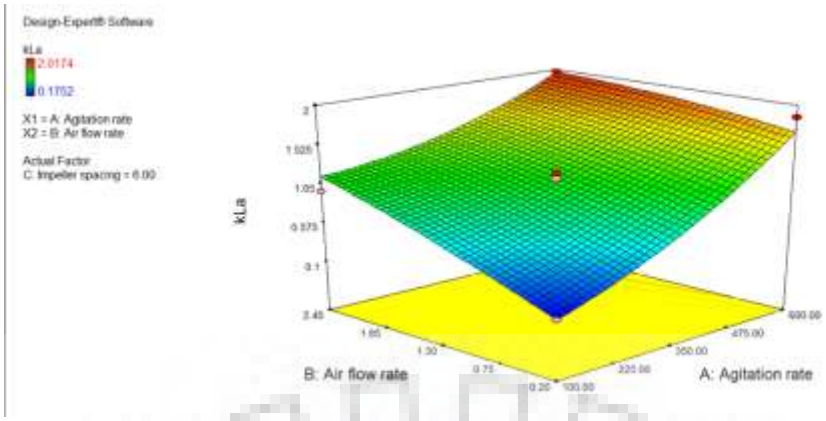


**(a)**

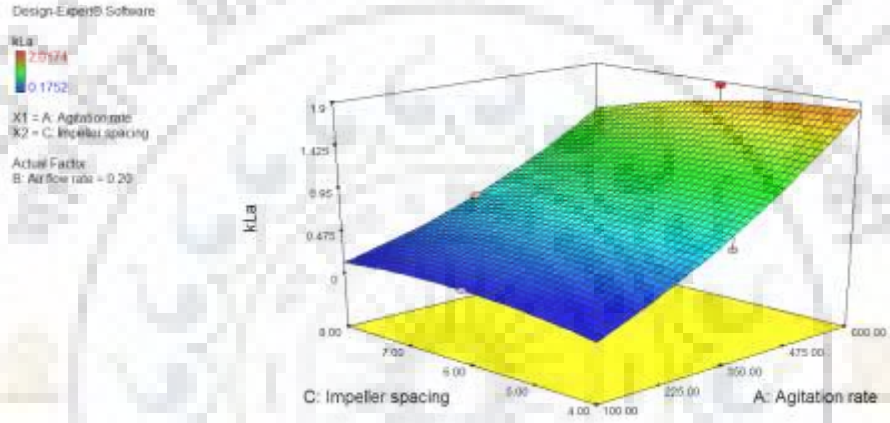


**(b)**

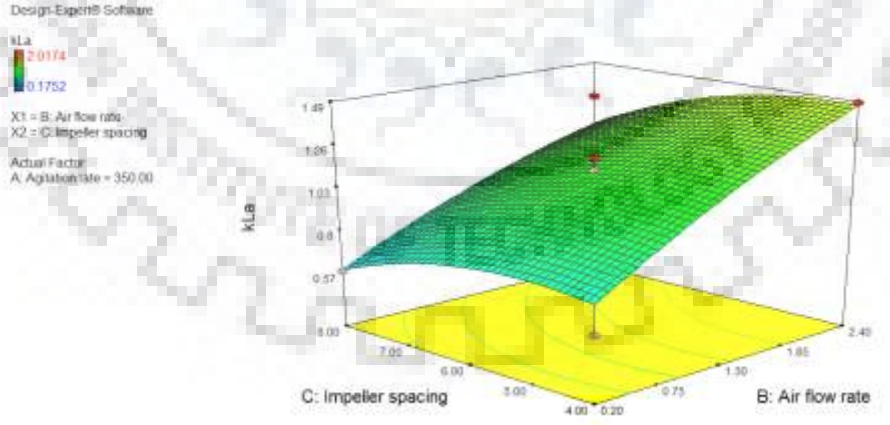


**(c )**

**Fig 5.12:** Dependece of $k_La$ for Rushton Impeller– Marine Propeller combination on possible combination of (a) agitation rate and air flow rate, (b) agitation rate and impeller spacing, (c) air flow rate and impeller spacing

In this case, Impeller spacing near 4 cm is considered better. As Impeller spacing is increased, the mass transfer coefficient is noticeably decreasing. In case of air flow rate, mass transfer is directly proportional to the flow rate. Optimum values of the three parameters A, B and C were found using this data. Four different batch fermentations were planned according to the process parameters laid out in Table 5.12 to understand the suitability of the proposed model.

**Table 5.12**: Experimental range of variables studied during designing of experiments for Rushton-Rushton Impeller Combination

| Run No. | Agitation (RPM) | Aeration (vvm) | Impeller spacing (cm) | $k_La$,1/min. |
|---|---|---|---|---|
| Optimized | 600 | 1.67 | 4.83 | 2.04 |
| 5 | 600 | 0.2 | 6 | 1.8581 |
| 10 | 350 | 0.2 | 6 | 0.7796 |
| 7 | 100 | 0.2 | 6 | 0.1752 |

### 5.2.2 Growth Curves for E.coli BL21

According to the standard procedure, strain of E.coli BL21 was inoculated in a flask at 37ºC with shaker at 180 rpm. The Optical Density was measured at regular intervals. The curve obtained is given in Fig 5.13. As can be clearly seen from the growth curve, E.coli BL21 is in lag phase till 2hrs after the incubation time. Exponential Phase last till 10 hr when the bacteria grows at a constant rate. After that it reaches stationary phase. Death Phase could be seen to occur after 12-14 hrs. So it will give maximum biomass concentration at approximately 8-10 hr run time of the bioreactor. The designed experiments will be conducted till 12 hrs due to the same reason.

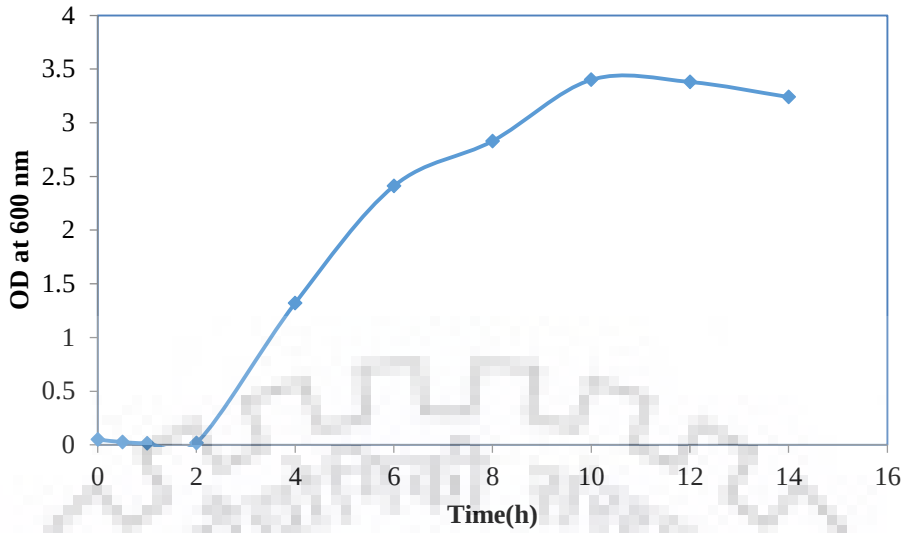


**Fig 5.13**: Growth Curve for Ecoli BL21

### 5.2.3 Rheological Properties of E.coli BL21

The Experiments on the bioreactor for E.coli BL21 could only be performed for Rushton-Rushton Impeller combination. The parameters used were derived from RSM Study as mentioned in Table 6. The first set of experiments were conducted for Agitation rate = 100 rpm, Air Flow Rate = 1LPM and Impeller Spacing = 6 cm. The Viscosity change according to the time of the sample taken from the bioreactor are represented in Fig 5.14. E.coli Viscosity is recorded highest when the inoculum was just added to the bioreactor i.e at 0h because it was in concentrated form. As the time progresses the 250 ml inoculum is equally distributed in the 5 litres of volume and after a certain period of time, viscosity reaches almost constant value. Viscosity Behaviour exhibited by EColi culture is Newtonian. The viscosity pattern observed in Fig 5.14 can be correlated to the optical density measurements for the the same interval of time in Fig 5.15.

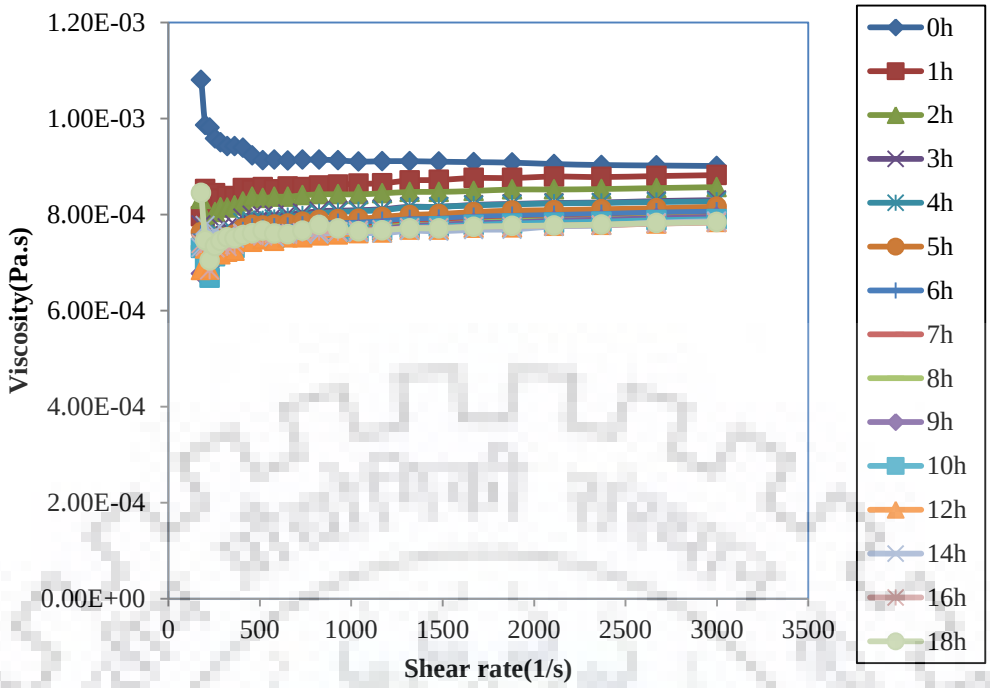


**Fig 5.14:** Viscosity variation with time for E.coli BL21 for A= 100 rpm, B= 1 LPM and C= 6cm

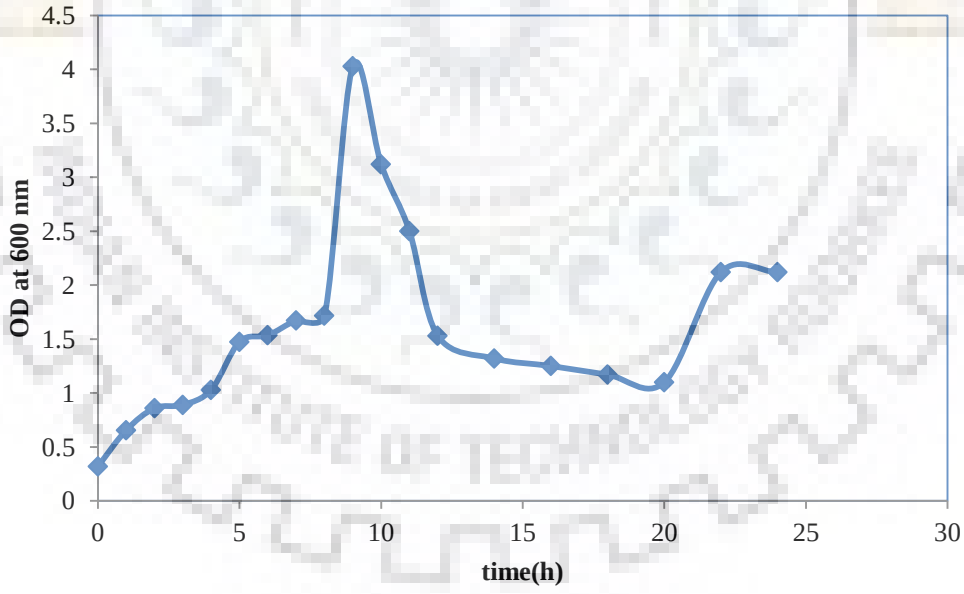


**Fig 5.15:** Optical density curve vs time for E.coli BL21 for A= 100 rpm, B= 1 LPM and C= 6cm

Dynamic Viscosity readings were also taken for the sample at different sample collection time to study the viscoelastic properties of the culture. The storage modus, loss modulus and

complex viscosity variation with time is represented in Fig 5.16, 5.17 and 5.18 respectively. Loss Modulus curve is hard to explain since it does not follow a pattern. Although it is smilar to the one exhibited by water. It implies the less significant rigid behaviour of the EColi culture. Storage Modulus on the other hand which implies storage of deformation energy is clearly highest at the start and decreases till 4 hr and then increases till 12 hr and then shows a decline again. This reflect the pattern of biomass concentration for these samples. Complex Viscosity also shows similar behaviour although it is seen to be lowest for 9hr and highest for 1 and 2hr samples.

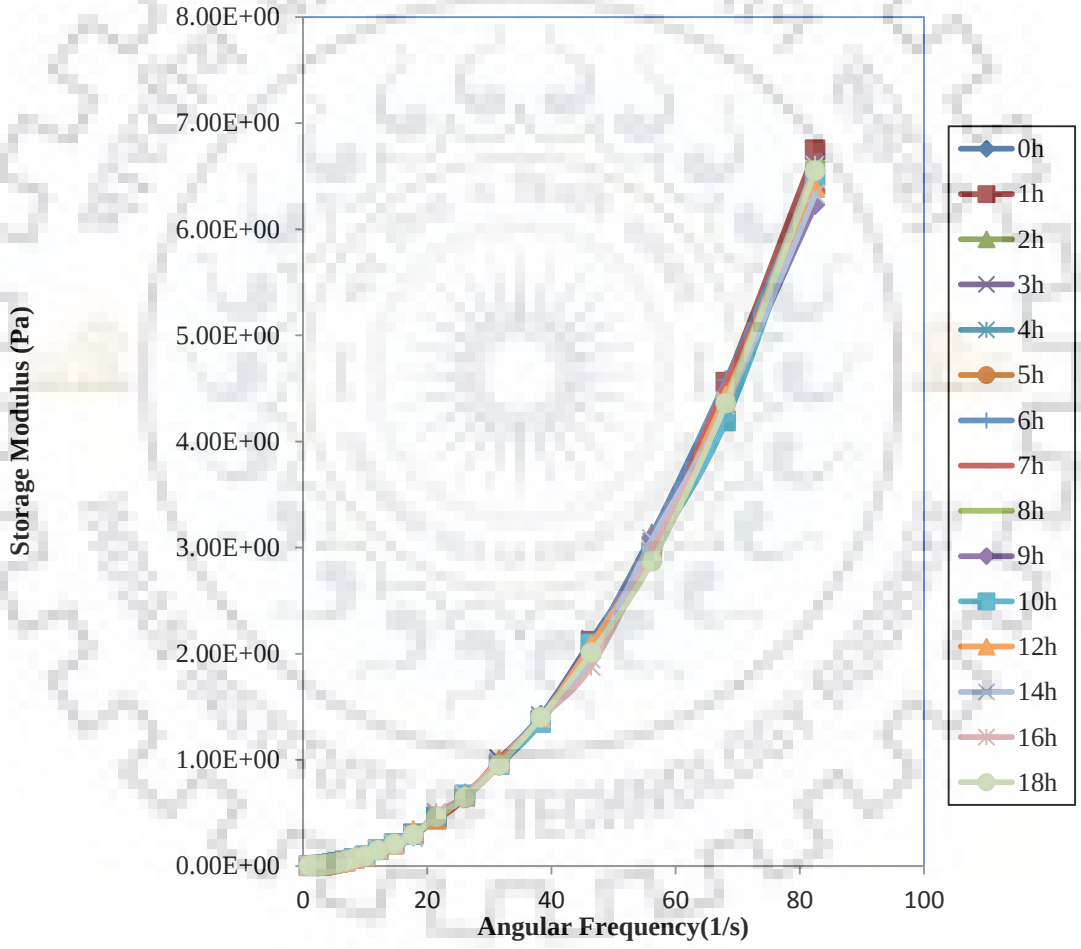


**Fig 5.16:** Storage Modulus vs angular Frequency curve for Ecoli culture for A= 100 rpm, B= 1 LPM and C= 6cm for sample collected at regular time interval.

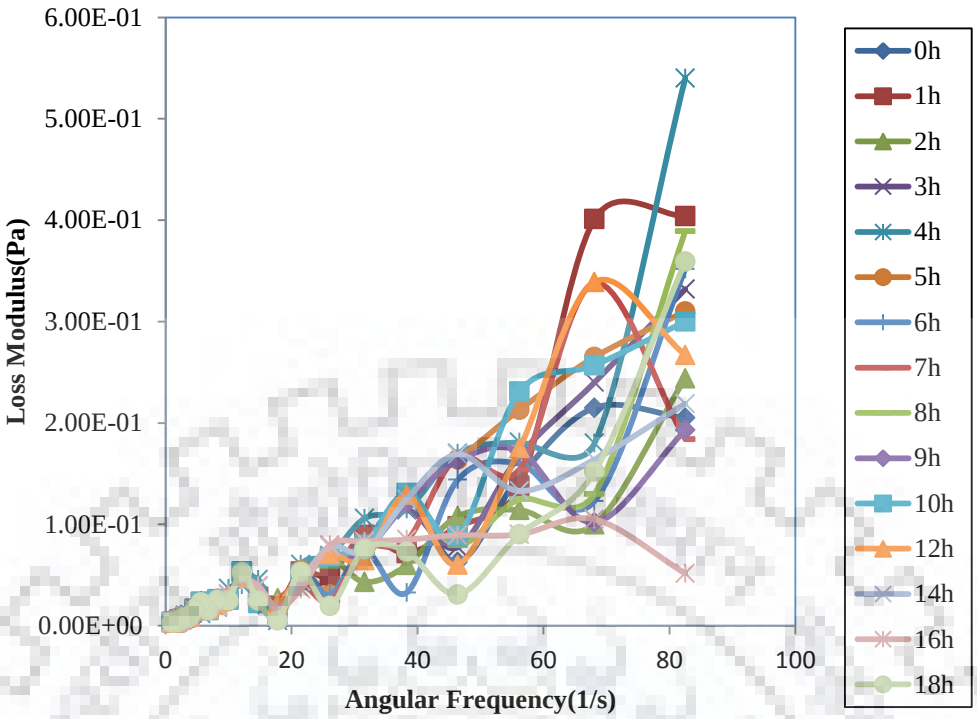


**Fig 5.17:** Loss Modulus vs angular Frequency curve for E.coli culture for A= 100 rpm, B= 1 LPM and C= 6cm for sample collected at regular time interval.

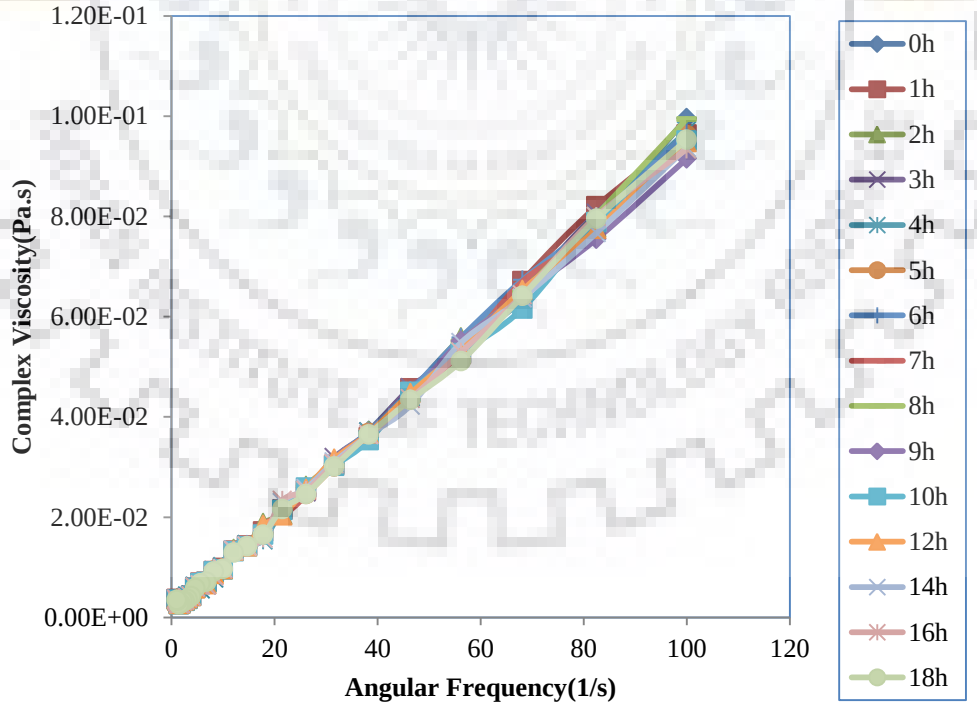


**Fig 5.18:** Complex vs angular Frequency curve for Ecoli culture for A= 100 rpm, B= 1 LPM and C= 6cm for sample collected at regular time interval

The second set of experiments were conducted for Agitation rate = 350 rpm, Air Flow Rate = 1LPM and Impeller Spacing = 6 cm. The Viscosity change according to the time of the sample taken from the bioreactor are represented in Fig 5.19. Similar pattern to the one in previous case is obtained. The two cases can be studied by comparing their optical density vs time curve (Fig 5.20). The highest biomass concentration obtained was 1.4 g/l. It can be clearly seen that biomass concentration is higher in case of second case which can be explained by a more effective mixing due to the higher agitation rate in case 2. Similar Dynamic Rheological measurements were done for this case as well to study Storage modulus, loss modulus and complex viscosity changes vs time (Fig 5.21, Fig 5.22, Fig 5.23). The results are similar to case 1. Unfortunately, other two set of experiments for Rushton-Rushton combination of Impeller could not be conducted since at 600 rpm there is excessive foaming which could not be controlled by the available antifoaming agents.

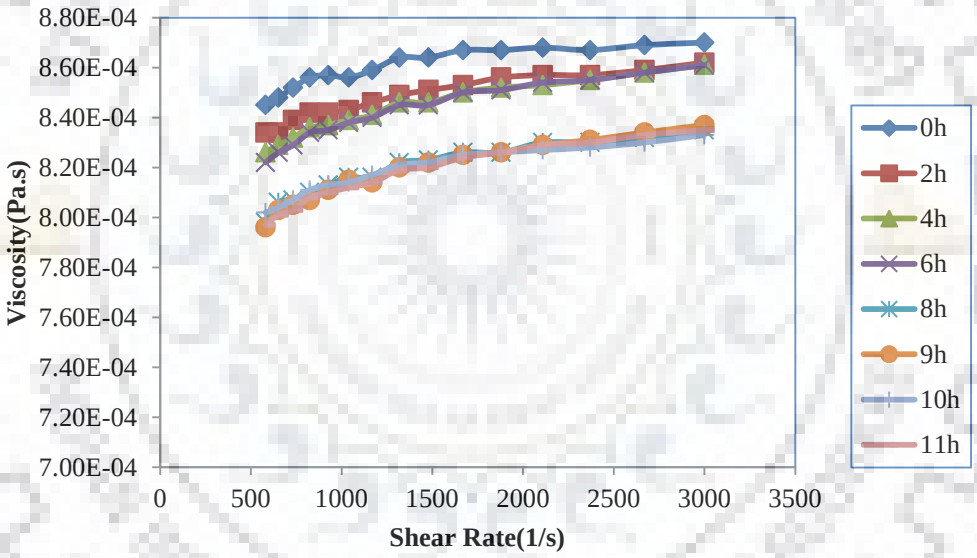


**Fig 5.19:** Viscosity variation with time for E.coli BL21 for A= 350 rpm, B= 1 LPM and C= 6cm.

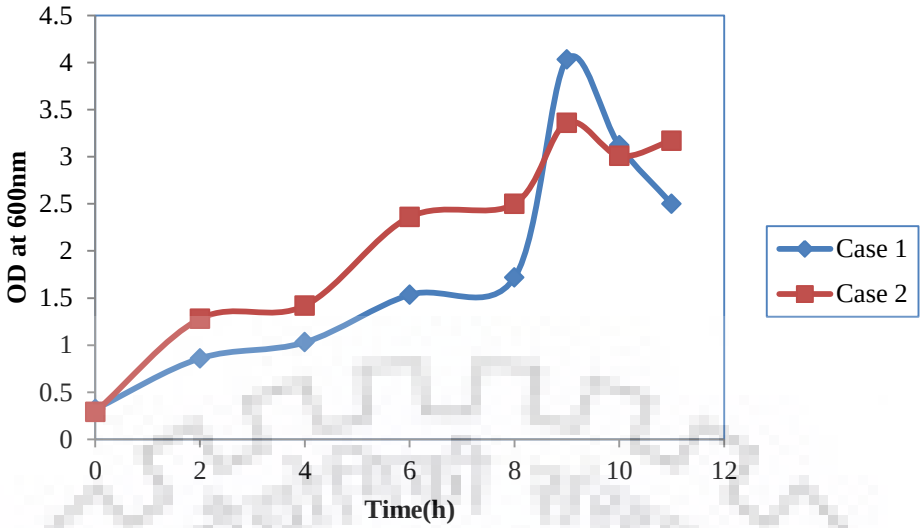


**Fig 5.20:** Optical Density curves for Case 1: A= 100 rpm, B= 1 LPM and C= 6cm And Case 2: A= 350 rpm, B= 1 LPM and C= 6cm.

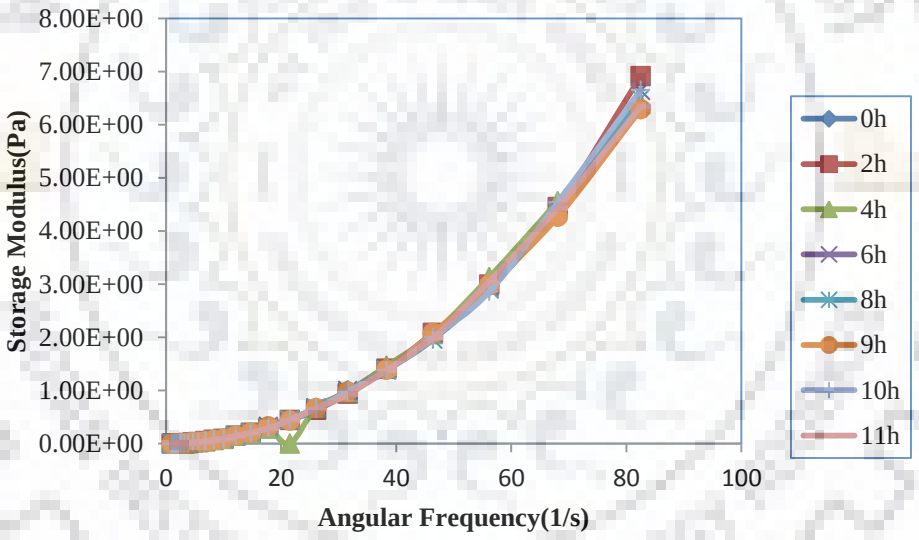


**Fig 5.21:** Storage Modulus vs angular Frequency curve for E.coli culture for A= 350 rpm, B= 1 LPM and C= 6cm for sample collected at regular time interval.

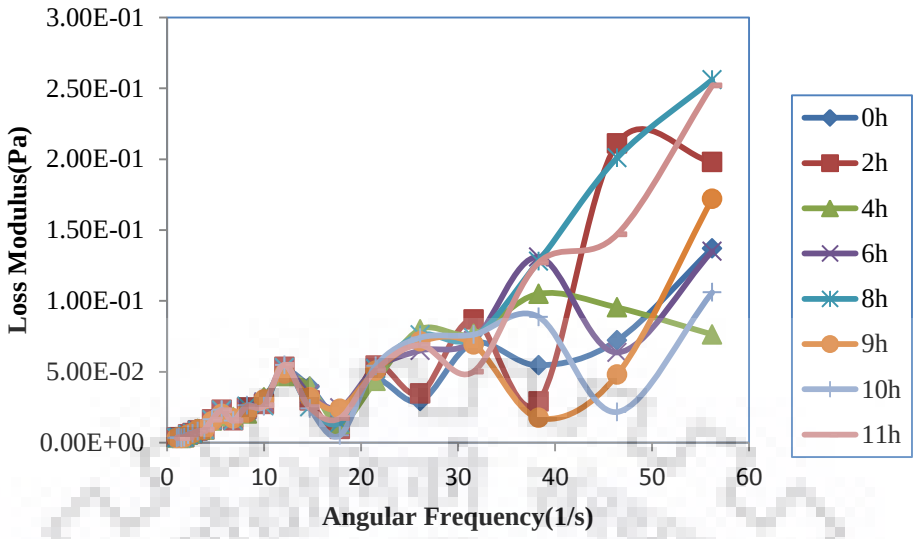


**Fig 5.22:** Loss Modulus vs angular Frequency curve for E.coli culture for A= 350 rpm, B= 1 LPM and C= 6cm for sample collected at regular time interval.

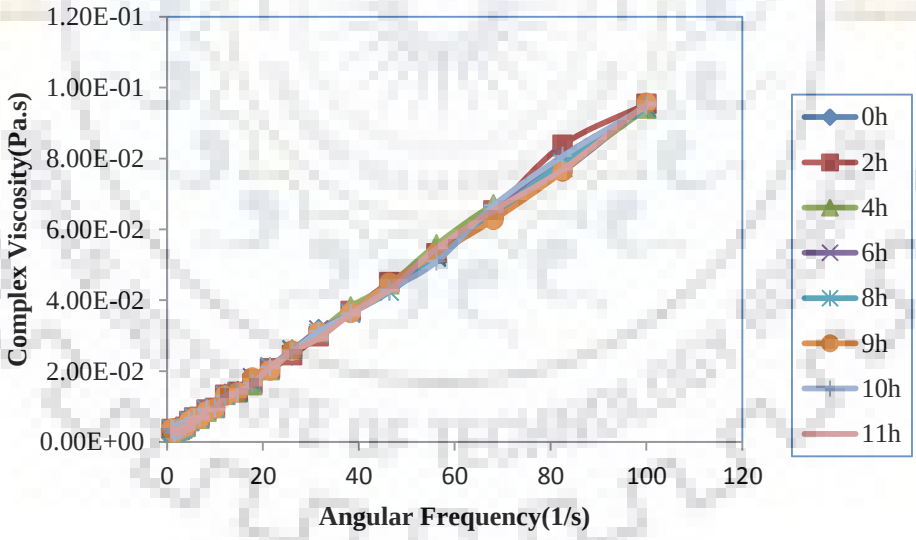


**Fig 5.23:** Complex Viscosity vs angular Frequency curve for E.coli culture for A= 350 rpm, B= 1 LPM and C= 6cm for sample collected at regular time interval.

## 5.3 *Botryococcus braunii (algae)*

For the *Botryococcus braunii*, Rheological measurements were first done for the inoculum at four different biomass concentrations. The culture is Newtonian as can be clearly seen by the linear Stress vs strain curve in Fig 5.25. For the highest concentration, the dynamic rheology is calculated as seen in Fig. 5.26. The inoculum is processed in a photobioreactor in the presence of air. The samples are taken at 8 hrs interval till the growth is stopped. It can be clearly noted from Fig 5.27 that viscosity is highest at 0h due to the addition of high concentration of inoculum which will then be mixed in the volume equally. The viscosity then decreases till 56 h. But will show increase again after that showing appreciable biomass formation as the time increases. Increasing biomass concentration with time can be validated by the optical density measurements in Fig 5.28. Dynamic Rheology measurements of this algae culture also yields similar results as E.coli (Fig 5.29, Fig 5.30, Fig 5.31). They signify the viscoelastic nature of the culture and less solid like properties.

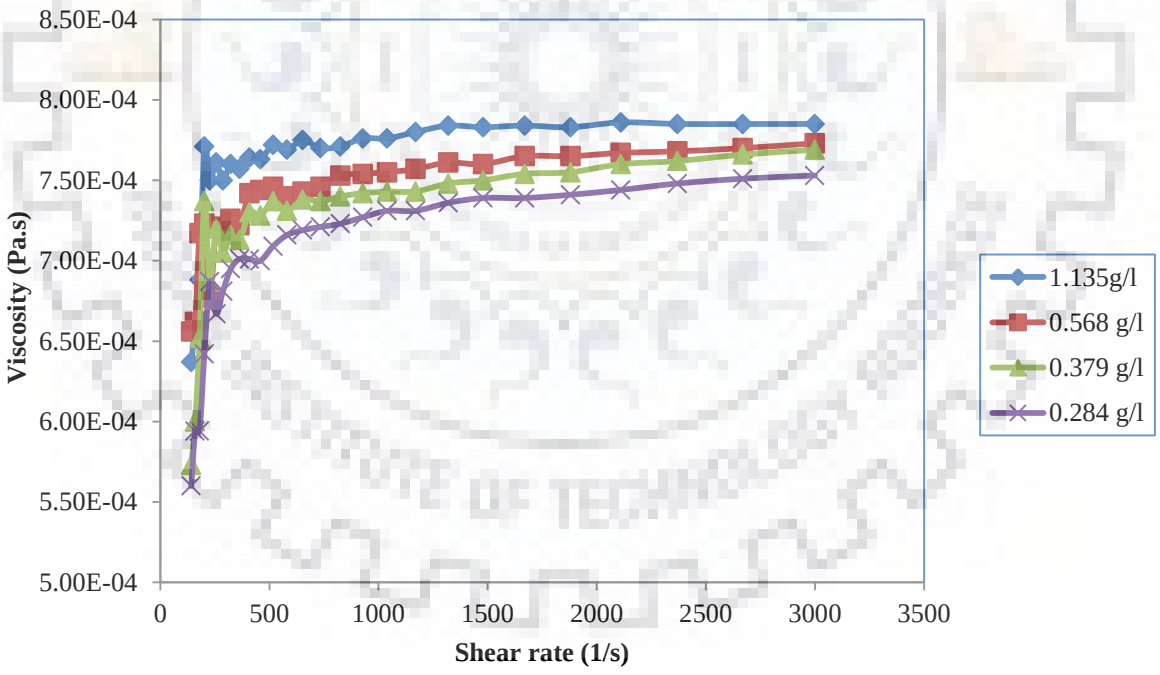


**Fig 5.24:** Viscosity vs shear rate curve for *Botryococcus braunii* at different concentration of biomass.

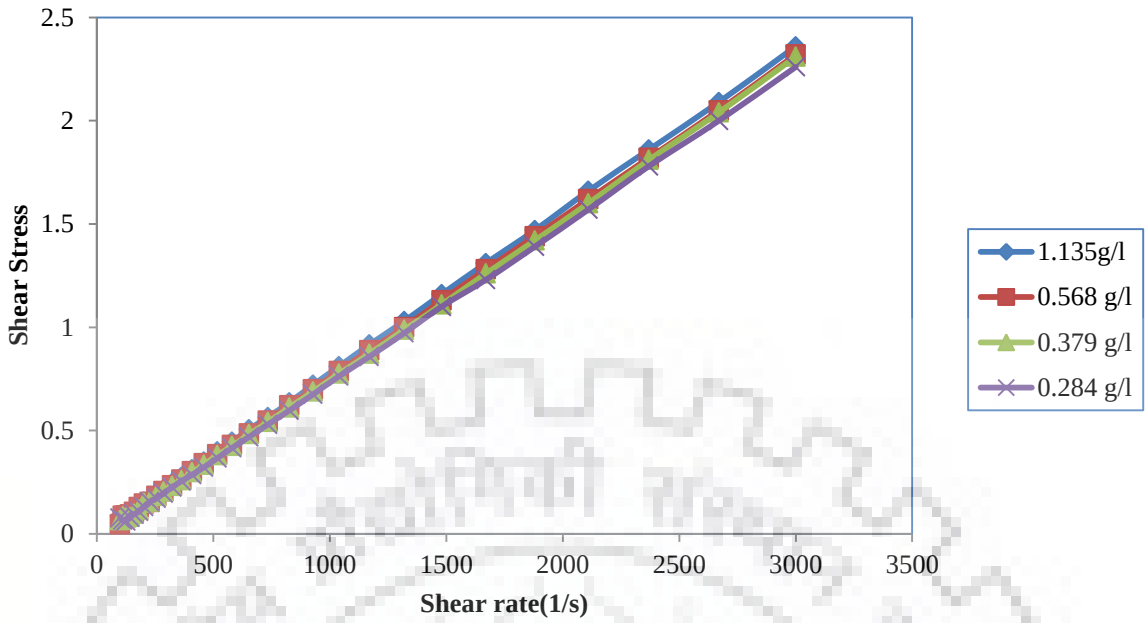


**Fig 5.25:** Shear stress vs Strain curve for *Botryococcus braunii* at different concentration of biomass

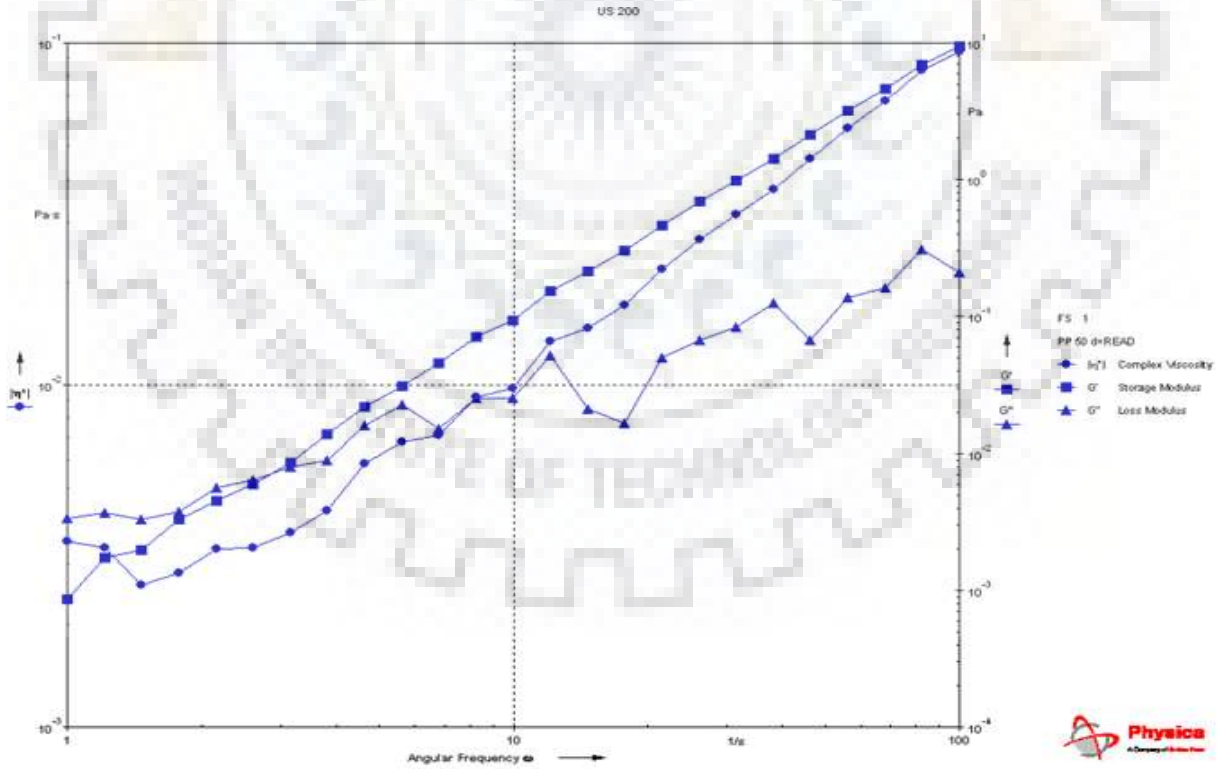


**Fig 5.26 :** Dynamic rheology of inoculum of *Botryococcus braunii*

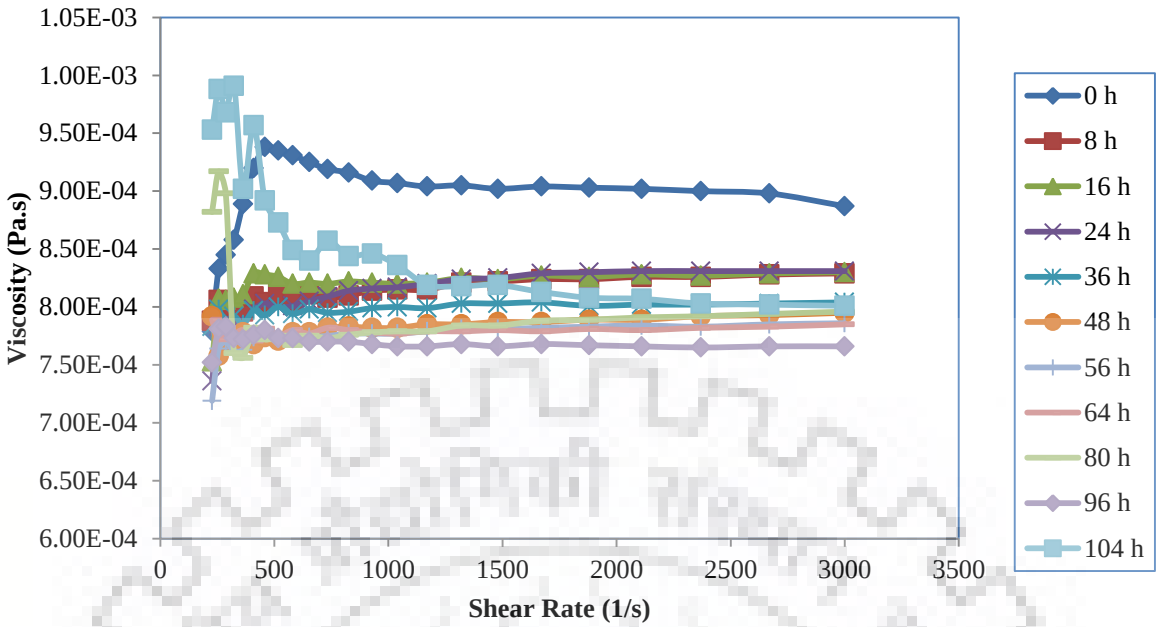


**Fig 5.27:** Viscosity curves for samples taken at regular time intervals during the fermentation of *Botryococcus braunii*

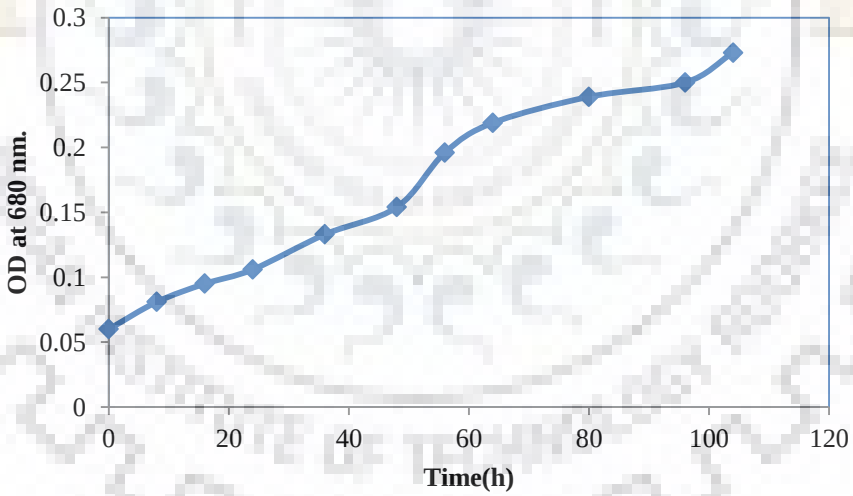


**Fig 5.28:** OD vs time for *Botryococcus braunii* fermented in a3 L photobioreactor

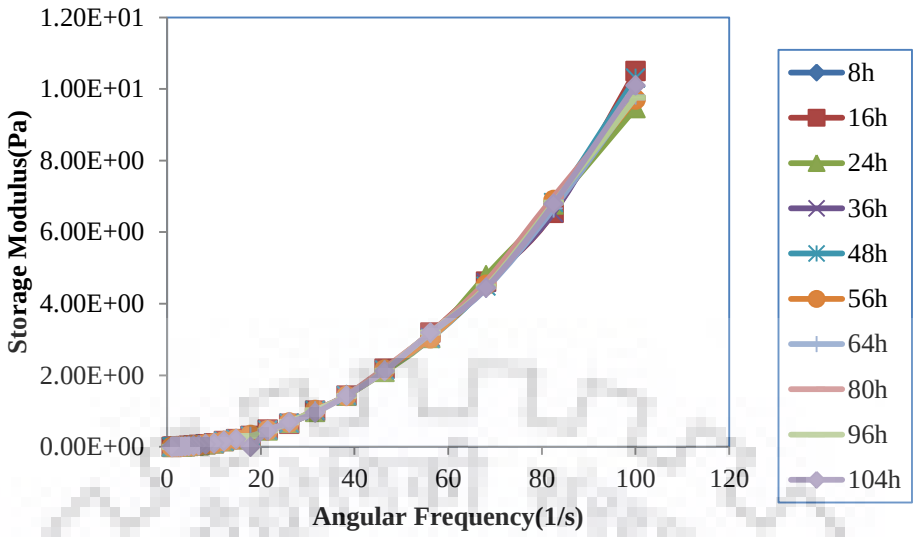


**Fig 5.29:** Storage Modulus vs angular Frequency curve for *Botryococcus braunii*

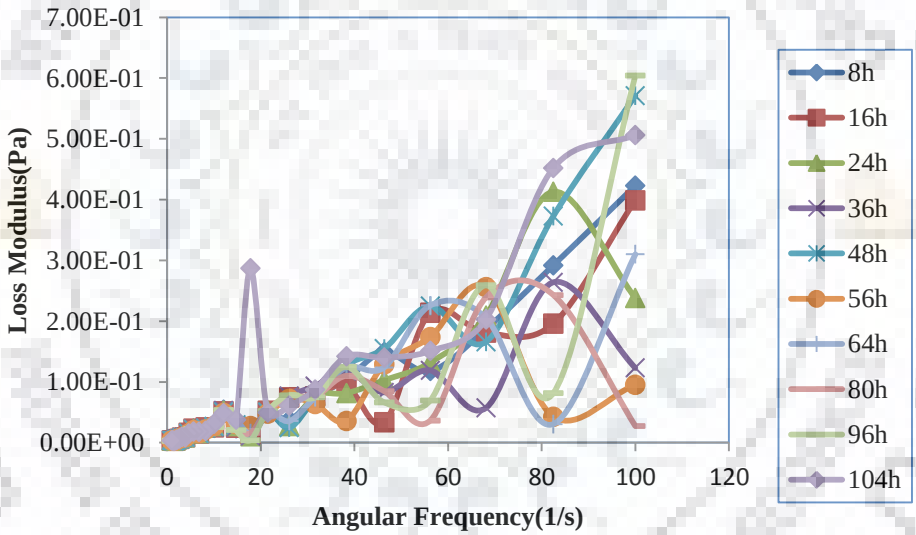


**Fig 5.30:** Loss Modulus vs angular Frequency curve for *Botryococcus braunii*

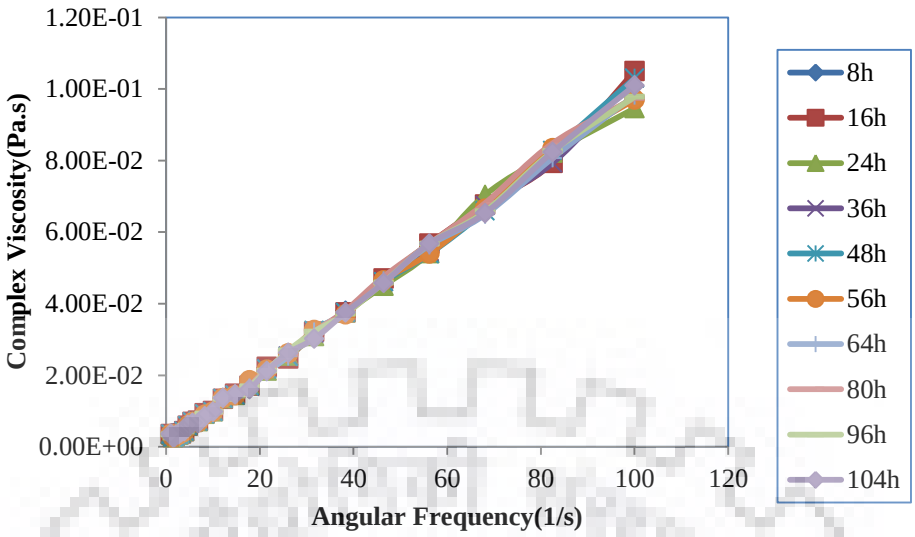


**Fig 5.31:** Complex Viscosity vs angular Frequency curve for *Botryococcus braunii*

Concentration was varied for algae suspension and oscillatory measurements were performed. Figure 5.32 shows a plot of the complex viscosity against concentration at frequency 100 Hz. η* for any given volume fraction is inversely proportional to frequency. The complex viscosity can be seen to be directly proportional to volume fraction.

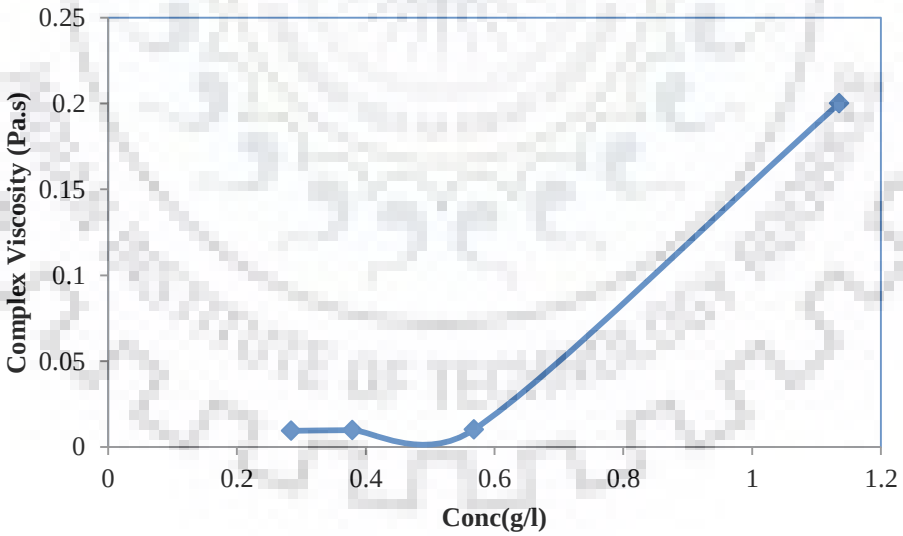


**Fig 5.32:** Complex Viscosity variation with biomass concentration for *Botryococcus braunii*

## 5.4 *Pichia stiptis* (Yeast)

*Pichia stiptis* is usually used in bioethanol production. It was grown in the reactor at 150 rpm and 30ºC. The sample was taken at regular intervals to measure the optical density and compute the rheology. Correlation factor for *Pichia stiptis* was 2.9665. Thus Conc vs time curve for the samples collected from the bioreactor is given in Fig 5.33. The highest biomass concentration obtained (9.14 g/l) in this case is comparatively higher than E.coli and Alagae case which can be verified from the literature as well. The viscosity readings were also taken for these samples and are illustrated in Fig 5.34. The behaviour here can also be considered Newtonian. Dynamic Rheology measurements for *Pichia stiptis* are given in Fig 5.35, Fig 5.36 and Fig 5.37. The curves obtained are similar to previous cases.

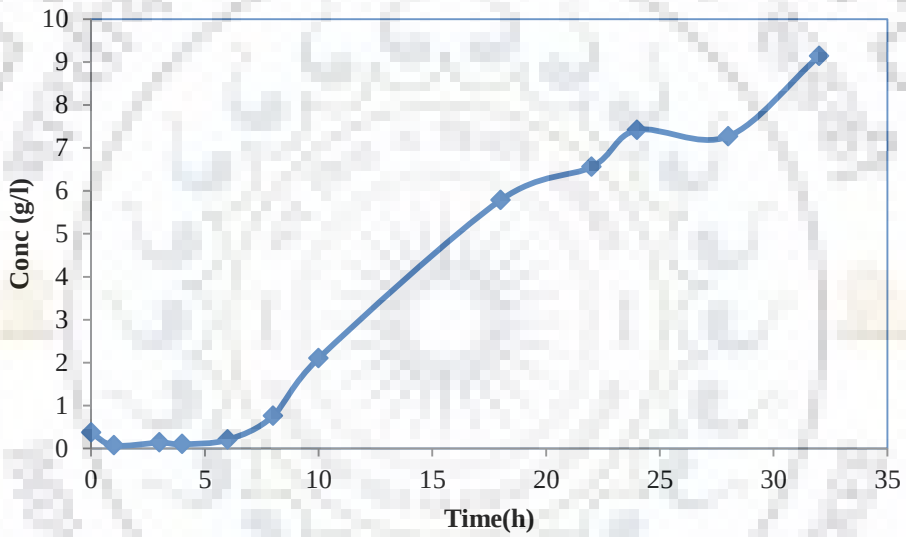


**Fig 5.33:** Concentration vs time curve for *Pichia stiptis* sample collected at different time from the reactor

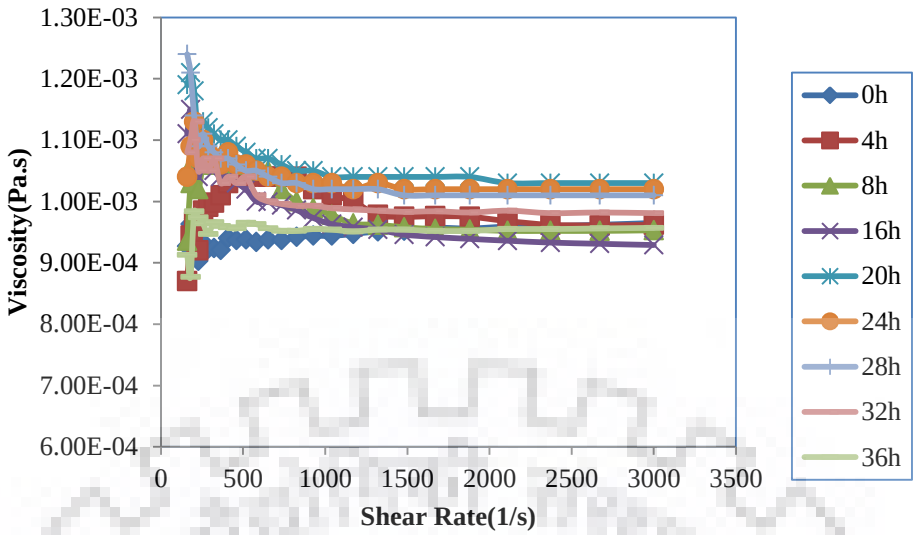


**Fig 5.34:** Viscosity curves for *Pichia stiptis* for samples collected at different time during the fermentation

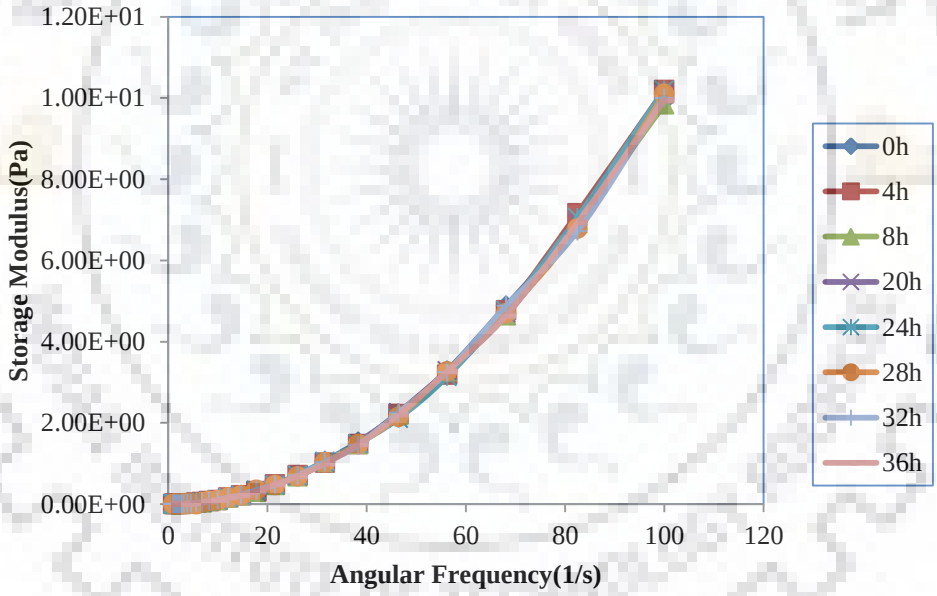


**Fig 5.35:** Storage Modulus vs angular Frequency curve for *Pichia stiptis*

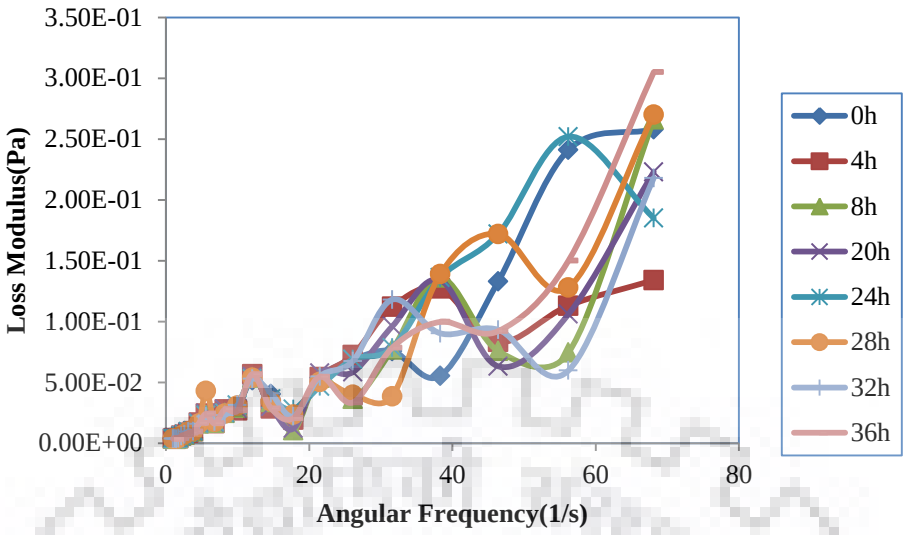


**Fig 5.36:** Loss Modulus vs angular Frequency curve for *Pichia stiptis*

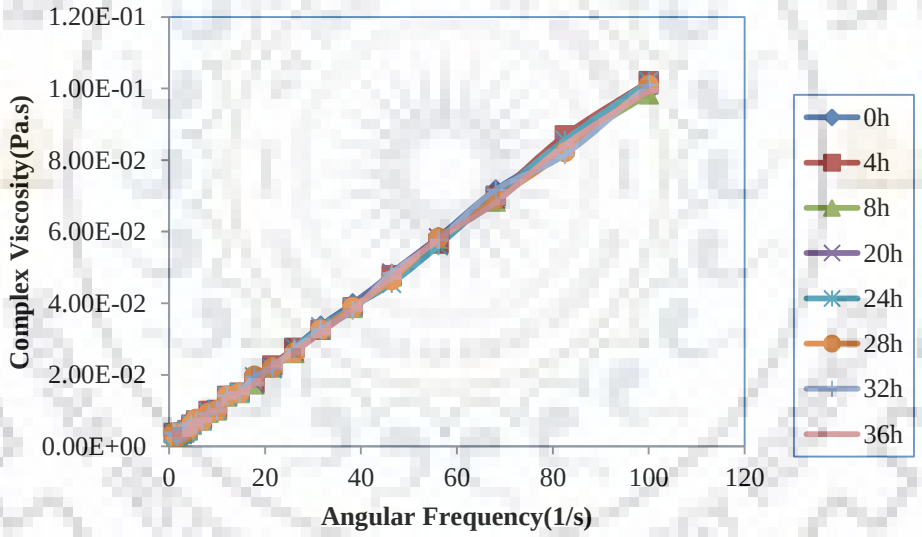


**Fig 5.37:** Complex Viscosity vs angular Frequency curve for *Pichia stiptis*

## 5.5 CFD model of a bioreactor

### 5.5.1 Geometry and Mesh

The geometry constructed in Gambit using the dimensions mentioned in Section 4.5 is given in Fig 5.38. The completely meshed Geometry is presented in Fig 5.39.

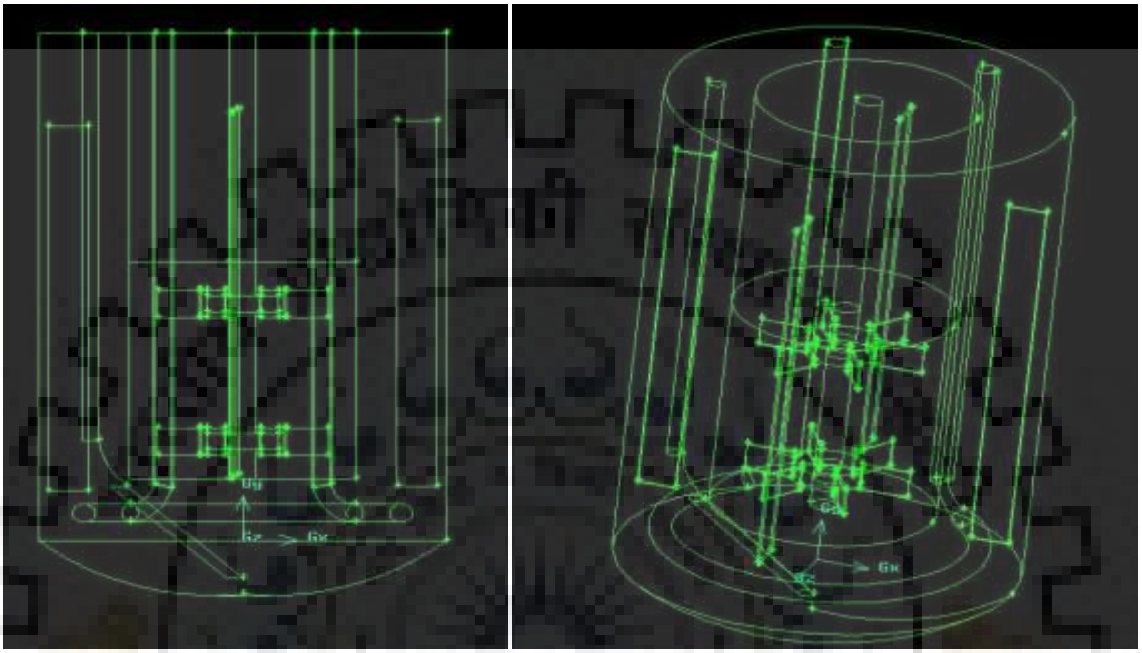

**(a)** **(b)**

**Fig 5.38:** Geometry of the bioreactor in (a) front view, (b) 3D view.

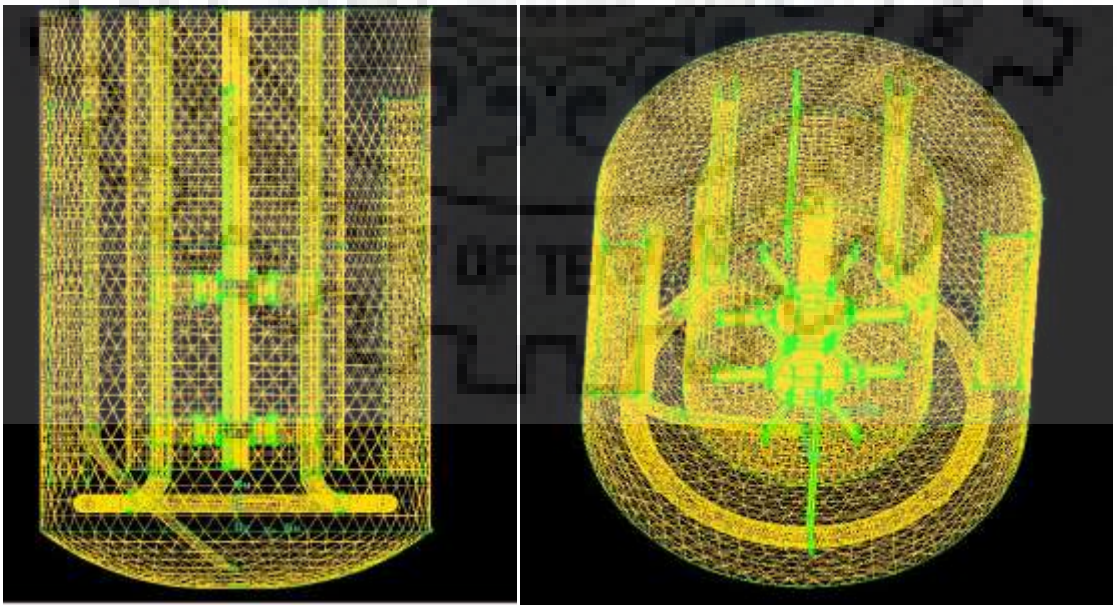

**(a)** **(b)**

**Fig 5.39:** Meshed Geometry of the bioreactor in (a) Front view, (b) 3D view

### 5.5.2 Flow Patterns

The velocity vector profile of the flow of the Newtonian Cultures having viscosity similar to water is shown in Fig 5.40

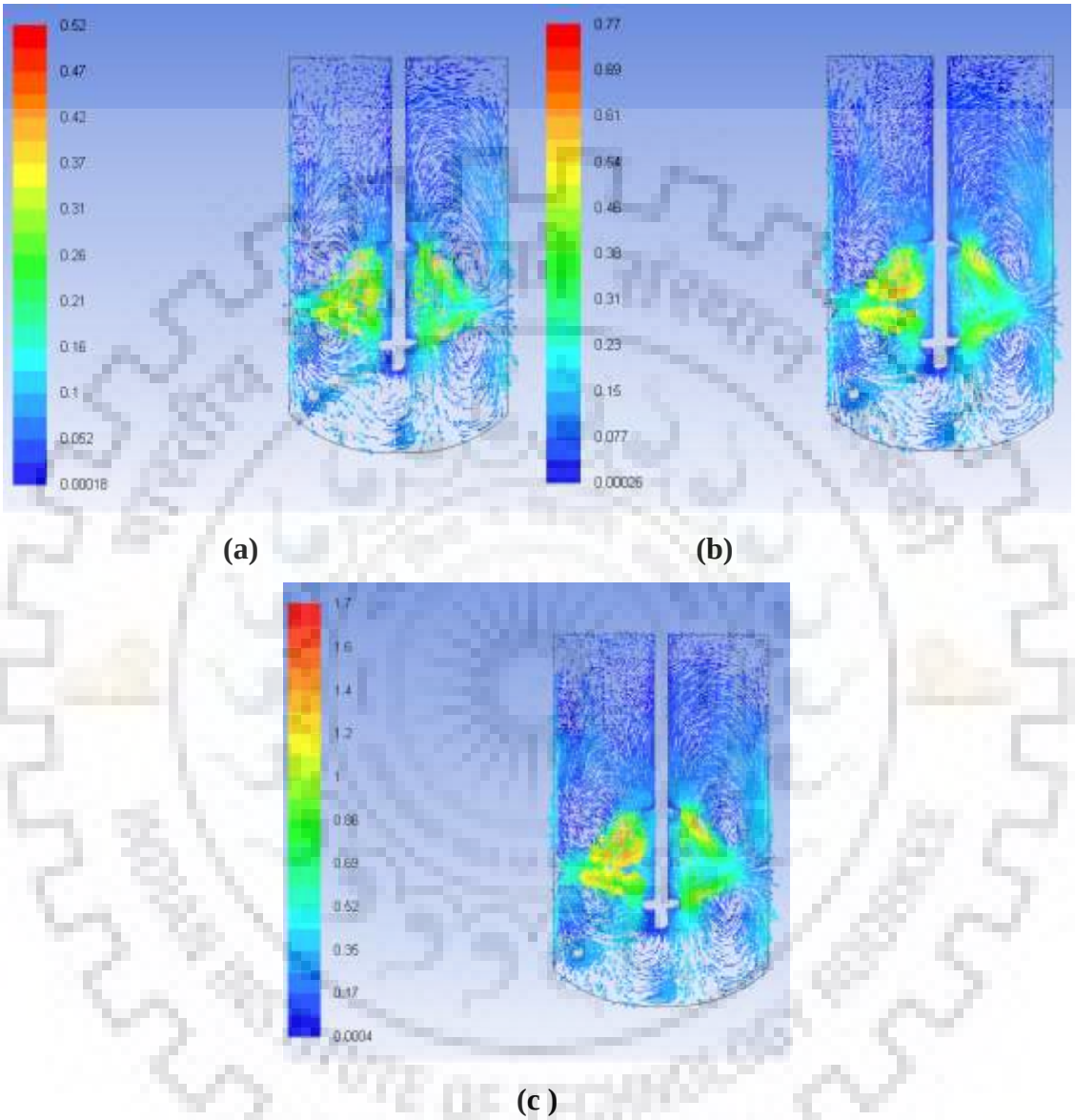


**Fig 5.40:** Velocity vector profile for (a) E.coli BL21 at 100 rpm, (b) *Pichia steptis* at 150 rpm and (c) E.coli BL21 at 350 rpm

The flow fields induced are shown in a vertical cross-sectional plane. The flow rate is maximum near the impellers.The field swept by the turbine blades has a very high velocity field. Moreover, tangential flow is set up because of the rotation of the volume of the fluid located between blades. As we move away from the impeller the flow decreases both in horizontal and vertical direction. Velocity is found to be maximum near the end of the blades.

The presence of two impellers has resulted in better mixing as can be seen from the profile. The velocity is high in the space between the impellers and the flow can be seen as forming a circular profile around the two impellers. The formation of recirculation loops between the two impellers can be clearly seen. Similar profiles are formed for *P. tricornutum* which has twice the viscosity of water. The simulation is done for different agitation rates. (Fig 5.41). Similarly, velocity profile for the fungus *Beauveria bassiana* was also obtained. It is a Non-Newtonian culture with power index n= 0.4221. (Fig 5.42)

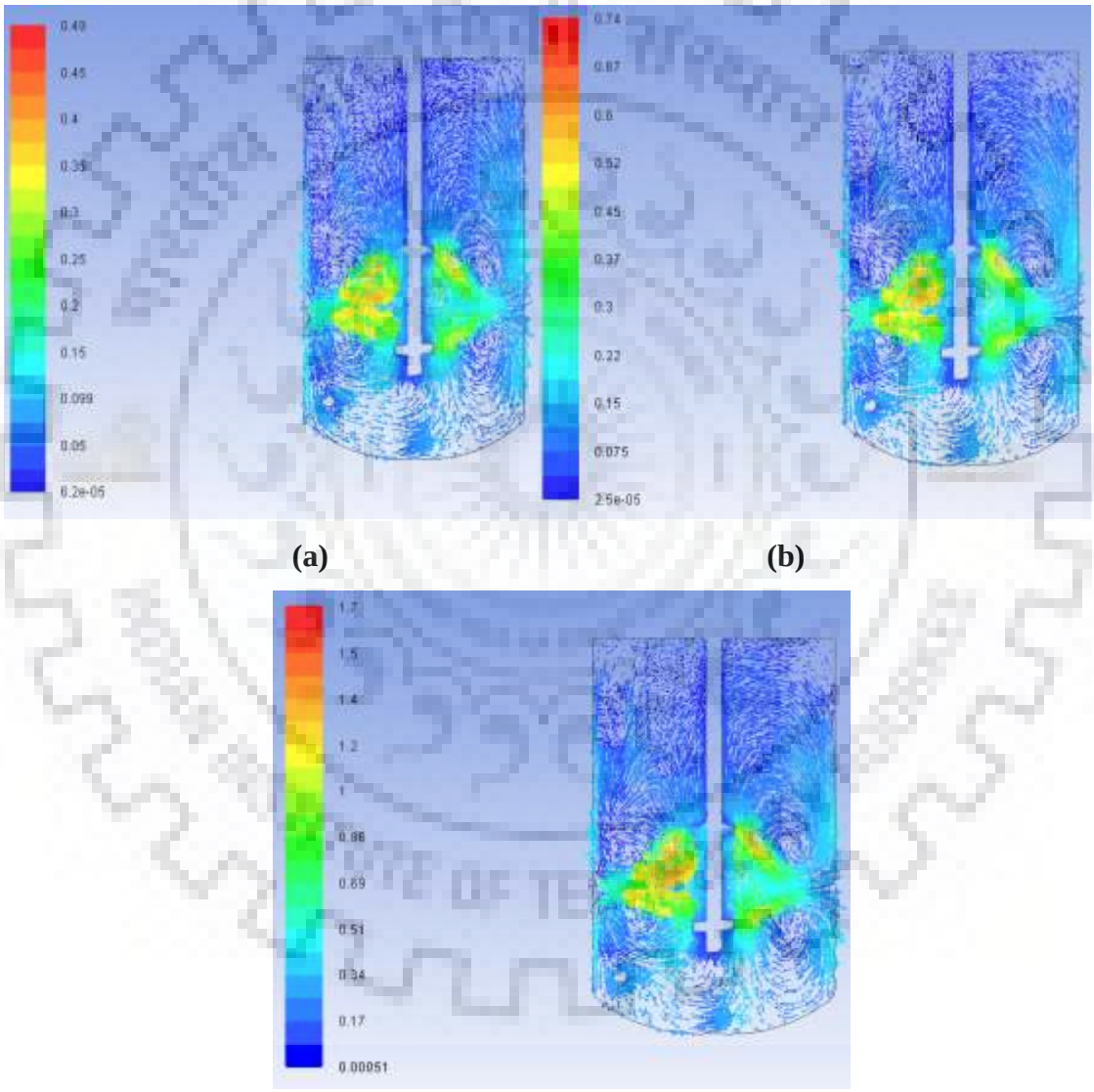


**Fig 5.41:** Velocity Vector Profile for algae *P. tricornutum* at agitation rate (a) 100 rpm, (b) 150 rpm, (c) 350 rpm.

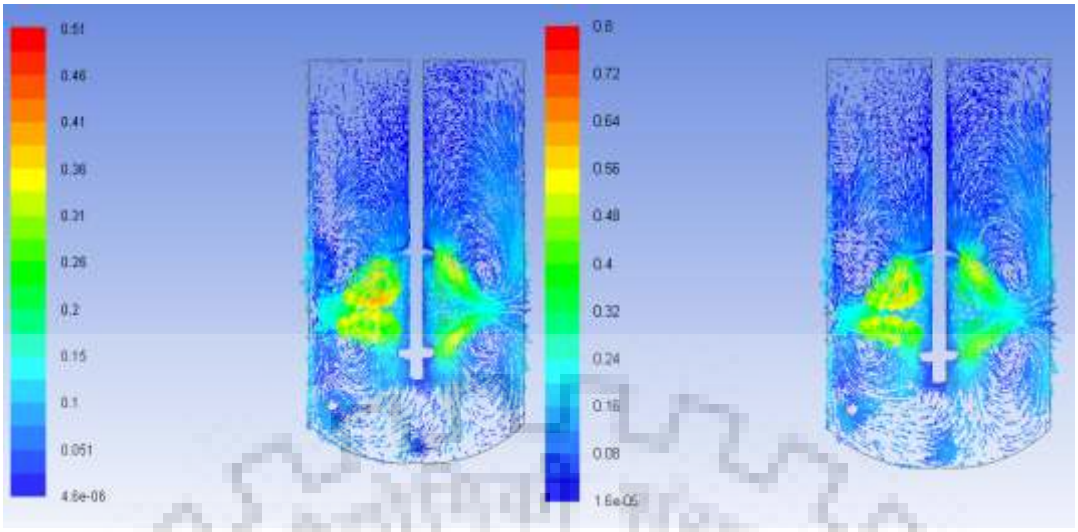


**(a)** **(b)**

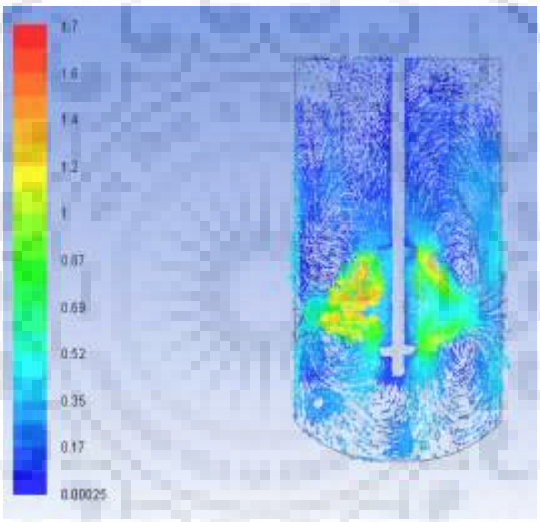


**(c)**

**Fig 5.42:** Velocity Vector Profile for Fungus *Beauveria bassiana* at agitation rate (a) 100 rpm, (b) 150 rpm, (c) 350 rpm.

The viscosity change does not seem to have prominent effect on the velocity profile. It can be clearly visualized by comparing the flow pattern of water, *P. tricornutum* and *Beauveria bassiana* at 600 rpm agitation speed (Fig 5.43).

Tip speed = ∏nd where n is Agitation rate and d is diameter of impeller

The non-dependency of tip speed on viscosity can be seen from Table 5.13

The empirical and CFD data for Tip speed are in agreement with each other

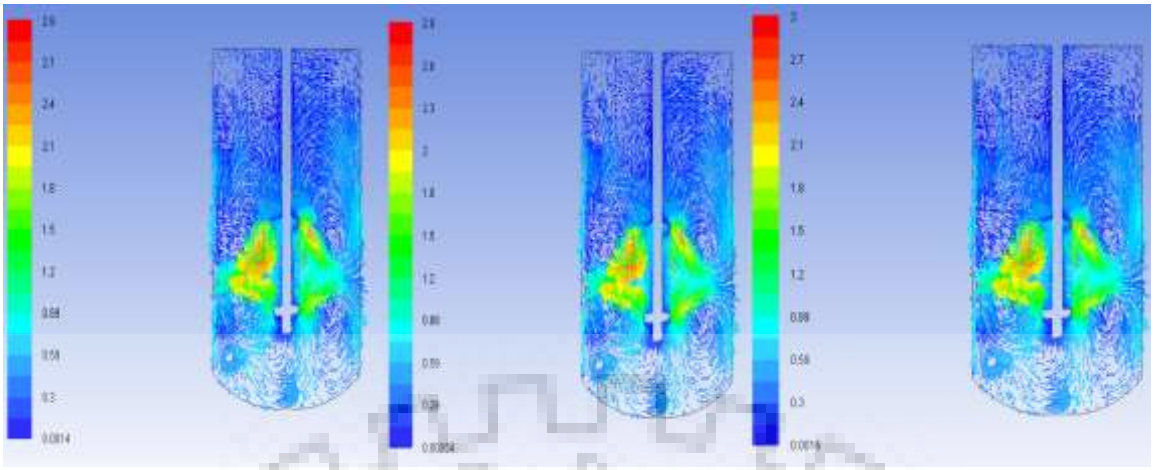

**(a)** **(b)** **(c)**

**Fig 5.43:** Velocity Profile at 600 rpm for (a) water, (b) *P. tricornutum* and (c) *Beauveria bassiana*

**Table 5.13**: Tip Speed values for different fluids used in CFD study

| **Culture** | **Agitation rate** | **Tip Speed m/s (CFD)** | **Tip Speed m/s (Empirical)** |
|---|---|---|---|
| Ecoli Bl21 | 100 RPM | 0.309 | 0.287 |
| *Pichia stiptis* | 150 RPM | 0.47 | 0.466 |
| Ecoli Bl21 | 350 RPM | 1.1 | 1.088 |
| Water | 600 RPM | 1.89 | 1.866 |
| *P. tricornutum* | 100 RPM | 0.3 | 0.287 |
| *P. tricornutum* | 150 RPM | 0.456 | 0.466 |
| *P. tricornutum* | 350 RPM | 1.1 | 1.088 |
| *P. tricornutum* | 600 RPM | 1.9 | 1.866 |
| *Beauveria bassiana* | 100 RPM | 0.31 | 0.287 |
| *Beauveria bassiana* | 150 RPM | 0.46 | 0.466 |
| *Beauveria bassiana* | 350 RPM | 1.1 | 1.088 |
| *Beauveria bassiana* | 600 RPM | 1.9 | 1.866 |

### 5.5.3 Distribution of Turbulent Kinetic energy

Kinetic energy profile is obtained for Newtonian and Non- Newtonian fluid was also obtained. However, Kinetic energy can be seen to be increasing with agitation rate and a better profile is obtained at higher agitation rate. Fig 5.44 show kinetic energy profile of *P. tricornutum* at different agitation rate

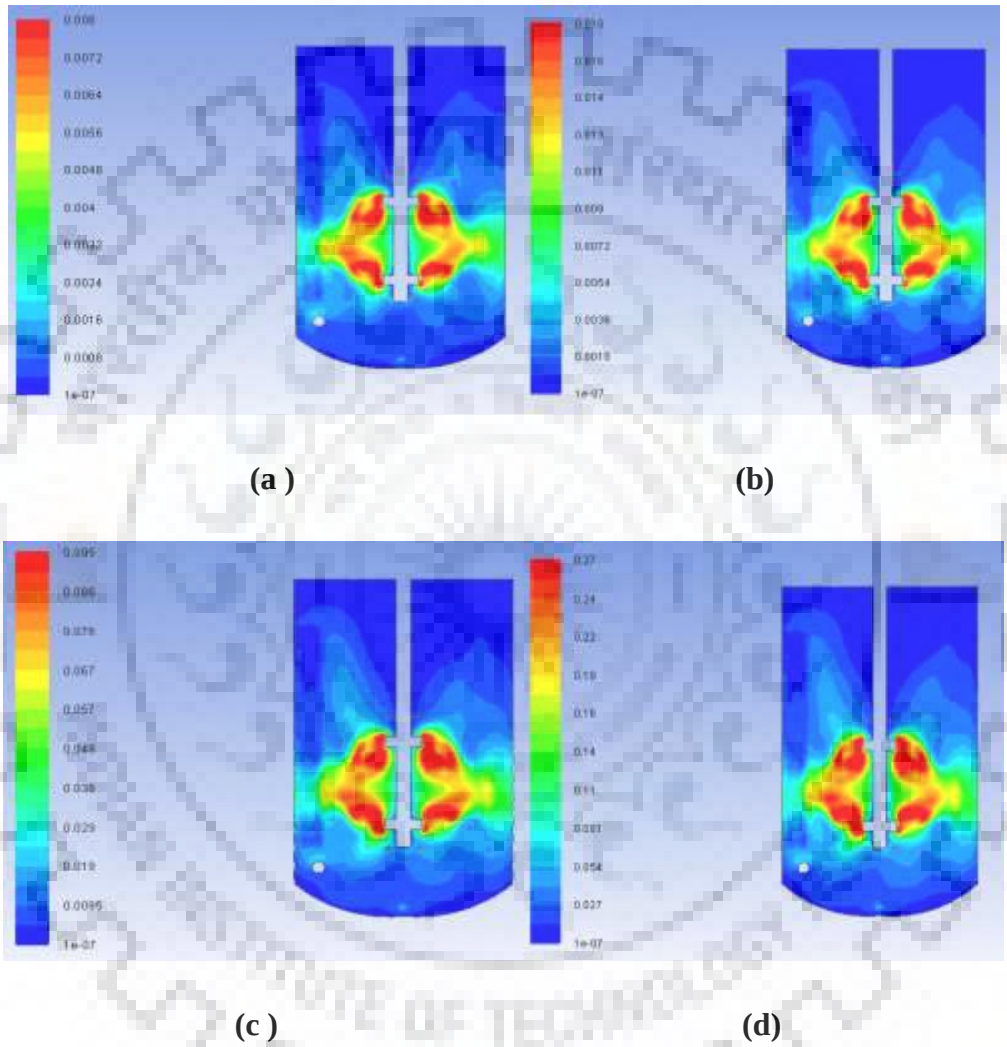


**Fig 5. 44**: Kinetic energy profile of *P. tricornutum* at agitation rates: (a) 100rpm , (b) 150 rpm, (c) 350 rpm and (d) 600 rpm

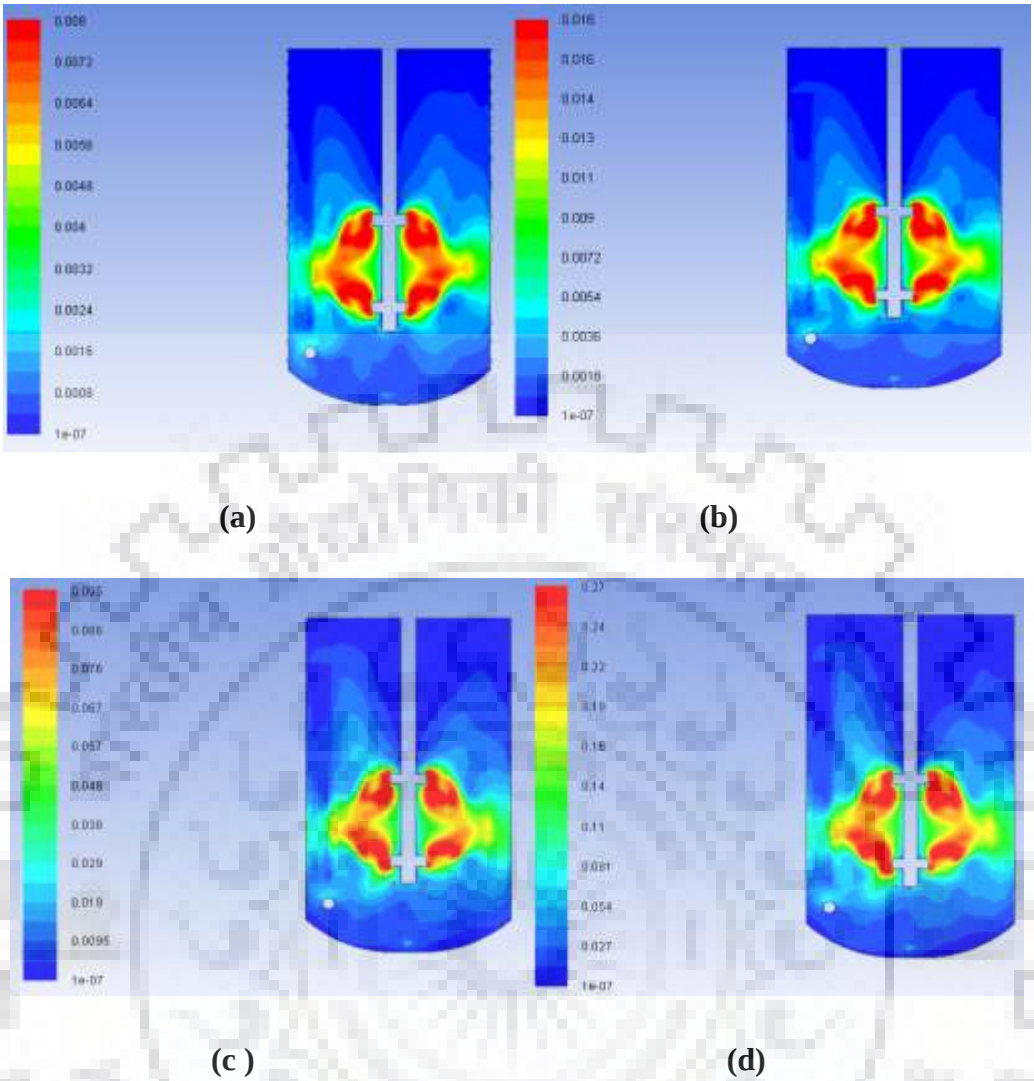


**Fig 5.45**: Kinetic energy profile of *Beauveria bassiana* at agitation rates: (a) 100rpm , (b) 150 rpm, (c) 350 rpm and (d) 600 rpm

The maximum values of kinetic energy are found near the impeller blades. Nearby the field swept by the turbine blade, the turbulent kinetic energy is quite high. Outside this domain, the turbulent kinetic energy quickly becomes very low. It can be seen that kinetic energy profiles are also not affected much by viscosity values. The maximum kinetic energy values are found in the vicinity of the blades. These values are although not high on the blades. The kinetic energy value decreases as we move vertically and horizontally away from the impeller.

### 5.5.4 Distribution of Dissipation Rate of the Turbulent Kinetic Energy

Figure 5.46 shows the dissipation rate profile of the turbulent kinetic energy in the horizontal plane for *P. tricornutum* at different agitation rates

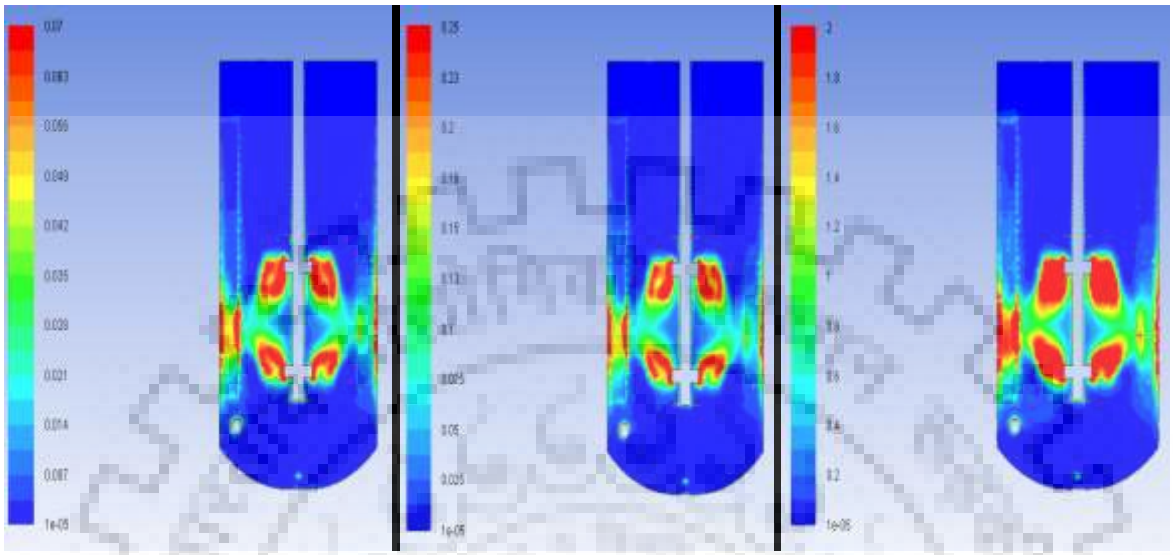

**(a)** **(b)** **(c)**

**Fig 5.46**: Kinetic energy dissipation rate profile of *P. tricornutum* at agitation rate: (a) 100 rpm, (b) 150 rpm and (c) 350 rpm

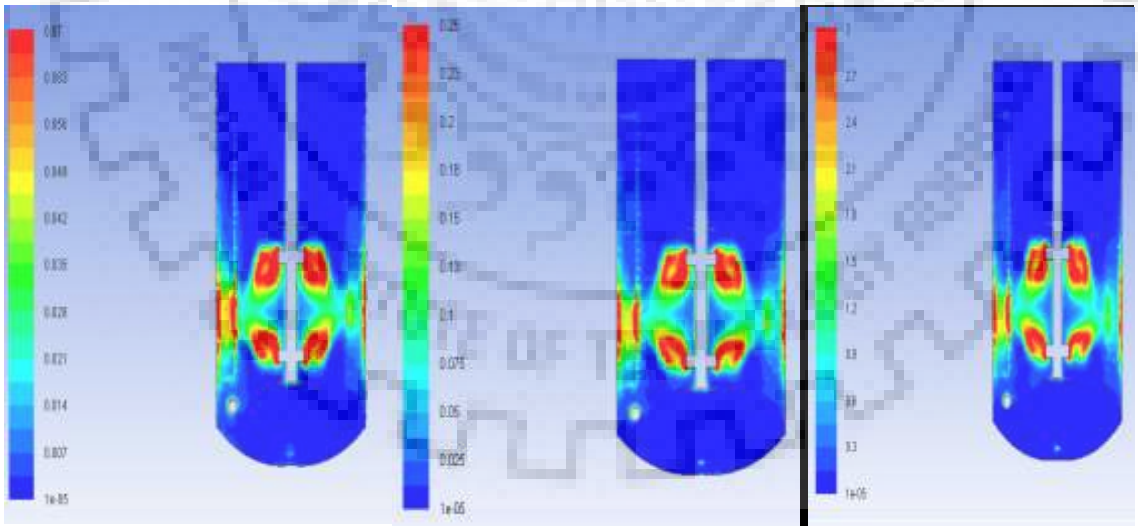

**(a)** **(b)** **(c)**

**Fig 5.47**: Kinetic energy dissipation rate profile of *Beauveria bassiana* at agitation rate: (a) 100 rpm, (b) 150 rpm and (c) 350 rpm

Similar profiles were seen in all the cases. However Energy dissipation rate increases with increasing agitation value. The profiles obtained in Fig 5.46 and 5.47 obtained are similar to that with the turbulent kinetic energy (Fig 5.44, Fig 5.45). The maximum values are found near the blade end. However, the dissipation rate becomes very weak outside the impeller domain. Viscosity independence of dissipation rate can be seen from Fig 5.48.

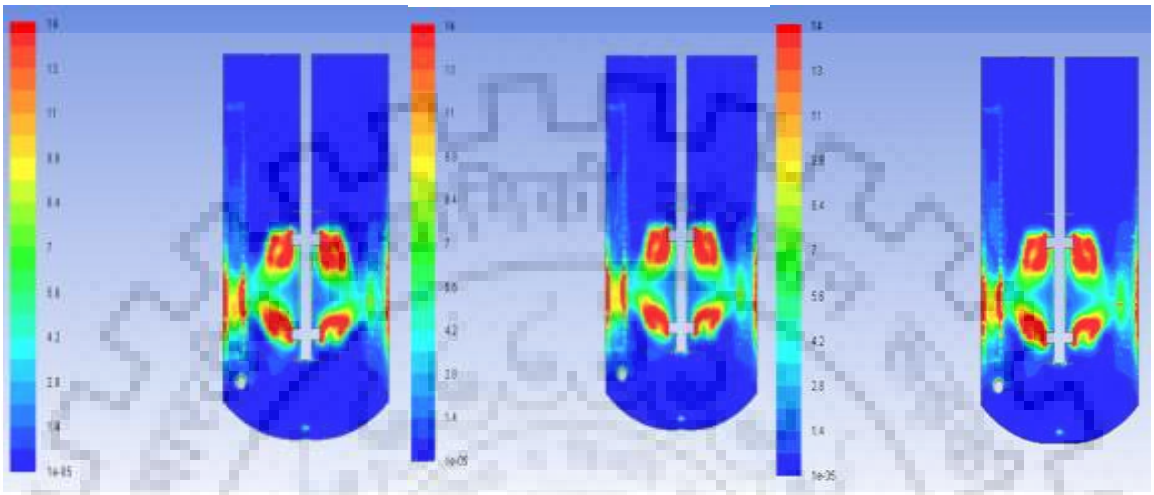

**(a)** **(b)** **(c)**

**Fig 5. 48:** Turbulence Kinetic Energy dissipation rate Profile at 600 rpm for (a) water, (b) *P. tricornutum* and (c) *Beauveria bassiana*

### 5.5.5 Mass Flow rate, Torque and Power Number Determination

Power can be calculated using the torque by the following equation

Power P = 2∏nζ

Where n is agitation rate of impeller in rev/s

ζ – Torque (N.m)

Furthermore, Power = Power Number x Density x Agitator speed$^3$ x Impeller Diameter$^5$

i.e . P = Np * ρ* $n^3$* $D^5$

Where P is Impeller power, Watts, Np is Power Number, ρ is Density of liquid, kg/m3 n is Agitator speed measured in revolutions / second and D – Impeller diameters in meters

Flow Number = Volumetric flow rate/ (agitation rate* Diameter of Impleller$^3$)

Table 5.14 gives the values of Mass flow rate, Power Number and flow number for the different cultures simulated in this study.

**Table 5.14:** Comparison of different dimensionless numbers for different culture and agitation rates

| Culture | Agitation rate | Torque(N.s) | Mass flow rate | Power (W) | Power number | Flow Number |
|---|---|---|---|---|---|---|
| E.coli Bl21 | 100 RPM | 0.0024 | 0.3834 | 0.0251 | 7.3383 | 1.0965 |
| *Pichia stiptis* | 150 RPM | 0.0055 | 0.5592 | 0.0857 | 7.4198 | 1.0661 |
| E.coli Bl21 | 350 RPM | 0.0301 | 1.3670 | 1.1027 | 7.5130 | 1.1170 |
| Water | 600 RPM | 0.0889 | 2.3920 | 5.5842 | 7.5523 | 1.1402 |
| *P. tricornutum* | 100 RPM | 0.0024 | 0.3650 | 0.0247 | 7.2159 | 1.0439 |
| *P. tricornutum* | 150 RPM | 0.0055 | 0.5691 | 0.0857 | 7.4198 | 1.0851 |
| *P. tricornutum* | 350 RPM | 0.0298 | 1.2960 | 1.0917 | 7.4381 | 1.0590 |
| *P. tricornutum* | 600 RPM | 0.0874 | 2.1818 | 5.4887 | 7.4232 | 1.0400 |
| *Beauveria bassiana* | 100 RPM | 0.0024 | 0.3735 | 0.0254 | 7.4300 | 1.0682 |
| *Beauveria bassiana* | 150 RPM | 0.0055 | 0.5513 | 0.0864 | 7.4741 | 1.0511 |
| *Beauveria bassiana* | 350 RPM | 0.0304 | 1.3540 | 1.1137 | 7.5879 | 1.1064 |
| *Beauveria bassiana* | 600 RPM | 0.0892 | 2.2590 | 5.6018 | 7.5761 | 1.0768 |

We can note here that mass flow rate and Power increases with agitation speed. Maximum Power number is found for 350 rpm indicating maximum power requirements at this agitation

speed. Power number was also seen to be highest for the culture with highest viscosity. Flow number in case of *P. tricornutum* was highest at 150 rpm while in case of *Beauveria bassiana*, it is highest for 350 rpm.

### 5.5.6 Mixing time Studies

Mass fraction of tracer at seven with respect to flow time at different points was measured. The Mass fraction vs flow plot for 'water like culture' is compared at different agitation rate for Pt 1 in Fig 5.49. It can be seen that mass fraction of tracer is reduced from 1 to 0 with time. The time taken for this is least in case of 600 rpm. As the agitation rate decreases, time taken for mass transfer of tracer to reach minimum increases. So mixing is achieved faster at higher agitation rate. The variation of tracer concentration with time at Points 2 and 3 are given in Fig 5.50.

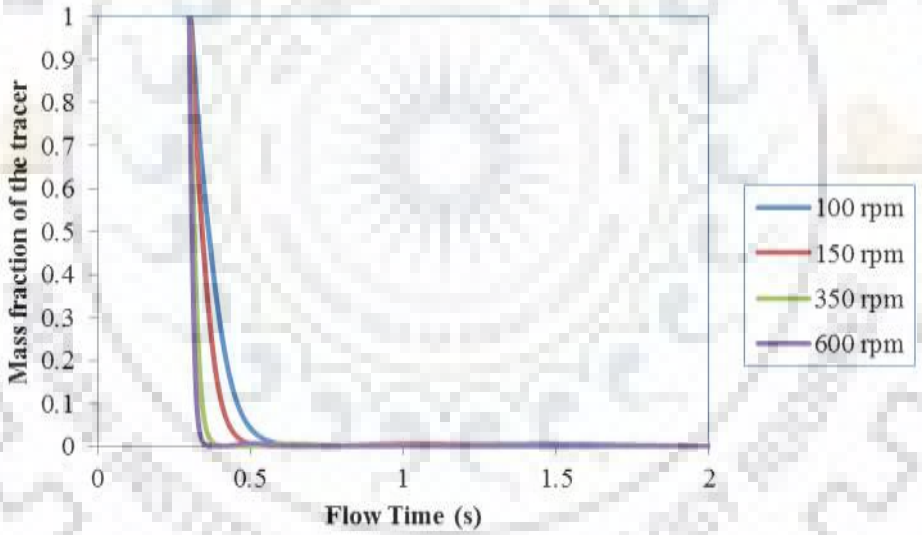


**Fig 5.49:** Mixing characteristics at Point 1 for Newtonian culture

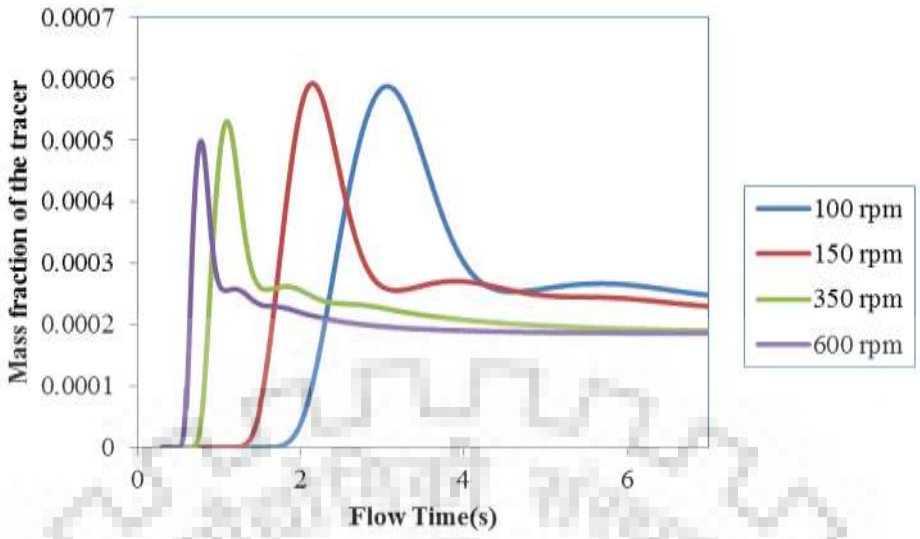


**(a)**

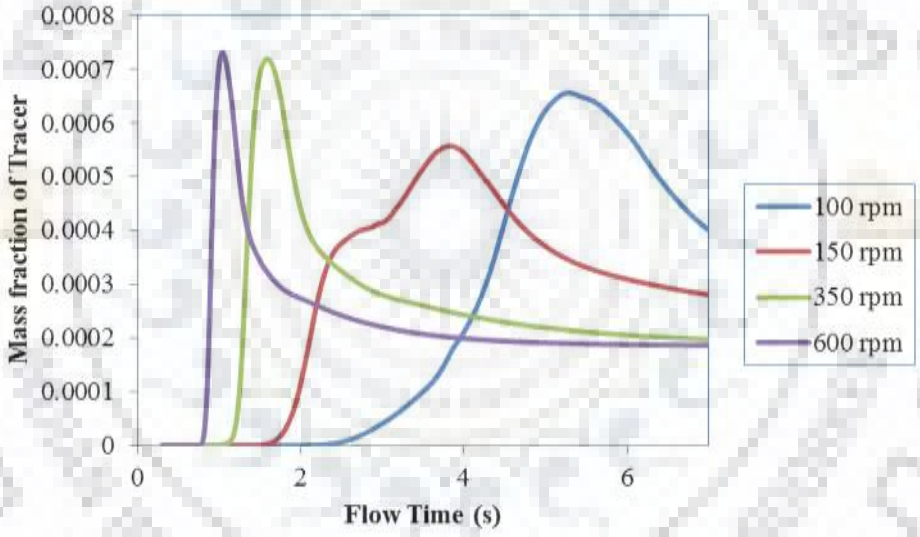


**(b)**

**Fig 5.50:** Mixing Characteristics for Newtonian culture at

(a) Point 2, (b) Point 3

Here the mass fraction of the tracer first increases and then reaches a minimum value. The flow time required to reach the minima and maxima is dependent on agitation rate. The mixing is fastest at 600 rpm

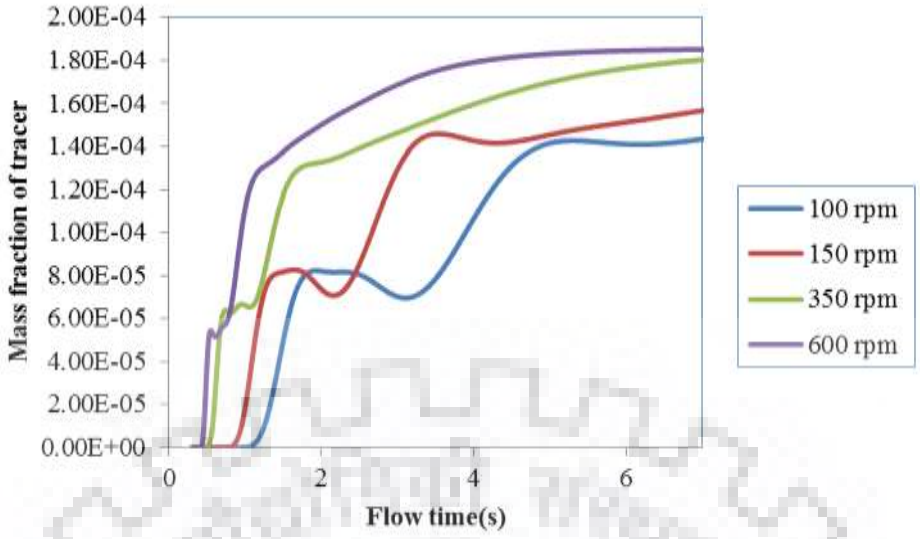


**(a)**

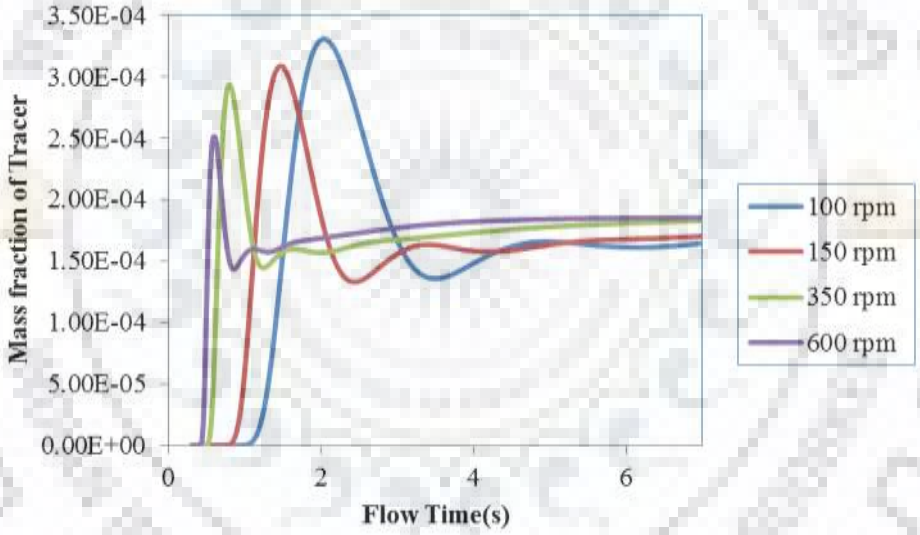


**(b)**

**Fig 5.51:** Mixing characteristics for Newtonian culture at

(a) Point 4, (b) Point 5

Similar pattern was recorded for points 4 and 5. However since these points are further from the tracer injection point, the time taken to initiate mixing is higher. The mixing stated the earliest at highest agitation rate. Fig 5.52 shows the mass tracer plot for points 6 and 7.

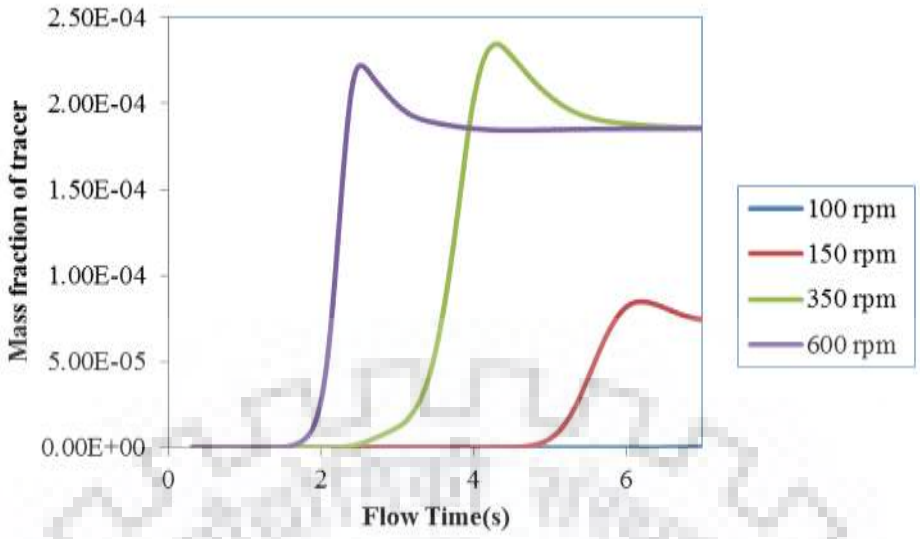


**(a)**

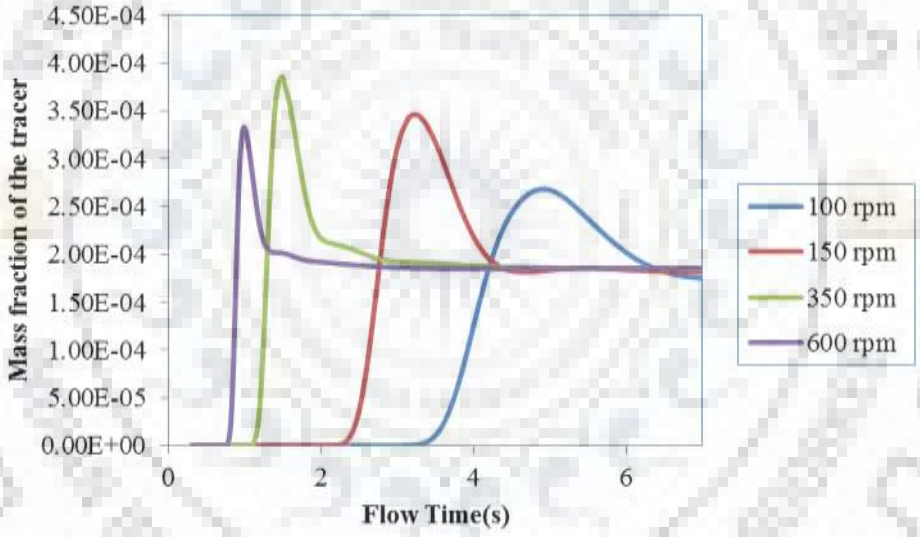


**(b)**

**Fig 5.52:** Mixing Characteristics for Newtonian culture at

(a) Point 6, (b)Point 7

For Point 6, the mixing profile is not even fully developed for 100 rpm agitation rate in the given 7s time of simulation. For Point 7, in case 600 rpm agitation rate mixing is done before 2s while for 100 rpm approx. 6.8 s were taken. Similar kind of results could be seen for *P. tricornutum* algae which is Newtonian in nature but has twice the viscosity of water. Fig 5.53 shows the mass fraction curve for *P.tricornutum* at all the tracking point for the tracer.

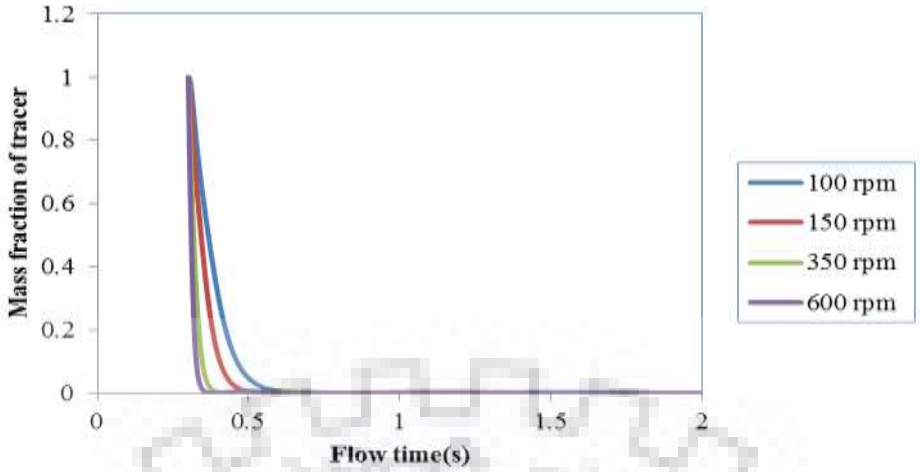
Mass fraction of tracer
Flow time(s)
100 rpm
150 rpm
350 rpm
600 rpm

**(a)**

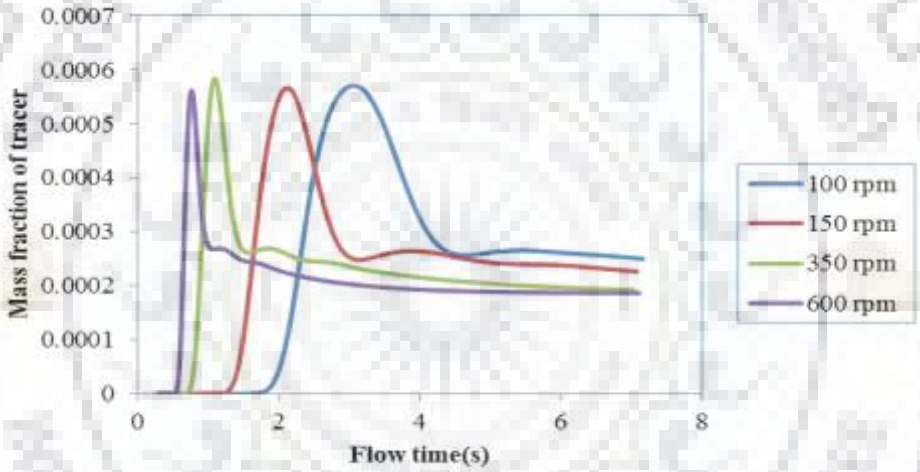
Mass fraction of tracer
Flow time(s)
100 rpm
150 rpm
350 rpm
600 rpm

**(b)**

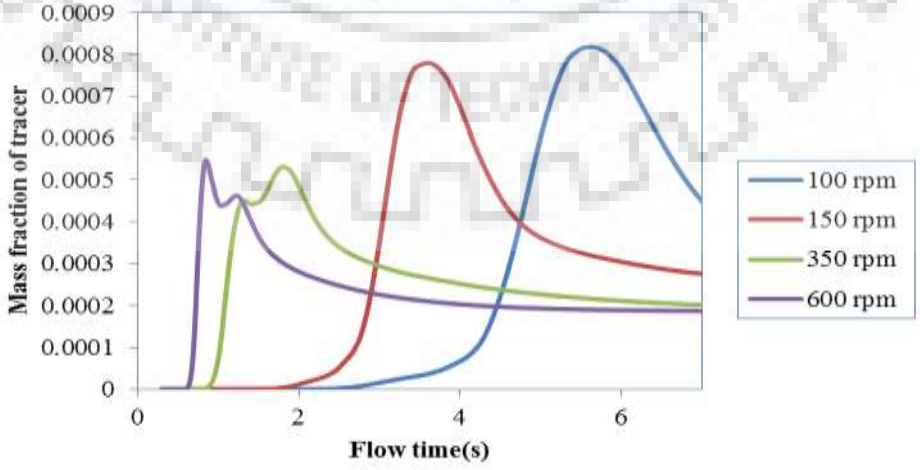
Mass fraction of tracer
Flow time(s)
100 rpm
150 rpm
350 rpm
600 rpm

**(c)**

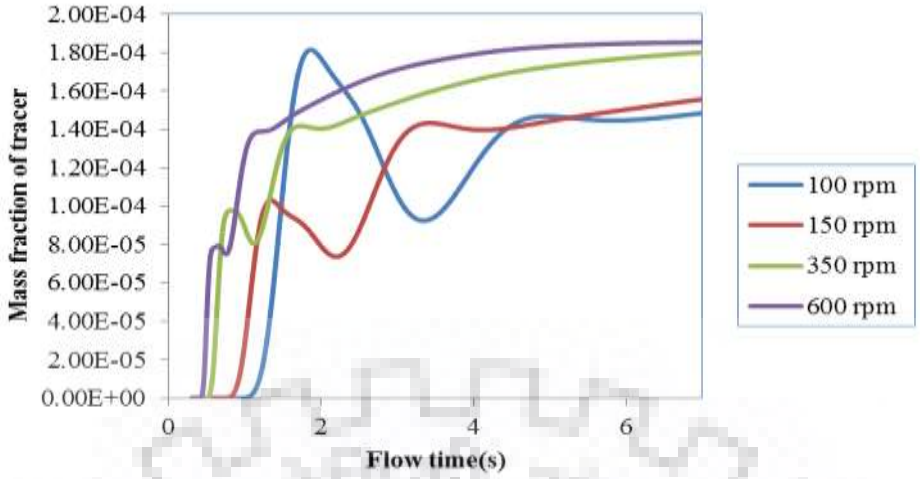
2.00E-04
1.80E-04
1.60E-04
1.40E-04
1.20E-04
1.00E-04
8.00E-05
6.00E-05
4.00E-05
2.00E-05
0.00E+00
Mass fraction of tracer
0
2
4
6
Flow time(s)
100 rpm
150 rpm
350 rpm
600 rpm

**(d)**

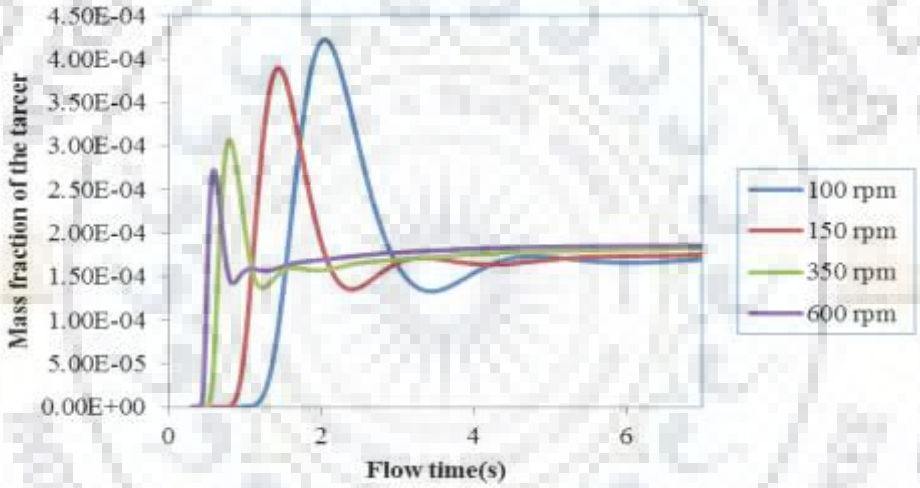
4.50E-04
4.00E-04
3.50E-04
3.00E-04
2.50E-04
2.00E-04
1.50E-04
1.00E-04
5.00E-05
0.00E+00
Mass fraction of the tarcer
0
2
4
6
Flow time(s)
100 rpm
150 rpm
350 rpm
600 rpm

**(e)**

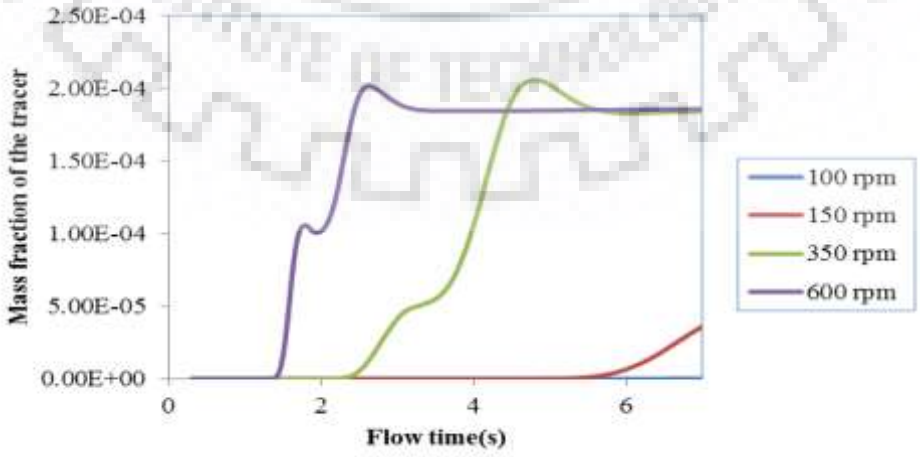
2.50E-04
2.00E-04
1.50E-04
1.00E-04
5.00E-05
0.00E+00
Mass fraction of the tracer
0
2
4
6
Flow time(s)
100 rpm
150 rpm
350 rpm
600 rpm

**(f)**

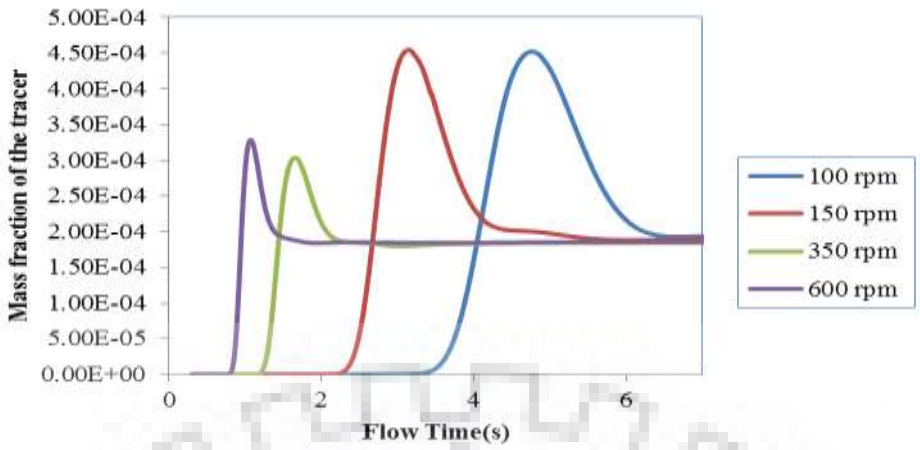


**(g)**

**Fig 5.53:** Mixing Characteristics for *P. tricornutum* at Point (a) 1, (b) 2, (c) 3, (d) 4, (e) 5, (f) 6 and (g) 7

In this case of point 3 and 4, mixing was not complete within the mixing time of 7s. For Point 6 lower agitation rate of 100 rpm, mixing was not even initiated within 7s. This can be attributed to the high viscosity of fluid. Mixing time is comparatively higher than that of Newtonian culture for all the points. For better comparison of viscosity effect on mass transfer of tracer, three different cultures: (a) E.coli BL21, (b) *P.tricornutum* and (c) *Beauveria bassiana*. Viscosity of *P.tricornutum* is twice of that of E.coli and *Beauveria bassina* is Non-Newtonian whose apparent viscosity can be as high as ten times of *P.tricornutum*. Fig 5.54 gives the tracer mass fraction comparison for all seven points for the three cultures at 100 rpm.

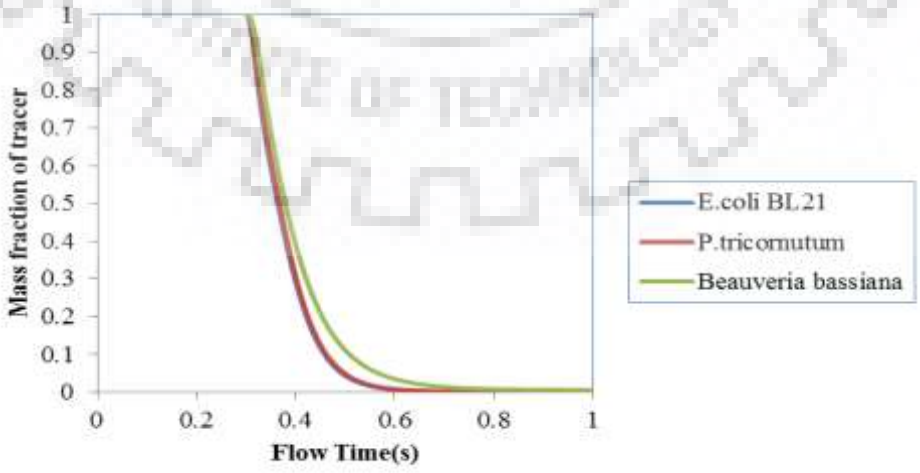


**(a)**

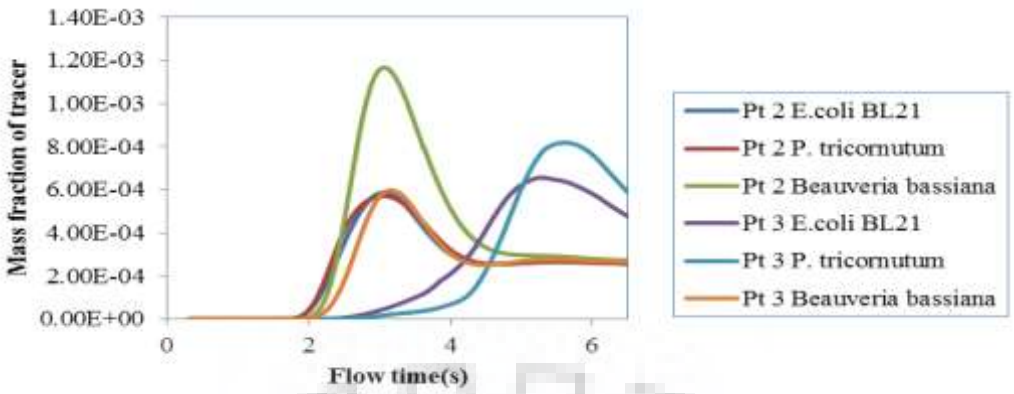


**(b)**

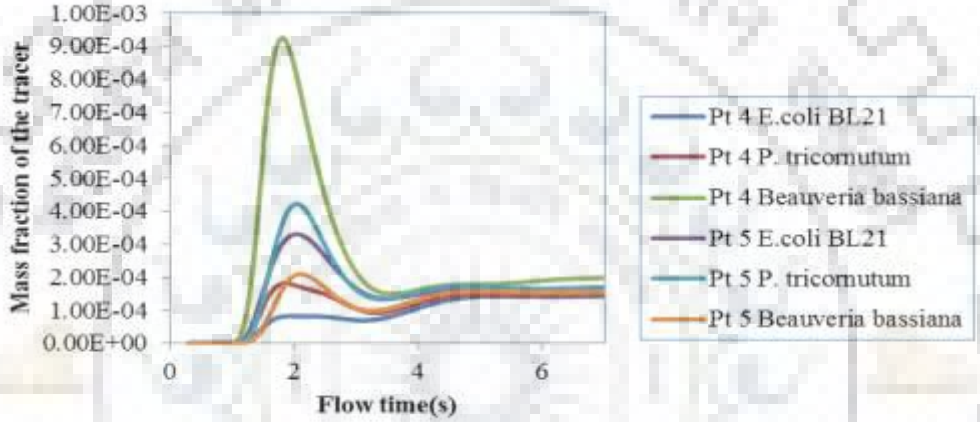


**(c)**

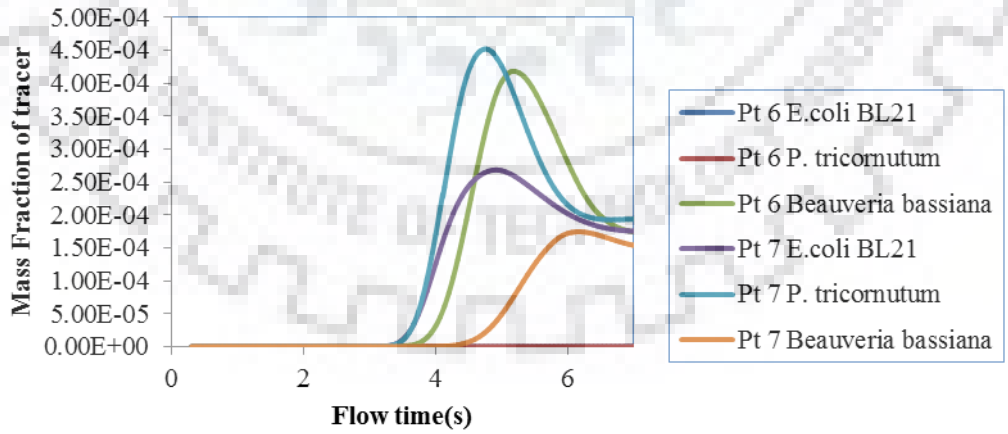


**(d)**

**Fig 5.54**: Mixing characteristics of tracer at 100 rpm for three different cultures of E.coli BL21, *P.tricornutum* and *Beauveria bassiana* at Points (a) 1, (b) 2 and 3, (d) 4 and 5, (d) 6 and 7

It can be seen that for all the points, minima and maxima reached by tracer is higher in case of *Beauveria bassina* which has the highest viscosity. Thus higher mass fraction of tracer is observed for culture with higher viscosity.

# CHAPTER 6
# CONCLUSION AND FUTURE SCOPE

## 6.1 Conclusion

The present work focuses of flow and mixing characteristics in bioreactors considering different cell culture environments. The rheological behaviors of different cell cultures were predicted experimentally.

Temperature dependence of viscosity is confirmed using the reference materials of CMC and Xanthun gum. Moreover for non-Newtonian fluids, consistency index (K) decreased with temperature for a constant concentration while power law index (n) increased with temperature. Conversely, consistency power law index increased with concentration for a constant temperature and power law index decreased with concentration. Dynamic rheological predictions were also done for the reference materials. Storage Modulus of 1% CMC solution was comparatively higher than 2% and 4 % CMC solution indicating higher ability to store elastic deformation energy. This may be due to higher degree of cross linking at 1% concentration. Loss modulus is a measure of energy dissipation indicating the hardness or stiffness of a material. The trend similar to storage modulus was observed where 1% solution was found to have the highest loss modulus. Similar trend was observed for complex modulus. In case of Xanthun gum, the storage modulus, loss modulus and complex viscosity were found to be directly proportional to frequency and concentration.

Response surface methodology (RSM) was used to find optimum parameters for operation of bioreactor for Newtonian fluid. It was done for two different combinations of impellers: (a) Rushton-Rushton and (b) Rushton impeller- Marine Propeller. Mass transfer was observed to be higher in case of Rushton- Rushton impeller combination. A quadratic regression model was developed correlating agitation rate, air flow rate and impeller spacing to mass transfer coefficient. Significance of this model was verified using ANOVA analysis, which confirmed that the second-order polynomial function is a good fit for the present experimental data.

The Rheological study of E.coli BL21 was then conducted at the obtained parameters. Viscosity of E.coli was recorded highest when the inoculum was just added to the bioreactor, i.e at 0 h. It was observed that the mass transfer is higher in case of higher agitation rate,

however, due to high foam formation agitation rate could not be increased beyond 350 rpm in the present bioreactor.

Dynamic Rheology measurements conducted for E.coli BL21, *Botryococcus braunii* and *Pichia stiptis* yield similar results and resemble the curves obtained for water. The Rheological studies conducted for *Botryococcus braunii* have shown that there is a complex viscosity is directly proportional to culture concentration. The presence of elasticity can be attributed to algae cell interparticle interaction and algae motility. The data shows that storage modulus was dominant. For biomass concentrations measured in this study, all three cultures displayed Newtonian behaviour.

The mixing characteristics of the present bioreactor system were studied numerically to predict dead point and to further enhance availability of nutrients and air in the bioreactor.
Computational fluid dynamics study was conducted for a 7L bioreactor with two Rushton impellers. The flow patterns and mixing behaviour was predicted using k-ε turbulent model and scalar transport models. The Flow field, turbulent kinetic energy and energy dissipation were predicted for 'water like' cultures, *P. tricornutum* and *Beauveria bassiana* at four different agitation rates. *P. tricornutum* viscosity is twice as that of water and Beauveria bassiana is a non-Newtonian fungal culture with apparent viscosity almost 20 times of that of water. It was found that the flow rate was maximum near the impellers and the viscosity change does not seem to have prominent effect on the velocity profile.
Further, the maximum values of turbulent kinetic energy and energy dissipation rates were found near the impeller blades. Nearby the field swept by the turbine blade, the turbulent kinetic energy was quite high. Outside this domain, the turbulent kinetic energy quickly becomes very low. It was also found that the mass flow rate and Power increases with agitation speed.
For mixing time studies, It was found that with a decrease in agitation rate the time taken for mass fraction of tracer to reach minimum increased. Therefore, higher mixing was achieved at higher agitation rate. Mixing time was shown to be increasing with viscosity. It can be seen that for all the points, minima and maxima reached by tracer is highest in case of *Beauveria bassina* which has the highest viscosity. Thus higher mass fraction is achieved for culture with higher viscosity. Mixing time was shown to be increasing with viscosity.

## 6.2 Future Recommendations

Higher biomass concentration of these cultures is to be studied for better understanding of viscosity effect to the design of the bioreactor, e.g. mathematical correlation between viscosity parameters and impeller tip speed can be investigated. Other highly viscous culture like fungus and plant can be rheologically characterized for better understanding.

CFD modelling of a bioreactor can be further refined for two phase mass transfer for better understanding of the real-time process. It can help eliminate a series of trial runs to find the optimum conditions to run a reactor.

# REFERENCES


1. Yaun Shi, Dewey D. Y. Ryu, Rabia Ballica, 1993.Rheological properties of mammalian cell culture suspensions: Hybridoma and HeLa cell lines. Biotechnology and Bioengineering, 41(7), 745 - 754
2. Hu-Ping Luo, Muthanna H. Al-Dahhan, 2003. Analyzing and Modeling of Photobioreactors by Combining First Principles of Physiology and Hydrodynamics. Wiley InterScience,
3. Antoine Souli`es, Jeremy Pruvost , Jack Legrand, Cathy Castelain, Teodor I. Burghelea, 2012. Rheological properties of suspensions of the green microalga Chlorella vulgaris at various volume fractions. Springer-Verlag Berlin Heidelberg, 52:589–605
4. F. Kerdouss, A. Bannari, P. Proulx , R. Bannari, M. Skrga, Y. Labrecque, 2007. Two-phase mass transfer coefficient prediction in stirred vessel with a CFD model. Computer & Chemical Engineering, 32 (2008) 1943–1955
5. Xinru Zhang , Zeyi Jiang ,Liang Chen , Aihui Chou , Hai Yan , Yi Y. Zuo , Xinxin Zhang,2013. Influence of cell properties on rheological characterization of microalgae suspensions. Bioresource Technology 139 (2013) 209–213.
6. P. Patrício, P. L. Almeida, R. Portela, R. G. Sobral, I. R. Grilo, T. Cidade, and C. R. Leal, 2014. Living bacteria rheology: Population growth, aggregation patterns, and collective behavior under different shear flows Phys. Rev. Vol. 90, Iss. 2. 022720
7. Victoria O. Adesanya, Damien C. Vadillo, Malcolm R. Mackley, 2012. The rheological characterization of algae suspensions for the production of biofuels. Journal of Rheology, 56, 925
8. Angel Wileman, Altan Ozkan, Halil Berberoglu, 2012. Rheological properties of algae slurries for minimizing harvesting energy requirements in biofuel production. Bioresource Technology 104 (2012) 432–439
9. Rabia Ballica, Dewey D. Y. Ryu,* Robert L. Powell, and Derek Owen,1992. Rheological Properties of Plant Cell Suspensions. Blotechnol. Prog. 1992, 8, 413-420
10. FLUENT Learning Modules. (2017, March 1). Retrieved August 5, 2017, from https://confluence.cornell.edu/display/SIMULATION/FLUENT Learning Modules

11. ANSYS FLUENT 12.0 Tutorial Guide, Retrieved July 27, 2017 from http://www.afs.enea.it/project/neptunius/docs/fluent/html/tg/main_pre.htm
12. Ahuja, A., Singh, A., 2009. Slip velocity of concentrated suspensions in Couette flow. J. Rheol. 53, 1461–1485.
13. Andersen, R., 2005. Algal Culturing Techniques. Academic Press, Burlington, MA, USA. ASME, 2010. Slurry Transportation Piping Systems. American Society of Mechanical Engineers Report B31.11-2002, New York, NY.
14. Berberoglu, H., Pilon, L., Jay, J., 2008. Effect of nutrient media on photobiological hydrogen production by Anabaena variabilis ATCC 29413. Int. J. Hydrogen Energy 33, 1172–1184.
15. Biller, P., Ross, A., 2011. Potential yields and properties of oil from the hydrothermal liquefaction of microalgae with different biochemical content. Bioresource Technology 102, 215–225.
16. Chen, F., 1997. Mixotrophic and heterotrophic growth of Haematococcus lacustris and rheological behaviour of the cell suspensions. Bioresource Technolnology. 62 (1–2), 19–24.
17. Newton Joseph M., Vlahopoulou Joanna, Young Z., 2017. Investigating and modelling the effects of cell lysis on the rheological properties of fermentation broths. Biochemical Engineering Journal 121, 38–48
18. Gabelle J.-C., Jourdier E., Licht R.B., Chaabane F.,Henaut I., Morchain J., Augier F., 2012. Impact of rheology on the mass transfer coefficient during the growth phase of Trichoderma reesei in stirred bioreactors. Chemical Engineering Science 75, 408–417.
19. Ahamed, A., Vermette, P., 2010. Effect of mechanical agitation on the production of cellulases by Trichoderma reesei RUT-C30 in a draft-tube airlift bioreactor. Biochemical Engineering Journal 49 (3), 379–387.
20. Albaek, M.O., Gernaey, K.V., Hansen, M.S., Stocks, S.M., 2011. Modeling enzyme production with Aspergillus oryzae in pilot scale vessels with different agitation, aeration, and agitator types. Biotechnology and Bioengineering 108 (8), 1828–1840.
21. Albaek, M.O., Gernaey, K.V., Hansen, M.S., Stocks, S.M., 2012. Evaluation of the energy efficiency of enzyme fermentation by mechanistic modeling. Biotechnology and Bioengineering 109, 950–961.
22. Allen, D.G., Robinson, C.W., 1991. The prediction of transport parameters in filamentous fermentation broths based on results obtained in pseudoplastic polymer-solutions. The Canadian Journal of Chemical Engineering 69 (2), 498–505.

23. Amanullah, A., et al., 2000. Agitation induced mycelial fragmentation of Aspergillus oryzae and Penicillium chrysogenum. Biochemical Engineering Journal 5 (2), 109–114.
24. Ascanio, G., Castro, B., Galindo, E., 2004. Measurement of power consumption in stirred vessels—A review. Chemical Engineering Research & Design 82 (A9), 1282–1290.
25. Bakonyi P., Nemest´othy N., and B´elafi-Bak´o K., 2012. Comparative Study of Various E. coli Strains for Biohydrogen Production Applying Response Surface Methodology. The ScientificWorld Journal.
26. Dubey S., Singh A., Banerjee U.C., 2011. Response Surface Methodology of Nitrilase production by recombinant *Escherichia coli.* Brazilian Journal of Microbiology 42: 1085-1092.
27. Ameur H., Bouzit M., 2012. Mixing in shear thinning fluids. Brazilian Journal of Chemical Engineering Vol. 29, No. 02, 349 – 358.
28. Montantea G., Mošťekb M., Jahodab M. , Magellia F.,2005. CFDsimulations and experimental validation of homogenisation curves and mixing time in stirred Newtonian and pseudoplastic liquids. Chemical Engineering Science 60 2427 – 2437.
29. Taghavi M., Zadghaffari R., Moghaddasa J., Moghaddasb Y., 2011. Experimental and CFD investigation of power consumption in a dual Rushton turbine stirred tank. Chemical engineering research and design 89 280–290.
30. Wu B., Chen S., 2007. CFD Simulation of Non-Newtonian Fluid Flow in Anaerobic Digesters. Biotechnology and Bioengineering, Vol. 99, No. 3, 700-711.